VIRAL GENETIC DETERMINANTS OF ZIKA VIRUS PATHOGENESIS

Derek Lynn Carbaugh

A dissertation submitted to the faculty at the University of North Carolina at Chapel Hill in partial fulfillment of the requirements for the degree of Doctor of Philosophy in the Department of Microbiology and Immunology

Chapel Hill
2020

Approved by:

Helen M. Lazear

Mark T. Heise

Aravinda M. de Silva

Ralph S. Baric

Nathaniel J. Moorman

ABSTRACT

Derek Lynn Carbaugh: Viral Genetic Determinants of Zika Virus Pathogenesis

(Under the direction of Helen M. Lazear)

Zika virus (ZIKV) is an emerging mosquito-borne flavivirus primarily transmitted by mosquitoes and ticks. Recent ZIKV outbreaks have produced serious human disease, including neurodevelopmental malformations and Guillain-Barré syndrome. These outcomes were not associated with ZIKV infection prior to 2013, raising the possibility that viral genetic changes could contribute to new clinical manifestations.

In my studies, I investigated the role of E protein glycosylation in ZIKV pathogenesis. I found that glycosylated viruses were highly pathogenic in *Ifnar1*$^{-/-}$ mice, whereas non-glycosylated viruses were attenuated, producing lower viral loads in the serum and brain when inoculated subcutaneously, but replicating equally well in the brain when inoculated intracranially. These results suggest that E glycosylation is advantageous in the periphery but not within the brain. Accordingly, I found that glycosylation facilitated infection of lectin expressing cells, possibly explaining the attenuation of non-glycosylated ZIKV in mice. Additionally, I found that adding a glycan back to the E protein at a different position (N67) does not functionally complement the loss of the glycan at position N154.

I also discovered two strain-specific determinants of ZIKV virulence in mice. I found that H/PF/2013 caused 100% lethality in *Ifnar1*$^{-/-}$ mice, whereas PRVABC59 caused no

lethality. Deep sequencing revealed a high-frequency variant (V330L) in PRVABC59 not present in H/PF/2013. I showed that the V330 variant is lethal on both strains, whereas the L330 variant is attenuating only on the PRVABC59 background. To investigate the remaining differences between the two strains, I made a panel of chimeric viruses with nucleotide sequences derived from H/PF/2013 or PRVABC59. I found that 6 nucleotide differences in the 3' quarter of the H/PF/2013 genome were sufficient to confer virulence in *Ifnar1*$^{-/-}$ mice.

Altogether, I confirmed that the E protein glycosylation mediates pathogenesis of ZIKV from both Asian and African-lineage strains, and I identified a large and previously unreported difference in virulence between two commonly used ZIKV strains, in two widely used mouse models of ZIKV pathogenesis (*Ifnar1*$^{-/-}$ and *Ifnar1*$^{-/-}$ *Ifngr1*$^{-/-}$ DKO mice). My studies emphasize how small genetic changes in viruses can lead to drastically different pathogenic phenotypes in common laboratory models.

ACKNOWLEDGEMNTS

The Lazear lab has been an excellent environment for me to both conduct my research, and also grow and develop as a scientist over the last five years. When I first came to UNC, I really wasn't sure what kind of lab I was looking for or what atmosphere best suited me as a scientist, but after my rotation with Helen, I knew. Helen's knowledge and enthusiasm about science, specifically obscure flaviviruses, was contagious and made me excited about my research. I want to thank Helen for all of the terrific one-on-one mentoring she gave me during my first year in the lab and the continued support to push me to reach my potential, and provided me with the encouragement and resources to achieve my goals.

I want to thank the rest of the quickly growing Lazear lab for being great lab members, as well as friends. But I want to especially thank Melisa for everything she does to keep the lab running smoothly, always fixing the autoclave, and always being there to talk about everything and anything.

I thank all members of the Heise, Moorman, Desilva, and Baric lab who have helped me over the past five years. I thank Doug and Boyd from the Baric lab for teaching me the reverse genetics system, and especially Boyd, for always being willing to pass on his vast knowledge and for all of his advice and suggestions on troubleshooting for all the times things did not work, which was a lot.

I thank Dixie Flannery, Michelle Hightower, Toni Baric and everyone in the Microbiology & Immunology offices for their administrative help. The 9th floor of BW would surely fall apart without everything that Toni does for everyone, and scheduling all of my committee meetings would have been much, much harder without Toni!

Lastly, I would like to thank all of my friends and family for their support during all of my studies. Especially my mom and dad who were there for me through all of the ups and downs in my life and have given me everything I have ever needed to get where I am at today.

.

TABLE OF CONTENTS

LIST OF FIGURES

LIST OF TABLES

LIST OF ABBREVIATIONS

AA – amino acid

Ab – antibody

ALFV – Alfuy virus

BMDM – bone marrow derived macrophages

BMDCs – bone marrow derived dendritic cells

C – capsid

cDNA – complementary deoxyribonucleic acid

ConA – concanavalin A

DCs – dendritic cells

DC-SIGN – dendritic cell-specific intercellular adhesion molecule-3-grabbing non-integrin

DENV – dengue virus

DNA – deoxyribonucleic acid

E – envelope

ED – envelope domain

EDI – envelope domain I

EDII – envelope domain II

EDIII – envelope domain III

ELISA – enzyme-linked immunosorbent assay

ER – endoplasmic reticulum

FFA – focus forming assay

FFU – focus forming unit

HDV – hepatitis delta virus

HIV – human immunodeficiency virus

HPI – hours post-infection

IFN – interferon

IFNAR1 – interferon alpha receptor 1

ISGs – interferon stimulated genes

JEV – Japanese encephalitis virus

LGTV – Langat virus

MAb – monoclonal antibody

MOI – multiplicity of infection

MVEV – Murray Valley encephalitis virus

NS – non-structural protein

NT – nucleotide

ORF – open reading frame

PCR – polymerase chain reaction

PNGase F – peptide-N-glycosidase F

pr – precursor protein

prM – precursor membrane protein

RNA – ribonucleic acid

ROS – reactive oxygen species

RT-PCR – reverse transcription polymerase chain reaction

sfRNA – subgenomic flavivirus RNA

SVP – subviral particle

TBEV – tick-borne encephalitis virus

UTR – untranslated region

VLP – virus like particle

WNV – West Nile virus

WT – wild type

YFV – yellow fever virus

ZIKV – Zika virus

xrRNA – Xrn1 resistant RNA

CHAPTER 1 – INTRODUCTION[1]

1.1 Summary

The *Flavivirus* genus, in the family *Flaviviridae*, includes human pathogens, such as West Nile virus (WNV), Japanese encephalitis virus (JEV), dengue virus (DENV), yellow fever virus (YFV), tick-borne encephalitis virus (TBEV), and Zika virus (ZIKV). Most flaviviruses are vector-borne, transmitted by mosquitoes and ticks. Many of these arboviruses are capable of causing severe diseases, such as encephalitis, hemorrhagic fever, and birth defects (1, 2). Thus, the endemic transmission of flaviviruses in certain regions of the world, as well as their emergence in new areas, represents a significant public health burden as well as a threat to livestock and wildlife(3–6).

1.2 Flavivirus genome organization and replication

Flaviviruses are enveloped, positive-sense single-stranded RNA viruses. The flavivirus genome is translated as a single open reading frame flanked by 5’ and 3’ untranslated regions (UTR) (7). The polyprotein is proteolytically cleaved co- and post-translationally by host and viral proteases into three structural proteins, capsid (C), premembrane/membrane (prM/M), and envelope (E), as well as seven non-structural proteins (NS1, NS2A, NS2B, NS3, NS4A NS4B, and NS5) (8–10).

---

[1]Parts of this chapter were first published in *Journal of Virology*, May 18;94(11):e00104-20.

Both prM and E are incorporated into the viral envelope in a highly ordered conformation. prM participates in the proper folding, maturation, and assembly of E during replication (9, 11). E facilitates membrane fusion between the virus and host cell, and is the primary viral protein against which neutralizing antibodies are produced (9, 12, 13). Flavivirus E proteins form head-to-tail homodimers, 90 of which assemble to form a virion surface with 2-fold, 3-fold, and 5-fold symmetry axes (14). Flavivirus E proteins are class-II fusion proteins with three distinct domains: domain I (EDI), domain II (EDII), and domain III (EDIII) (Fig 1.1A) (10, 15–19). EDI and EDII are discontinuous, forming a central β-barrel and elongated dimerization region, respectively, while EDIII forms a continuous C-terminal, immunoglobulin-like domain (15). There is ~40% amino acid identity among the flavivirus E proteins. After virion attachment to the cell and endocytosis, flexible hinges that connect the three E domains enable irreversible conformational changes during pH-dependent membrane fusion inside the endosome (10, 13, 15, 19). Flavivirus replication and assembly occurs on endoplasmic reticulum (ER) membranes, with encapsidated genomes acquiring their envelope as they bud into the ER lumen. The pr peptide is positioned at the distal end of EDII within the heterodimer where it obscures the fusion loop on E proteins of immature virions (20). Transit of assembled virions through the acidic compartments of the trans-Golgi network results in a reorganization of the surface of the virus particle. This pH-dependent change in virion structure exposes a cleavage site on prM and the pr portion is cleaved by host furin-like proteases in the Golgi to form mature, infectious particles (9, 10, 21, 22).

1.3 Zika virus

ZIKV is a mosquito-borne flavivirus, closely related to DENV, whose natural transmission cycle circulates between vectors from the *Aedes* genus and mammalian hosts (23). ZIKV was first isolated in 1947 from the blood of a sentinel rhesus monkey in the Zika forest near Entebbe, Uganda (24). Over the next sixty years, serological and entomological data revealed small sporadic outbreaks in Africa and southeast Asia (25–29). In 2007 the first ZIKV outbreak outside of Africa and Asia was reported on Yap Island, Federated States of Micronesia (30). Symptomatic patients showed signs of fever, rash, conjunctivitis, arthralgia, and arthritis, termed Zika fever. Serological estimates suggest that more than 70% of the population had been exposed to ZIKV (30). This outbreak highlighted the potential of ZIKV to spread to new locations and cause illness in humans. Subsequently, ZIKV spread from Southeast Asia, across the Pacific Ocean, and into the Americas, with outbreaks in Cambodia in 2010 (31), in French Polynesia in 2013-2014 (32), and most notably in Brazil in 2015 (33). The spread of ZIKV to the Western Hemisphere also was accompanied by unexpected clinical manifestations that had not been associated with ZIKV prior to 2013. The 2013-2014 ZIKV outbreak in French Polynesia was associated with an increase in Guillain-Barré syndrome, an autoimmune neuropathy that can result in weakness, paralysis, and death (2, 34, 35), while the outbreak in Brazil and the rapid spread of ZIKV to many countries in the Americas (33, 36–38) has revealed that ZIKV infection during pregnancy can cause a broad range of congenital malformations termed congenital Zika syndrome (2, 39, 40). It is unknown why such severe disease manifestations were only revealed during the most recent ZIKV outbreak, but one explanation could be viral

genetic changes. Phylogenetic analyses have grouped ZIKV into two major lineages: African and Asian, with strains that emerged in the Pacific Islands and Latin America belonging to the Asian lineage (41). Analysis of the viral genetic changes that have evolved over time is vital to fill major gaps in our knowledge regarding ZIKV genetic determinants of pathogenesis.

1.4 Flavivirus envelope protein glycosylation

Many flaviviruses contain an N-linked glycosylation site (N-X-S/T) at amino acid N154 of E, where a glycan is added to the amide nitrogen of the asparagine (Asn, N) residue as the emerging protein is being translated (42). However, the number and position of predicted glycosylation sites are not conserved among all flaviviruses, nor among different strains of the same virus (43–47) (Fig. 1.1 B-C). For instance, most WNV strains (such as NY99) are glycosylated at N154, but some strains, such as Kunjin, are not (48). Similarly, all Asian lineage ZIKV strains, such as H/PF/2013 and PRVABC59, are glycosylated at N154, whereas some of the African lineage ZIKV strains are not (29, 49). The prototype ZIKV strain includes both glycosylated and non-glycosylated variants, all designated “MR766”, which can be a source of confusion in the literature (50–52). DENV is unique among flaviviruses in that its E protein contains two N-linked glycosylation sites, one at N67 and a second at N153, which are present in most strains of the four DENV serotypes (8, 47, 53). E glycosylation plays important roles in viral attachment and cell entry, replication, transmission, and pathogenesis. The effects of glycosylation are particularly important for these vector-borne viruses because the process of protein glycosylation differs between mammalian and insect cells.

1.5 Protein glycosylation in mammalian and insect cells

In mammalian cells, glycosylation takes place in the ER-Golgi complex where a network of glycotransferases and glycosidases enzymatically synthesize a diverse array of glycan structures (42, 54, 55). Briefly, a lipid-linked oligosaccharide, synthesized from the lipid dolichol, serves as a carrier of the glycan. Dol-PP-$GlcNAc_2Man_5$ is enzymatically synthesized on the cytoplasmic side of the ER membrane and then translocated across the membrane into the ER lumen where further monosaccharides are added. The final glycan structure is transferred co-translationally to the Asn residue of an appropriate N-X-S/T motif via an oligosaccharyltransferase. Further processing takes place in the ER-Golgi complex, where glycosidases trim the mannose residues before glycotransferases extend the “antennae” of the glycans to produce larger hybrid or complex structures. Many flaviviruses have avian amplifying hosts (e.g. WNV, JEV). Although glycosylation processes in avian cells have not been described as extensively as mammalian cells, bird-derived viruses likely have similar glycan structures as mammalian-derived viruses, as influenza viruses derived from chicken eggs, human embryonic lung fibroblast, or Madin-Darby canine kidney cells contain similar glycan structures, though at different frequencies (56, 57).

Protein glycosylation in insect cells has been best studied in organisms such as mosquitoes, fruit flies, and moths (58, 59). Ticks are another important arthropod vector of flaviviruses, but glycosylation pathways in tick cells have not been extensively described. The N-linked glycosylation pathway in insects begins like the mammalian pathway, with the synthesis and transfer of an oligosaccharide precursor, Dol-PP-$GlcNAc_2Man_9$, to an appropriate Asn on a newly synthesized polypeptide (59). Studies of

N-linked glycosylation in mosquito cells suggest carbohydrate structures are not further processed to generate complex carbohydrates, but instead remain high mannose or paucimannose (3-mannose-residue) oligosaccharides (60–62). Because flaviviruses typically cycle between vertebrate and arthropod hosts, distinct glycan structures added by these host cells contribute to different properties of the viruses initiating each round of infection, as arthropod-derived virions with simple sugars initiate infection in vertebrate hosts, and vertebrate-derived virions with complex sugars initiate infection in arthropod vectors. This is important because the structure of the carbohydrate can have an impact on its function, such as binding to cell surface attachment factors and initiating infection (63).

1.6 Envelope protein glycosylation and attachment

The first step in viral entry is virion binding to the cell surface. Cell surface molecules that facilitate virus binding and infection, but do not trigger fusion of viral and cellular membranes, are referred to as attachment factors (19). One family of attachment factors are lectins, proteins that bind carbohydrates, many in a calcium dependent manner (C-type lectins) (19, 64). Two extensively studied C-type lectins are dendritic cell-specific intercellular adhesion molecule-3-grabbing nonintegrin (DC-SIGN or CD209) and its paralog DC-SIGN-related protein (DC-SIGNR, L-SIGN, or CD209L). DC-SIGN is highly expressed in macrophages and dendritic cells (DCs), while DC-SIGNR is expressed on microvascular endothelial cells, especially in the liver sinusoids, lymph nodes, and placental villi (64). DC-SIGN and DC-SIGNR have been implicated in aiding the infection of numerous viruses such as human immunodeficiency virus (HIV), Ebola virus, Marburg virus, hepatitis C virus, human cytomegalovirus, Sindbis virus, and severe acute

respiratory syndrome coronavirus, as well as flaviviruses such as DENV and WNV (65–75).

Glycosylated E protein interacts with cell surface lectins, facilitating attachment and infectivity (32, 33, 35-46). WNV strains containing E glycosylation at position N154 use DC-SIGN as an attachment factor, leading to enhanced infection compared to non-glycosylated strains (67). DC-SIGNR has been shown to promote WNV infection much more efficiently than did DC-SIGN, particularly when the virus was grown in mammalian cells, and this was dependent upon E glycosylation at N154 (81). However, mutant WNV E proteins containing an N-linked glycosylation site at position N67 allowed WNV to interact with DC-SIGN (79). The DC-SIGN interactions were dependent on the incorporation of high mannose sugars at position N67, whereas DC-SIGNR recognized WNV bearing either complex or high mannose sugars (79). Likewise, JEV mutants containing glycosylation at position N67 showed enhanced DC-SIGN binding in HEK293T cells overexpressing DC-SIGN compared to viruses glycosylated at N154 (82). In contrast to the single glycan on most flavivirus E proteins, DENV is glycosylated at N67 and N153 (8, 47, 53). A Cryo-EM study demonstrated that the carbohydrate recognition domain of DC-SIGN binds preferentially to glycans present at N67 on DENV particles (77). Hacker et al. showed all four DENV serotypes had N-linked glycans added to both N67 and N153 of the E protein in both mammalian and mosquito cells, and viruses derived from both cell types were equally effective at infecting DC-SIGN expressing human monocytes and DCs (80). In DENV derived from mammalian cells, the N-linked glycans were a mix of high mannose sugars and complex sugars, while the N-linked glycans on mosquito-derived virus were a mix of high-mannose sugars and paucimannose sugars (80). Another study

revealed DENV lacking E glycosylation lost the ability to infect DC-SIGN and DC-SIGNR expressing cells (78). Altogether, these studies show that the location of the flavivirus E protein glycosylation motif, as well as the cell type the virus is propagated in, influence the final structure of the N-linked glycan, which in turn can influence virus binding to cell surface attachment factors and infectivity (Fig. 2). This is intriguing because E glycosylation also can impact the host antibody (Ab) response that is elicited to control the viral infection. A subset of highly potent, broadly neutralizing monoclonal Ab (MAb) to DENV (MAb 747(4)A11 and MAb 747(4)B7) were sensitive to glycosylation at N153 of DENV, showing lower activity against a naturally non-glycosylated DENV-4 strain compared to glycosylated strains (87). Conversely, studies of the arenavirus Lassa virus, showed envelope protein glycosylation acts as a shield, impairing the protective efficacy rather than the induction of neutralizing MAb, thereby preventing efficient antibody-mediated virus control (88). This is similar to one of the best characterized glycan shields found on the HIV Env protein, with 18-33 glycans per gp120 monomer (89). The extent of these post-translational modifications, combined with the intrinsic flexibility of the trimeric Env and constant evolution of the glycan shield, renders HIV Env an immunologically challenging target (90–93). These data highlight the importance of understanding the biology of viral envelope protein glycosylation for vaccine development efforts against these pathogenic viruses.

1.7 Envelope protein glycosylation and replication

E glycosylation plays a role in flavivirus attachment, however the roles of E glycosylation in flavivirus replication and assembly are less clear. Ablating N154 glycosylation on TBEV resulted in impaired secretion of virus-like particles (VLPs) (94) as

well as altered conformation of secreted E protein and a corresponding decrease in infectivity (95). This effect was observed for E protein secreted from mammalian cells, but not tick cells, suggesting cell type-dependent effects of E glycosylation. Similarly, removal of the N-linked glycosylation site in E significantly reduced the release of WNV subviral particles (SVPs) but these non-glycosylated SVPs were more infectious than glycosylated SVPs, particularly on mosquito cells (96). Studies with ZIKV have shown glycosylation at N154 of the E protein significantly influenced expression, production, and secretion of the ZIKV E protein ectodomain as well as virus production and infectivity with VLPs (97). The reduction of virion or particle release may be due to impaired trafficking along the ER-Golgi secretory pathway in the absence of appropriate E protein glycosylation. It also may be the consequence of incorrect E folding or interference with E dimerization, since glycosylation at N154 may stabilize the antiparallel E dimer conformation by keeping the fusion loop in place (18). However, ZIKV mutants lacking N154 glycosylation exhibit equivalent viral replication in mammalian and mosquito cells compared to glycosylated viruses (52, 98, 99). Nonetheless, these studies suggest flavivirus E glycosylation can influence viral particle assembly, secretion, and infectivity.

In addition to N154 glycosylation, DENV also contains a glycosylation site at N67 of the E protein. Mondotte et al. found that E glycosylation was not essential for DENV replication in insect cells, although ablating the glycosylation at N67 (N67Q), but not N153 (N153Q) resulted in a dramatic decrease of viral particle assembly or release in mammalian cells (83). Similarly, Bryant et al. observed that DENV E glycosylation at N67 was important for growth in mammalian cells (100). However, though non-glycosylated (N67Q) virus was able to replicate in mosquito cells, a compensatory mutation arose

(K64N) introducing a new glycosylation site, suggesting glycosylation at N67 (or nearby N64) is selected in mosquito cells. Interestingly, non-glycosylated mutants replicated similarly in inoculated *Aedes aegypti* mosquitoes, with no change in their glycosylation status (100).

In contrast, Lee et al. found that N67 glycosylation was dispensable for efficient DENV release from mammalian cells, depending on the amino acid substitution introduced to abolish glycosylation (53). Ablating the glycosylation motif with a substitution of the Thr at position 69 of the N67 N-X-S/T motif, with a larger and more hydrophobic residue such as Val or Leu, retained efficient growth, whereas the introduction of an Ala residue at the same site reduced virus growth by >100-fold relative to the wild-type virus (53). Additionally, the conservative substitution of Asn to Gln at position 67 was markedly less detrimental for viral growth than the nonconservative change of Asn to Asp. Furthermore, Lee et al. found that a compensatory mutation (N124S) at a non-adjacent region in the E protein partially rescued the growth defect of the T69A mutant, without generating a novel glycosylation site (53). Moreover, they found strain origin of the E protein influenced the impact of ablating the glycan on viral growth (53). Ablating the E glycosylation at N67 of the DENV2 16681 strain prevented growth in mammalian cells, but was well tolerated in a chimeric virus encoding the prM and E proteins from strain PUO-218 which differs from 16681 at 4 residues. A region in DII, between residues 120 and 126, appears to play a role in overcoming the attenuated growth associated with ablation of the N67 glycan (53). These observations highlight that it can be challenging to define whether the glycan per se mediates infection, as opposed to the specific amino acid residues that comprise the glycosylation signal. For example,

different amino acid substitutions at E154/156 of WNV conferred distinct avian host and vector competence phenotypes independent of E-protein glycosylation status (101). Thus, in addition to the specific effects of E glycosylation, the underlying amino acids at E residues 67 and 154 also may affect viral attachment and infectivity.

1.8 Envelope protein glycosylation and flavivirus transmission

Most flaviviruses are transmitted between hosts by arthropod vectors (mosquitoes or ticks), which acquire the virus during a blood meal (102). Vector-borne transmission requires the ingested virus to cross the midgut barrier and spread to the salivary glands to be transmitted to a new vertebrate host during a subsequent feeding (103, 104). Viruses must overcome multiple factors in the vector to be efficiently transmitted, including vector antiviral responses and tissue barriers (103, 104).

E protein glycosylation plays a role in flavivirus transmission via several mechanisms. Moudy et al. showed that non-glycosylated WNV replicated less efficiently than glycosylated WNV in *Culex* mosquitoes and was transmitted less efficiently (105). Interestingly, they found nearly all of the mosquitoes infected with non-glycosylated WNV transmitted a revertant virus, suggesting a strong selective pressure favoring glycosylated WNV in mosquitoes (105). E protein glycosylation could facilitate viral transmission across vector barriers by several mechanisms. Soluble carbohydrate-binding proteins could form a link between the virus and midgut surfaces or cell surface lectins could facilitate attachment to mosquito cells (106). In addition to facilitating transmission through attachment, the E glycan may also play a role in evading vector antiviral responses. Wen et al. found that ZIKV E N154 glycosylation promoted midgut invasion by inhibiting the reactive oxygen species (ROS) antiviral response (107). They further

showed that ablating E glycosylation (T156I), prevented mosquito infection via the oral route, whereas there was no effect on infection by intrathoracic injection, which bypasses the midgut.

Fontes-Grafias, et al. similarly showed that non-glycosylated ZIKV was very inefficient at infecting *Ae. aegypti* mosquitoes via a blood meal (99). However, in contrast to the ability of E glycosylation to facilitate attachment to mammalian cells, they showed that ZIKV with non-glycosylated E (N154Q), resulted in increased viral attachment, virion assembly, and infectivity of progeny virus in C6/36 mosquito cells compared to glycosylated virus (99). Another study showed ablating E glycosylation of DENV also increased virus entry but reduced virion release in C6/36 cells (53). These studies suggest the absence of E glycosylation is beneficial for infecting C6/36 cells in culture, but seems to be detrimental to the virus in mosquitoes. Thus, E protein glycosylation can aid flavivirus transmission by subverting tissue barriers and immunity-related pathways in arthropod vectors.

Though flaviviruses primarily are transmitted by arthropod vectors, vector-independent transmission has been documented in a variety of circumstances including TBEV in unpasteurized milk, JEV among pigs, and WNV, Bagaza virus, and Tembusu virus among birds (108–113). An S156P mutation that ablated E glycosylation in Tembusu virus resulted in impaired transmission among ducks, suggesting that E glycosylation could facilitate vector-independent as well as vector-borne transmission of flaviviruses (114).

1.9 Envelope protein glycosylation and pathogenesis

Since E glycosylation can play a role in flavivirus attachment, replication, and transmission, it is not surprising that it also contributes to pathogenesis for some flaviviruses. Several studies have suggested a role for E protein glycosylation as a molecular determinant of neurovirulence. The 1999 emergence of WNV in the United States was characterized by large-scale mortality in wild birds, a phenomenon that had not been observed in earlier WNV outbreaks, as well as many cases of encephalitis in humans (115). In studies comparing WNV strains from the 1999 outbreak to historical WNV strains, E glycosylation was associated with increased brain infection and lethality in mice (116). Beasley et al. confirmed these findings by generating infectious clones of glycosylated virulent (NY99), and non-glycosylated attenuated (ETH76a) WNV strains and measuring their lethality in mice (117). They swapped the prM-E sequences of ETH76a into the NY99 infectious clone, or mutated residue N154 to abolish glycosylation in NY99, both of which resulted in attenuation of the virus to a level comparable to wild-type ETH76a. Furthermore, a mutation that added the glycosylation to the ETH76a E protein on the NY99 backbone yielded a virus with virulence equivalent to wild-type NY99, indicating E protein glycosylation mediated the observed differences in virulence.

Other groups have generated chimeras of attenuated and highly virulent flaviviruses to analyze the role of viral E proteins in neuroinvasiveness (the ability of the virus to spread into the central nervous system from peripheral tissues) and neurovirulence (the ability of the virus to cause disease within the nervous system). Prow et al. generated a panel of Murray Valley encephalitis virus (MVEV) and Alfuy virus (ALFV) E protein mutants (118). MVEV causes encephalitis in humans, and isolates from

clinical material or mosquitoes are highly neuroinvasive in weanling mice (119, 120). In contrast, ALFV, a subtype of MVEV, has not been associated with human disease, and isolates are poorly neuroinvasive in weanling mice (121, 122). Their results showed that motifs within the E protein, including the absence of glycosylation and unique substitutions in the flexible hinge region, contribute to the reduced neuroinvasiveness of ALFV compared to MVEV (118).

However, multiple groups have generated chimeric viruses of neuroinvasive and non-neuroinvasive flaviviruses, and were unable to restore the neuroinvasive phenotype. A chimeric DENV4, containing the E glycoproteins of TBEV, was not neuroinvasive in adult BALB/c mice (123). Likewise, chimeric viruses consisting of the DENV4 backbone and the prM-E genes of Langat virus (LGTV) were not neuroinvasive (124). Chimeric WNV/DENV4 virus, in which the prM-E of WNV were put on the DENV4 backbone, lost the neuroinvasive properties of WNV (125), and replacing the prM-E of YFV, which is non-neuroinvasive, with prM-E of the neuroinvasive JEV, did not result in a virus that was neuroinvasive (126). These data suggest that prM and E of neuroinvasive flaviviruses are not sufficient to confer neuroinvasiveness to non-neuroinvasive flaviviruses.

To address the role of JEV E protein glycosylation in pathogenesis, especially the location and number of N-linked glycosylation on E proteins, Liang et al. generated three JEV mutants: one with glycosylation at N67, one with glycosylation at N67 plus N154, and one with no glycosylation on the E protein (N154A) (82). They found reduced viral growth in cell culture, as well as reduced neurovirulence and neuroinvasiveness in mice infected with the non-glycosylated or N67-only glycosylated virus compared to the wild-type JEV with glycosylation at only N154 (82). The virus with both N67 and N154 E

glycosylation exhibited efficient replication in culture and neurovirulence in mice, but reduced neuroinvasiveness compared to the wild-type virus (82). The authors proposed that neurotropic flaviviruses with a single E protein glycosylation at N154 might have an enhanced ability to cross the blood-brain barrier, though the mechanism by which this would occur is unclear. Notably, the non-neuroinvasive flaviviruses DENV and YFV have two or zero E glycosylation sites, respectively.

Several recent studies with ZIKV have investigated whether N154 glycosylation contributes to neuroinvasion. After the large ZIKV outbreak in 2015 in Latin America, and the unexpected clinical manifestations associated with the outbreak, including neurodevelopmental malformations (congenital Zika syndrome) and Guillain-Barré syndrome (2), many studies have sought to identify the causative determinants of new disease phenotypes. All contemporary ZIKV isolates encode an N-linked glycosylation site in the E protein at position N154 but this glycosylation site is absent in many historical ZIKV isolates (29, 127, 128). Non-glycosylated (N154A) ZIKV mutants generated on the prototype strain MR766 background were attenuated in *Ifnar1*$^{-/-}$ mice inoculated via a subcutaneous route, replicating to lower levels in serum and brain and causing less lethality compared to glycosylated virus (52, 98). Similarly, non-glycosylated (N154Q) mutants generated from Asian-lineage ZIKV strain FSS13025 also produced lower viral loads in the serum and brain compared to glycosylated virus, and were not virulent via a subcutaneous inoculation route (99).

Many of these studies identify a potential role for E glycosylation in flavivirus neurovirulence and pathogenesis. However, several studies conclude that the E glycosylation is a neuroinvasive determinant, implying that E glycosylation facilitates

trafficking across the blood-brain barrier. Studies with WNV and chimeric viruses made this conclusion based on the difference in lethality between peripheral inoculation routes (subcutaneous, intraperitoneal, or intravenous) and intracranial inoculations, observing that mice succumb to non-glycosylated viruses via intracranial but not peripheral routes. However, many of those studies did not measure viral loads in the serum of mice infected peripherally, and those that did found lower viral loads in mice infected with non-glycosylated viruses. Such findings are similar to the results of more recent studies with ZIKV, in which non-glycosylated viruses are attenuated in the periphery, which likely contributes to lower viral loads in the brains, regardless of any effect of E glycosylation on neuroinvasion. Thus, whether E glycosylation truly mediates neuroinvasion (and the mechanism by which it might do so) remains an open question.

1.10 Flavivirus strain variation and pathogenesis

Different strains of the same virus can have differential pathogenic outcomes in humans or animal models. For instance, WNV NY99 is lethal in mice, whereas WNV ETH76a and most WNV KUNV strains are not (117, 129). Similarly, MVEV is lethal in mice and pathogenic in humans, while ALFV, a subtype of MVEV, is attenuated (119–122). Different ZIKV strains also have varying degrees of virulence. ZIKV is grouped into two major phylogenetic lineages, African and Asian (29, 41). African lineage strains have been shown to be more virulent than some Asian strains and their pathogenicity is associated closely with the degree of inflammatory immune responses in mice (130). Interestingly, highly similar contemporary Asian strains, isolated during the recent outbreaks in the Western Hemisphere, have shown a wide range of pathogenic outcomes in different mouse models. ZIKV does not replicate efficiently in wild-type

C57BL/6 mice because ZIKV NS5 protein does not antagonize mouse STAT2 (131, 132). Thus, various immunodeficient mouse models are used to study ZIKV pathogenesis, and the two most commonly used systems (*Ifnar1*$^{-/-}$ mice and *Ifnar1*$^{-/-}$ *Ifngr1*$^{-/-}$ DKO mice) largely have been assumed to yield comparable results. *Ifnar1*$^{-/-}$ mice lack the type I interferon-αβ (IFN-αβ) receptor, while *Ifnar1*$^{-/-}$ *Ifngr1*$^{-/-}$ DKO mice lack both the type I IFN-αβ receptor, as well as the type II IFN-γ receptor. Type I IFNs are essential for activating the antiviral innate immune response and are well known for their ability to directly induce an antiviral response within infected and surrounding cells through the upregulation of molecules that can antagonize virus replication (133). Type II IFN signals through a different receptor and has effects that are independent from type I IFN. As a part of the innate immune response, they are predominantly produced by natural killer cells during infection. Type II IFNs promotes antiviral immunity through its regulatory effects on the innate immune response and acts as a key link between the innate immune response and activation of the adaptive immune response (133). A ZIKV strain isolated in 2013 from French Polynesia (H/PF/2013) and a strain isolated in 2015 from Brazil (Paraiba_01/2015) both have been shown to cause 100% and 80% lethality in *Ifnar1*$^{-/-}$ mice, respectively (134, 135). In contrast, a ZIKV strain isolated in 2010 from Cambodia (FSS13025) was only 20-30% lethal in *Stat2*$^{-/-}$ or *Ifnar1*$^{-/-}$ mice, and a strain isolated in 2015 from Puerto Rico (PRVABC59) was not lethal in either mouse model (136). However, the H/PF/2013, Paraiba_01/2015, FSS13025, and PRVABC59 strains were uniformly lethal in *Ifnar1*$^{-/-}$ *Ifngr1*$^{-/-}$ DKO mice (137–140). These data indicate ZIKV strain-specific contributions to virulence in mice, and highlight that differences in

pathogenesis may not be evident in highly susceptible models, such as *Ifnar1*$^{-/-}$ *Ifngr1*$^{-/-}$ DKO mice.

1.11 Flavivirus RNA determinants of replication and pathogenesis

The Flavivirus open reading frame (ORF) is flanked by a 5’ UTR of about 100 nucleotides (nt) and by a 3’ UTR of about 400 to 800 nt. The 3’ UTR contains large stem loop structures (SL). This secondary RNA structure is conserved among all flavivirus genomes and is essential for virus replication (141–143). A conserved sequence, located just 5’ of the 3’ terminal SL structure contains a highly conserved 8 nt sequence, called the 3’ cyclization sequence (3’ CYC). An exact complement of the 8 nt 3’ CYC sequence is located in the capsid coding region near the 5’ end of the genome. Genome cyclization due to the 3’–5’ long distance RNA–RNA interaction is required for the initiation of minus strand RNA synthesis but not for translation (141–143).

Other RNA structures in the 3’ UTR result in the generation of small RNAs that impact flavivirus replication via multiple mechanisms. A key characteristic common to all arthropod-borne flavivirus infections tested to date is the generation and accumulation of a small 300–500-base subgenomic flavivirus RNA (sfRNA) (144). Flavivirus sfRNAs are generated by stalling of the cellular 5′–3′-exoribonuclease, Xrn1 in mammalian hosts and its homolog Pacman in insects, on the 3’UTR structures as it attempts to degrade viral positive-sense transcripts inside infected cells. The functions of sfRNA have been implicated in the induction of pathogenicity in mice and cytopathicity in cell culture, evasion of type I and type II IFN responses, decreased mRNA turnover, enhanced virus replication in mammalian cells, and for the infection and subsequent transmission by the mosquito vector (145–152).

1.12 Conclusions

The *Flavivirus* genus contains numerous viruses that are capable of causing a wide array of pathologic phenotypes in humans and mouse models. Phylogenetic analyses have sought to identify viral determinants that correlate to pathogenesis. One highly studied flavivirus determinant of pathogenesis is the N-linked glycosylation site on the E protein. N-linked glycosylation is a common post-translational modification which has significant effects on protein conformation and function (42). It is a complex process that is highly host cell- specific (42). Not all flaviviruses possess an E glycosylation but for many flaviviruses E glycosylation impacts viral fitness, infectivity, replication, and virulence. The producing cell type, whether from arthropod versus vertebrate cells or specific cell types within a host, likely impacts the nature of the glycan added to flavivirus E proteins, but the ultimate effect of these distinct glycan structures on viral transmission, infection, and pathogenesis remains incompletely understood. It is unclear why DENV uniquely maintains two E glycosylation sites, or conversely how YFV maintains efficient transmission, infection, and virulence without E glycosylation. Understanding the impact of the viral E glycosylation on the host Ab response could improve the development of vaccines and diagnostics, particularly for DENV and ZIKV. Whether flavivirus E glycosylation is a bona fide neuroinvasive determinant or simply enhances viral replication in the periphery, resulting in higher infection levels in the brain, requires further investigation. It is also unclear why such highly similar ZIKV strains result in differential pathogenesis in different mouse models. Answers to these questions will further our knowledge of flavivirus replication and pathogenesis and potentially aid in combating these pathogenic viruses.

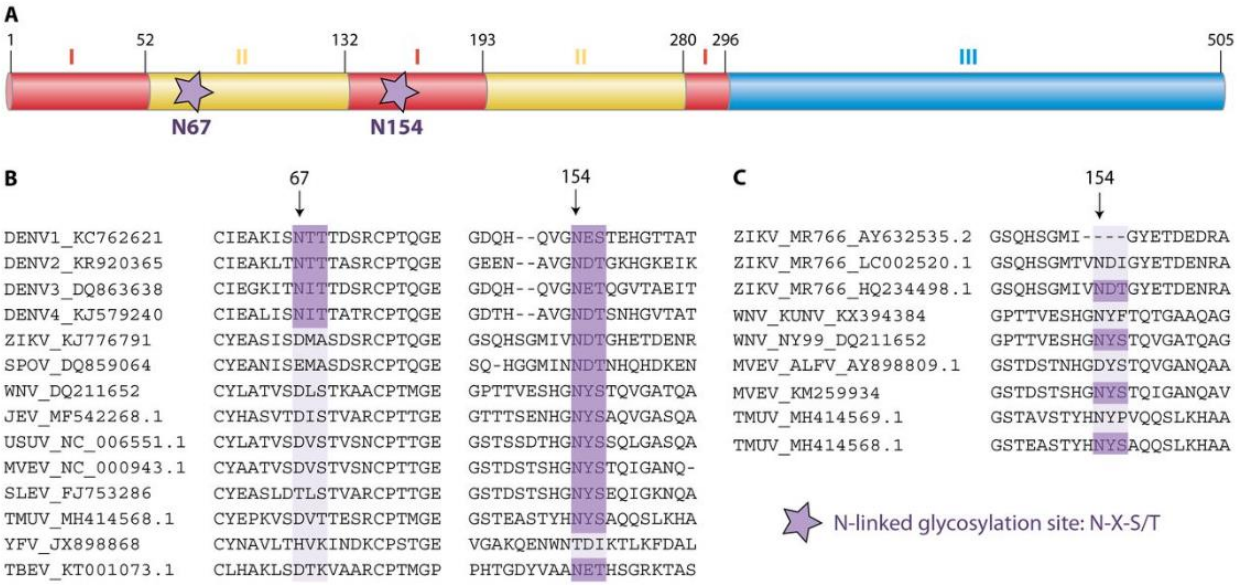

Figure 1.1. Flavivirus E protein glycosylation sites. (A) Domain organization of DENV E; stars indicate the glycosylation sites at asparagine (N) residues 67 and 154. Numbers indicate amino acid residues comprising E domain I (red); domain II (yellow), and domain III (blue). (B) Glycosylation at N154 is highly conserved among flaviviruses, whereas glycosylation at N67 is unique to DENV. Genebank accession numbers for each virus are indicated. (C) Glycosylation at N154 can differ among different strains of the same flavivirus.

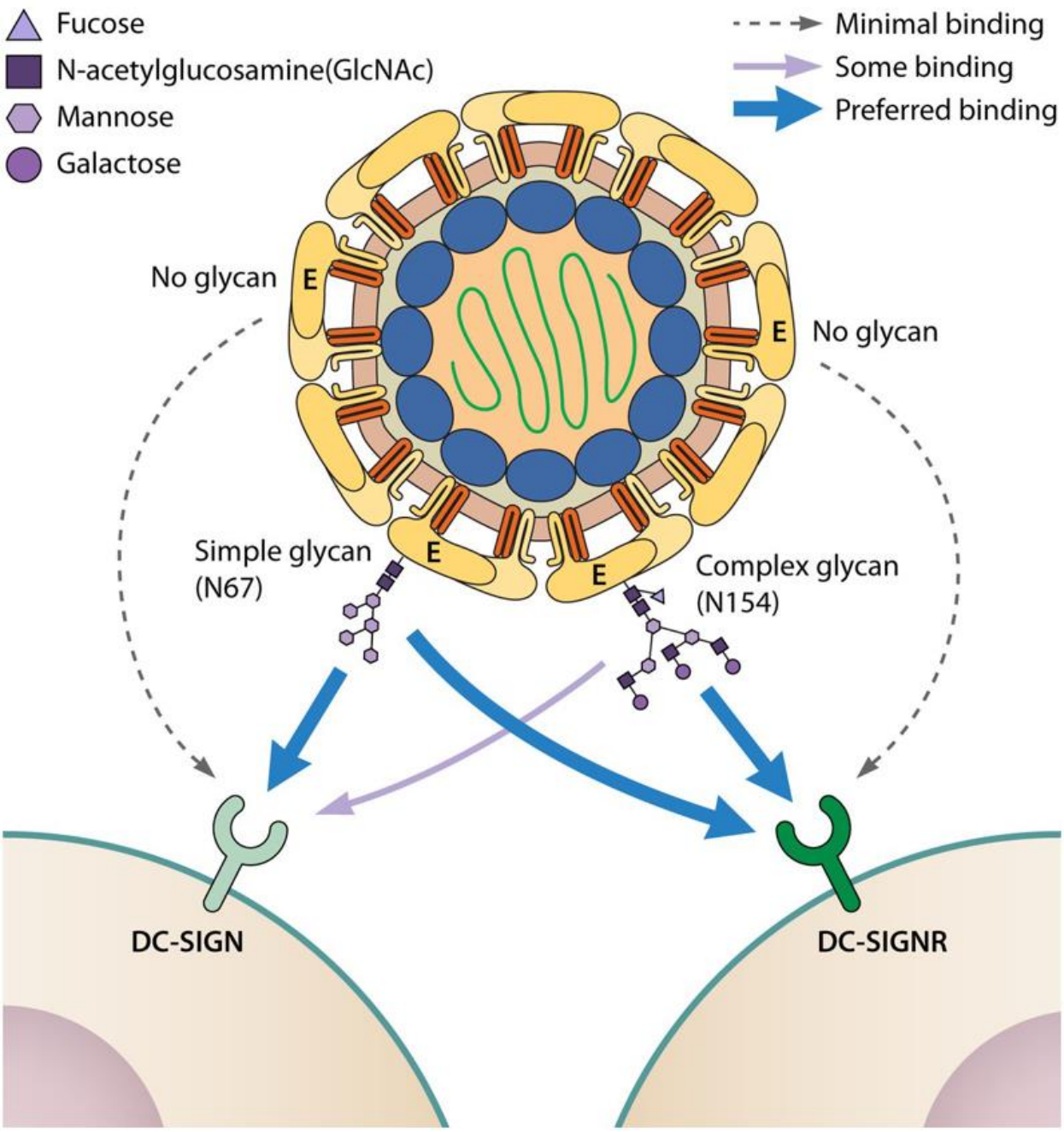

Figure 1.2. Glycan structure influences E binding to attachment factors. Flaviviruses with non-glycosylated E have minimal binding to the lectins DC-SIGN or DC-SIGNR, whereas glycosylation at N67 or N154 facilitate virus binding to cell-surface lectins. Simple (high mannose) glycans are preferentially added at N67 and facilitate binding to DC-SIGN or DC-SIGNR expressing cells. In contrast, complex glycans are preferentially added at N154 and favor binding to DC-SIGNR rather than DC-SIGN.

CHAPTER 2 – ENVELOPE PROTEIN GLYCOSYLATION MEDIATES ZIKA VIRUS PATHOGENSIS[1]

2.1 Summary

Zika virus (ZIKV) is an emerging mosquito-borne flavivirus. Recent ZIKV outbreaks have produced serious human disease, including neurodevelopmental malformations (congenital Zika syndrome) and Guillain-Barré syndrome. These outcomes were not associated with ZIKV infection prior to 2013, raising the possibility that viral genetic changes could contribute to new clinical manifestations. Nearly all contemporary ZIKV isolates encode an N-linked glycosylation site in the envelope (E) protein (N154) but this glycosylation site is absent in many historical ZIKV isolates. Here, we investigated the role of E protein glycosylation in ZIKV pathogenesis using two contemporary Asian-lineage strains (H/PF/2013 and PRVABC59) and the historical African-lineage strain (MR766). We found that glycosylated viruses were highly pathogenic in *Ifnar1*$^{-/-}$ mice. In contrast, non-glycosylated viruses were attenuated, producing lower viral loads in the serum and brain when inoculated subcutaneously, but replicating equally well in the brain when inoculated intracranially. These results suggest that E glycosylation is advantageous in the periphery but not within the brain.

_____

[1]Parts of this chapter were first published in *Journal of Virology*, May 2019, 93(12):e00113-19.

Accordingly, we found that glycosylation facilitated infection of cells expressing DC-SIGN and DC-SIGNR, suggesting that inefficient infection of lectin-expressing leukocytes could explain the attenuation of non-glycosylated ZIKV in mice. Additionally, we show that glycosylating the E protein at a different position (N67) does not functionally complement the loss of the glycan at position 154, but instead further attenuated the virus.

2.2 Importance

It is unclear why the ability of Zika virus (ZIKV) to cause serious disease, including Guillain-Barré syndrome and birth defects, was not recognized until recent outbreaks. One contributing factor could be genetic differences between contemporary ZIKV strains and historical ZIKV strains. All isolates from recent outbreaks encode a viral envelope protein that is glycosylated, whereas many historical ZIKV strains lack this glycosylation. We generated non-glycosylated ZIKV mutants from contemporary and historical strains and evaluated their virulence in mice. We found that non-glycosylated viruses were attenuated and produced lower viral loads in serum and brains. Our studies suggest envelope protein glycosylation contributes to ZIKV pathogenesis, possibly by facilitating attachment to and infection of lectin-expressing leukocytes.

2.3 Introduction

Zika virus (ZIKV) is an emerging flavivirus primarily transmitted by mosquitoes. Most ZIKV infections are asymptomatic, with approximately 20% resulting in self-limiting illness, including maculopapular rash, fever, and/or conjunctivitis (2, 153). Historically,

ZIKV was not associated with significant human disease. However, recent ZIKV outbreaks have featured new clinical manifestations. The 2013-2014 ZIKV outbreak in French Polynesia was associated with an increase in Guillain-Barré syndrome, an autoimmune neuropathy that can result in weakness, paralysis, and death (2, 34, 35). The subsequent detection of ZIKV in Brazil in 2015 and the rapid spread of ZIKV to many countries in the Americas (33, 36–38) has revealed that ZIKV infection during pregnancy can cause a broad range of congenital malformations termed congenital Zika syndrome (2, 39, 40).

ZIKV is grouped into two major phylogenetic lineages, African and Asian. All contemporary American strains belong to the Asian lineage, and genetic analyses support a model of a single introduction of ZIKV to Brazil from the South Pacific (37, 38, 127). It is unknown why severe disease manifestations such as congenital Zika syndrome were only revealed during the most recent ZIKV outbreak, but non-exclusive explanations include i) the ability of a large outbreak with good surveillance to reveal rare outcomes, ii) different host genetic or immune status in Latin America compared to regions where ZIKV circulated previously, and iii) genetic changes in ZIKV strains resulting in altered tropism and/or enhanced pathogenesis (154). Amino acid substitutions that may contribute to the increased rate of transmission and/or pathogenicity have been identified by comparative genomic and phylogenetic analyses (41, 155, 156). Differences in the non-structural protein 1 (NS1) and pre-membrane protein (prM) have been associated experimentally with enhanced transmission or virulence of American strains (127, 157–159). These analyses also have revealed a difference in the N-linked glycosylation motif (N-X-S/T) at amino acid 154 of the ZIKV

envelope (E) protein. Many African-lineage ZIKV isolates lack the glycosylation motif either due to a 4-6 amino acid deletion or a T156I substitution, whereas all Asian-lineage strains, including ones from recent outbreaks, contain an intact glycosylation signal (29, 128). This is significant because N-linked glycosylation on E is associated with enhanced mosquito transmission and/or increased virulence in vertebrates for other flaviviruses, including West Nile virus (WNV), Japanese encephalitis virus (JEV), tick-borne encephalitis virus, and others (82, 95, 105, 114, 116–118, 160–163).

In this study, we investigated the role of E glycosylation in ZIKV pathogenesis across Asian- and African-lineage ZIKV strains. We used site-directed mutagenesis to ablate the glycosylation motif with a single amino acid substitution (N154Q) in a previously described infectious clone of the Asian-lineage ZIKV strain H/PF/2013 (164). We generated a new infectious clone of another widely used Asian-lineage ZIKV strain, PRVABC59, and ablated the glycosylation motif with either an N154Q or a T156I substitution. Finally, we used our previously reported infectious clones derived from the prototype African-lineage ZIKV strain MR766 TVP 14270 with a 4 amino acid deletion ablating the glycosylation site, as well as mutants with a restored glycosylation signal or 4 amino acids restored with a T156I mutation ablating the glycosylation signal (164). We show that mutant viruses lacking E glycosylation are avirulent in *Ifnar1*$^{-/-}$ mice and are attenuated in overall replication *in vivo*. We also show that the lectins DC-SIGN and DC-SIGNR facilitate infection of glycosylated virus in cell culture. Additionally, we show that the addition of a glycan at position N67 did not functionally complement the loss of glycosylation at N154. Our results indicate N-linked glycosylation of the ZIKV E protein

at position N154 mediates infection and pathogenesis and suggest the glycan may enhance infectivity via cell surface lectins.

2.4 Results

N154Q mutation ablates E glycosylation.

To evaluate the role of E glycosylation in ZIKV infection, we used site-directed mutagenesis to introduce a single amino acid substitution (N154Q) that ablates the glycosylation motif (N-X-S/T) in a previously described infectious clone of ZIKV strain H/PF/2013 (Fig. 2.1A)(164). Consensus sequencing of virus released from electroporated Vero cells confirmed the two engineered nucleotide changes (Fig. 2.1B). We compared the growth of the H/PF/2013 isolate, wild-type (WT) clone, and N154Q mutant viruses in Vero cells and found equivalent replication kinetics (Fig. 2.1C). To verify the glycosylation status of the viral E protein, we immunoprecipitated lysates from infected Vero cells with monoclonal antibody (MAb) 1M7, a human MAb that binds the conserved fusion loop of E. We digested the immunoprecipitates with peptide N-glycosidase F (PNGase F) to remove all N-linked carbohydrates. When probed by western blot with MAb 4G2, E protein from H/PF/2013 isolate virus and WT infectious clones exhibited a smaller molecular weight after PNGase F treatment, indicating glycan cleavage (Fig. 2.1D). However, the size of the N154Q E protein was unaffected by PNGase F digestion, indicating that the mutant E protein was not glycosylated. Compared to ZIKV, DENV E protein exhibited a greater size shift upon PNGase F digestion, as expected because DENV E has two glycosylation sites (N67 and N153) (80). We further confirmed the glycosylation state of the viral E protein by lectin blot, using biotinylated-concanavalin A (ConA), a mannose/glucose binding lectin, to probe E

protein immunoprecipitated from infected Vero cells. Consistent with the results from PNGase F digestion, the H/PF/2013 isolate and WT clone E proteins were detected by ConA, whereas the N154Q E protein was not (Fig. 2.1E).

Ifnar1 heterozygous mice are not susceptible to ZIKV disease.

Since E glycosylation has been described as a neuroinvasion determinant of ZIKV and other flaviviruses (98, 117), we next evaluated the virulence of the N154Q mutant in mice. ZIKV does not replicate efficiently in wild-type C57BL/6 mice because ZIKV NS5 protein does not antagonize mouse STAT2 (131, 132). Thus, mouse models of ZIKV pathogenesis typically employ mice lacking IFN-αβ signaling, usually through genetic loss of the IFN-αβ receptor (*Ifnar1*$^{-/-}$) alone or in combination with the IFN-γ receptor, or by treatment of wild-type mice with IFNAR1-blocking MAb (MAR1-5A3) (136, 140, 165–169). Treatment with MAR1-5A3 results in increased ZIKV viremia (with higher MAb doses producing higher viremia) but does not elicit the weight loss and lethality observed in *Ifnar1*$^{-/-}$ mice (166), implying that partial loss of IFNAR1 activity may allow sufficient ZIKV replication to study pathogenic phenotypes. Thus, we sought to determine if mice with a single copy of *Ifnar1* were more susceptible to ZIKV infection than mice with two copies. We crossed *Ifnar1*$^{+/-}$ mice to generate mixed litters of *Ifnar1*$^{+/+}$, *Ifnar1*$^{+/-}$, and *Ifnar1*$^{-/-}$ mice, which we infected at 4 to 6 weeks of age with $1x10^3$ FFU of ZIKV H/PF/2013 isolate by a subcutaneous route in the footpad. Weight loss and lethality were measured for 14 days (Fig. 2.2 A and B). *Ifnar1*$^{+/+}$ and *Ifnar1*$^{+/-}$ mice did not lose weight and did not succumb to infection, whereas *Ifnar1*$^{-/-}$ mice began losing weight at 5 days post-infection (dpi) and all *Ifnar1*$^{-/-}$ mice succumbed to the virus by 7 dpi. To determine if *Ifnar1*$^{+/-}$ mice sustained increased viral replication compared to

Ifnar1$^{+/+}$ mice in the absence of overt disease (similar to MAR1-5A3-treated mice), we measured viral loads in the serum at 2, 4, and 6 dpi by qRT-PCR (Fig. 2.2 C). *Ifnar1*$^{+/-}$ mice had similar viral loads in the serum compared to *Ifnar1*$^{+/+}$ mice, whereas *Ifnar1*$^{-/-}$ mice had >100-fold higher viral loads in the serum compared to *Ifnar1*$^{+/+}$ and *Ifnar1*$^{+/-}$ mice. These results indicate that one copy of *Ifnar1* is sufficient to restrict ZIKV infection, so we used *Ifnar1*$^{-/-}$ mice for all subsequent pathogenesis experiments.

ZIKV E N154Q is attenuated upon subcutaneous but not intracranial inoculation.

To evaluate the role of E glycosylation in ZIKV pathogenesis we infected 5- to 6-week old *Ifnar1*$^{-/-}$ mice with 1x10^3 FFU of WT or N154Q virus by a subcutaneous route in the footpad and evaluated weight loss and lethality (Fig. 2.3A and B). Mice infected with WT clone virus began losing weight at 4 days post-infection (dpi) and all mice succumbed by 7 dpi, consistent with previous studies with the H/PF/2013 isolate virus (166). In contrast, mice infected with the N154Q virus lost weight from 5 to 7 dpi but recovered and all mice survived. Studies with ZIKV and other flaviviruses have identified a role for E glycosylation in neuroinvasion (98, 116, 117), so we tested whether the N154Q mutant regained virulence if the blood-brain barrier was bypassed. We infected WT and *Ifnar1*$^{-/-}$ mice with 1x10^3 FFU of WT or N154Q virus by intracranial inoculation and found that both viruses caused equivalent weight loss and lethality (Fig. 2.3C-E). Six of 7 *Ifnar1*$^{-/-}$ mice infected with the N154Q mutant died, while one mouse lost weight and recovered. WT mice lost weight from 4 to 6 dpi, but all mice recovered and all mice survived infection with both viruses. Overall, these results indicate that ZIKV N154Q remains neurovirulent, even though this virus was attenuated via a subcutaneous inoculation route.

ZIKV E N154Q has impaired replication in vivo.

Since the ZIKV N154Q virus was avirulent following subcutaneous inoculation, but lethal upon intracranial inoculation, we tested whether E glycosylation mediated neuroinvasion as well as invasion into other specialized tissue compartments, such as the eyes and testes, compared to peripheral tissues such as the serum and spleen. We infected 5-week-old *Ifnar1*$^{-/-}$ mice with 1x10^3 FFU of WT or N154Q virus via subcutaneous footpad inoculation and measured viral loads in the serum at 2, 4, and 6 dpi (Fig. 2.4.A) and viral loads in tissues 6 dpi by qRT-PCR (Fig. 2.4B-E). Compared to the WT virus, ZIKV N154Q produced lower viral loads in the serum at all time points, as well as reduced viral loads in the brain and eyes. In contrast, viral loads in the spleen and testes were not affected by E glycosylation. These results indicate that ZIKV H/PF/2013 N154Q, lacking the E glycosylation, is attenuated and produced lower viremia, which could contribute to lower viral loads detected in some tissues.

Low levels of ZIKV detected in the brains of N154Q-infected mice could result from delayed or inefficient neuroinvasion by the non-glycosylated virus. Alternatively, the attenuated mutant could revert in the periphery, producing WT virus that infects the brain. To distinguish these possibilities, we extracted RNA from brains 6 days after footpad inoculation with ZIKV N154Q and evaluated viral E sequences by Sanger sequencing. Based on sequencing chromatograms, 7 of 10 brains contained a mixture of WT and N154Q virus, 1 brain contained predominantly WT virus, and 2 brains contained predominantly N154Q virus. To determine whether the N154Q mutant was stable in the periphery, we performed Sanger sequencing on RNA extracted from serum 2 days after infection with ZIKV N154Q. We found that serum from 2 of 5 mice

sequenced contained a mixture of WT and N154Q virus while the N154Q mutation was maintained in 3 mice. We next sequenced virus from brains harvested 5 to 8 days after intracranial inoculation with ZIKV N154Q and found that the N154Q mutation was maintained in 6 of 6 mice. Altogether, these data suggest selection favoring glycosylated virus in peripheral tissues but not within the brain of ZIKV-infected *Ifnar1*$^{-/-}$ mice.

Asian and African lineage strains lacking the E glycosylation are attenuated.

ZIKV strain H/PF/2013 was isolated from an outbreak in French Polynesia in 2013, which preceded the emergence of ZIKV in the Americas and only retrospectively was associated with cases of congenital Zika syndrome (32, 170–172). Since other reports of a role for E glycosylation in mediating ZIKV virulence used an African-lineage strain or a Cambodian strain from 2010 (99), we sought to determine if glycosylation mediated similar effects on virulence and tissue invasiveness in a contemporary ZIKV strain from Latin America. We generated a new infectious clone of another widely used contemporary Asian lineage strain, PRVABC59 (Puerto Rico, 2015) (Fig. 2.5A) (173). Due to the high nucleotide identity between H/PF/2013 and PRVABC59 (>99%), we were able to use the same restriction endonuclease sites to partition the viral genome across four plasmids, as previously described (164). Following digestion, ligation*, in vitro* transcription, and electroporation into Vero cells, infectious virus was recovered. The virus was passed once on Vero cells and titered by focus-forming assay. The open reading frame of the WT infectious clone was sequenced, and we confirmed no new mutations were introduced compared to the reference genome sequence for this strain (accession number KU501215). We used site-directed mutagenesis to introduce a

single amino acid substitution (N154Q) to ablate the glycosylation motif (N-X-S/T). We also made a second mutant virus with the glycosylation motif ablated by a T156I mutation, as this variant has been detected in ZIKV strains isolated from mosquitoes in Africa in the 1970s and 1980s (29, 174). The region surrounding the introduced mutation was sequenced (Fig. 2.5B). All four viruses replicated equivalently in Vero cells (Fig. 2.5C). We performed PNGase F digestion (Fig. 2.5D) and lectin blotting (Fig. 2.5E) on immunoprecipitated E protein from Vero cells infected with PRVABC59 isolate, WT clone, N154Q mutant, and T156I mutant viruses to confirm the E glycosylation state. PNGaseF digestion produced a size shift for the PRVABC59 isolate and WT clone E proteins, but not the two mutants (Fig. 2.5D). Lectin blotting showed a band for the PRVABC59 isolate and the WT clone E proteins, but no band was detected for the two mutants lacking the E glycosylation (Fig. 2.5E). These results indicate that ZIKV PRVABC59 isolate and WT clone E protein are glycosylated and that this glycosylation is ablated by either N154Q or T156I mutations.

We next tested the virulence of the PRVABC59 viruses in *Ifnar1*$^{-/-}$ mice. We inoculated 5-to-6-week-old mice with 1x10^3 FFU of PRVABC59 isolate, WT clone, N154Q, or T156I viruses via subcutaneous footpad infection and measured viral loads in the serum at 2, 4, and 6 dpi (Fig. 2.6A) and tissues at 6 dpi by qRT-PCR (Fig. 2.6B-E). The WT clone produced viral loads similar to the isolate virus. However, both non-glycosylated mutants produced lower viral loads than WT viruses at all time points in the serum, as well as in the brain and eyes, indicating that, like strain H/PF/2013, ZIKV PRVABC59 infection is mediated by E protein glycosylation *in vivo*. Similar to strain H/PF/2013, glycosylation did not impact ZIKV PRVABC59 viral loads in the spleen or

testes. The observation that N154Q and T156I mutants produced very similar viral loads is consistent with a specific role for glycosylation in ZIKV infection, rather than an effect of the Asn residue itself. As for experiments with ZIKV H/PF/2013, we used Sanger sequencing to evaluate viral E sequences from brains harvested 6 days after footpad infection with ZIKV PRVABC59 N154Q or T156I. In contrast to the H/PF/2013 strain, we found that the mutations were maintained in all 11 brains evaluated (5 N154Q and 6 T156I). These results could indicate that E glycosylation provides a selective advantage for ZIKV H/PF/2013 but not PRVABC59. Alternatively, E glycosylation may be advantageous for both strains, but our stock of H/PF/2013 N154Q virus could contain revertants at a level below the sensitivity of our Sanger sequencing assay, allowing for more rapid selection and amplification *in vivo* compared to the PRVABC59 viruses.

H/PF/2013 and PRVABC59 are both Asian-lineage ZIKV strains, closely related to ZIKV strains circulating in the Americas (41, 175). However, the prototype ZIKV strain, MR766, is an African-lineage strain isolated from a sentinel rhesus macaque in 1947 and subsequently maintained by extensive passage in suckling mouse brains (~150 passages) (24). Likely due to this long history, several variants of MR766 have been used by different groups and non-identical sequences deposited in NCBI (50, 176). Among the many differences in reference sequences for ZIKV strains named "MR766" is the glycosylation signal at N154, with some sequences encoding an intact glycosylation signal (accession number HQ234498.1), some with a T > I point mutation that ablates the glycosylation signal (accession number LC002520.1), and others with a 4-6 amino acid deletion that ablates the glycosylation signal (accession numbers DQ859059.1, AY632535.2, and NC_012532.1). To determine whether different MR766

variants exhibited similar virulence *in vivo*, we compared two MR766 isolates obtained from the World Reference Center for Emerging Viruses and Arboviruses: TVP 14270 (SM 150, 2/7/2011) and M4946 (SM 146 10/14/1952). By Sanger sequencing, we determined that M4946 had an intact glycosylation signal at N154, whereas TVP 14270 had a 4 amino acid deletion ablating this signal. We infected 7- to 10-week old *Ifnar1*$^{-/-}$ mice with 1x10^3 FFU of MR766 isolate strains by subcutaneous footpad inoculation. Consistent with a role for E glycosylation in mediating ZIKV virulence, mice infected with M4946 (+gly) lost weight faster and exhibited 100% lethality by 9 dpi, whereas only 20% of mice infected with TVP14270 (-gly) succumbed (Fig. 2.7A and B). These results are consistent with our previous studies which used MR766 TVP14270 (-gly) (166). We previously reported an infectious clone derived from MR766 TVP 14270 (-gly), as well as mutants that restored the N154 glycosylation signal (+gly) or restored the 4 amino acid deletion but with the T156I mutation ablating the glycosylation signal (164). To compare the virulence of these isogenic mutants, we infected 5-week-old *Ifnar1*$^{-/-}$ mice with 1x10^3 FFU of MR766 +gly, -gly, and T156I clone viruses via subcutaneous footpad inoculation and measured viral loads in serum at 2 and 4 dpi (Fig. 2.7C), and in tissues at 4 dpi (Fig. 2.7C-F). Tissues were harvested at 4 dpi, rather than 6 dpi, because mice succumbed to the +gly virus by 5 dpi, consistent with reports of MR766 +gly being more pathogenic than Asian lineage strains (136) and MR766 -gly being less pathogenic than H/PF/2013 (166). Similar to ZIKV H/PF/2013 and PRVABC59, we observed lower viral loads at all time points in the serum, as well as in the brain, but not in the testes or spleen, with the -gly and T156I viruses, compared to mice infected with the +gly virus. In the eyes, we found significantly lower viral loads with the -gly virus, but not the T156I

virus, compared to the +gly infected mice. Altogether, our data indicate ZIKV lacking the E protein glycosylation, in both African and Asian lineage strains, are attenuated compared to viruses with E protein glycosylation.

Lectins DC-SIGN and DC-SIGNR mediate infection of glycosylated ZIKV.

All non-glycosylated ZIKV that we tested (6 viruses from strains H/PF/2013, PRVABC59, and MR766) replicated equivalently to their glycosylated counterparts in Vero cells but produced significantly lower viremia in *Ifnar1*$^{-/-}$ mice. One explanation for the *in vivo* attenuation of non-glycosylated viruses is lower infectivity due to an inability to bind to attachment factors. The lectins DC-SIGN (CD209) and DC-SIGNR (L-SIGN or CD209L) mediate attachment and entry of flaviviruses including DENV (83, 177, 178), WNV (67, 79, 81), and JEV (82, 84). DC-SIGN is highly expressed in macrophages and dendritic cells, while DC-SIGNR is expressed on microvascular endothelial cells, especially in the liver sinusoids, lymph nodes, and placental villi (64). To test whether ZIKV E glycosylation facilitates lectin-mediated attachment and infectivity, we used Raji cells and Raji cells expressing DC-SIGN (Raji-DC-SIGN) or DC-SIGNR (Raji-DC-SIGNR) and measured infection by flow cytometry. We confirmed that DC-SIGN and DC-SIGNR were expressed on the surface of the appropriate cell type, but not parental Raji cells (Fig. 2.8A). Cells were infected with ZIKV (strain PRVABC59) WT clone, N154Q mutant, T156I mutant, or UV inactivated WT clone virus at a multiplicity of infection (MOI) of 5 and intracellular E protein was measured 24 hours post-infection (hpi) by flow cytometry (Fig. 2.8B and C). No E protein signal was detected in cells infected with UV-inactivated virus, confirming that our assay measured viral infection and replication, not residual inoculum. In the absence of exogenous lectin expression,

Raji cells were not efficiently infected with ZIKV. However, WT ZIKV, with glycosylated E protein, infected Raji cells expressing exogenous DC-SIGN, and to a greater extent, DC-SIGNR. Infection by non-glycosylated ZIKV (N154Q or T156I) was not augmented by DC-SIGN expression. Unexpectedly, the N154Q mutant was able to infect DC-SIGNR expressing cells (albeit to a lower extent than WT virus), while DC-SIGNR did not augment infection by the T156I mutant. Altogether, these data suggest E glycosylation facilitates ZIKV infection of lectin-expressing leukocytes, which could contribute to lower viremia produced by non-glycosylated ZIKV *in vivo*.

We also used flow cytometry to measure infection of two epithelial cell lines commonly used in ZIKV studies, Vero and A549. Both of these cell lines lack DC-SIGN expression (data not shown), suggesting entry occurs via different attachment factors. Consistent with the equivalent replication we observed for non-glycosylated ZIKV in Vero cells (Fig. 2.1E and Fig. 2.5E), N154Q and T156I mutants exhibited similar infection efficiency in Vero cells (~75% compared to ~85% of the cell population for WT virus) (Fig. 2.9A and B). Compared to Vero cells, A549 cells were less permissive to all viruses, but infection was more dependent on E glycosylation (~5% infection with N154Q and T156I viruses compared to ~20% for WT) (Fig. 2.9C and D). The effect of E glycosylation on A549 cell infection also was evident in multi-step growth curves, which showed that PRVABC59 N154Q and T156I mutants were attenuated by 10 to 100-fold compared to the WT clone (Fig. 2.9E). Likewise, replication of the H/PF/2013 N154Q mutant was significantly attenuated in A549 cells compared to the WT clone (Fig. 2.9F). These data suggest the E glycosylation mediates ZIKV infection in A549 cells but is dispensable in Vero cells.

The number and location of ZIKV E glycosylation sites affect replication in cell culture.

We next tested whether the location of the glycosylation on E affected ZIKV replication. Since DENV has a second glycosylation site at position N67 of E in addition to N154, we choose this site to add a second glycan to ZIKV E. To evaluate whether E glycosylation at position 67 of ZIKV could functionally complement the loss of the glycosylation at position 154, we used site-directed mutagenesis to introduce a glycosylation motif (DMA > NTT; GAC ATG GCT > AAC ACG ACA) at position 67 of the E protein in ZIKV strain H/PF/2013 (generating mutant D67N) as well as on the N154Q background (D67N/N154Q) (Fig. 2.10A) (52). To verify the glycosylation status of the viral E proteins, we infected Vero and C6/36 cells with WT ZIKV or glycosylation mutants N154Q, D67/N154Q, or D67, or DENV. We immunoprecipitated cell lysates with MAb 1M7 and probed by western blot with MAb 4G2. The molecular weight of E for each virus was as expected, corresponding to the number of glycosylation sites present on each E protein (Fig 2.10B). Virus lacking glycosylation (N154Q) had the smallest E protein size. WT and D67N/N154Q E proteins (each with a single glycan), were ~2kD larger than N154Q, while D67N E protein (two glycans) was ~4kD larger than N154Q. ZIKV D67N E protein was similar in size to DENV, which naturally is glycosylated at both D67 and N153. Mammalian and mosquito cell derived viruses produced similar size patterns, indicating similar utilization of E protein glycosylation sites in both cell types. We further verified the glycosylation status of each viral E protein by lectin blot using ConA. WT ZIKV, D67N/N154Q, D67N, and DENV E proteins were detected by ConA, whereas the N154Q E protein was not (Fig. 3.1B). We next compared the growth

kinetics of the H/PF/2013 isolate, WT clone, N154Q mutant, D67N/N154Q mutant, and D67N mutant viruses in Vero, A549, and C6/36 cells (Fig. 2.10C-E). In Vero cells, the isolate, WT clone and N154Q mutant replicated equivalently, whereas D67N/N154Q and D67N were both attenuated by ~1000-fold at 24, 48 and 72 hpi. In A549 cells, the isolate and WT clone replicated equivalently, whereas the N154Q mutant was attenuated by about ~100-fold at all time points, and the D67N/N154Q and D67N mutants were further attenuated, by ~10,000 fold compared to the WT clone. In C6/36 cells, the isolate, WT clone, N154Q mutant, and D67N/N154Q mutant all replicated equivalently, while the D67N mutant was attenuated by ~10-100-fold at all time points. These data indicate having two glycans on ZIKV E severely attenuates the virus in all cell types tested, while having a single glycan at position N67 is attenuating in Vero and A549 cells, but tolerated in C6/36 cells, suggesting the number and position of the glycan on E effects ZIKV replication in a cell-type specific manner.

To further analyze the effect of the location of E glycosylation on ZIKV replication, we measured infection by flow cytometry of Vero, A549, Raji, Raji-DC-SIGN, and Raji-DC-SIGNR cells (Fig 2.11A-C). Cells were infected at a MOI of 1 with ZIKV H/PF/2013 WT, N154Q, D67N/N154Q, or D67N virus derived from C6/36 cells. Cells were stained at 24 hpi with Alexa Fluor 488-conjugated ZIKV MAb 4G2 to detect intracellular E protein. In Vero cells, WT virus infected ~60% of the cells, while N154Q infected ~75%, D67N/N154Q infected ~80%, and D67N infected ~90% of cells. In A549 cells, WT virus infected ~25% of the cells, while N154Q infected ~12%, and D67N/N154Q infected ~19% of the cells. Surprisingly, D67N had the highest infectivity in A549 cells of ~40%. The Vero and A549 flow cytometry data matches the replication

seen in our multistep growth curves, with the exception of the D67N virus in A549 cells, which replicated poorly at all time points compared to WT, but had the highest level of E positive cells at 24 hpi by flow cytometry. In the absence of exogenous lectin expression, Raji cells were not efficiently infected with ZIKV. However, WT ZIKV, with glycosylation at position N154 of E protein, infected Raji cells expressing exogenous DC-SIGN, and to a greater extent, DC-SIGNR. Infection by non-glycosylated N154Q was not augmented by DC-SIGN expression, but the N154Q mutant was able to infect DC-SIGNR expressing cells (albeit to a lower extent than WT virus), consistent with previous experiments using the PRVABC59 strain. The single glycosylated D67N/N154Q and the double glycosylated D67N viruses showed significantly higher levels of infected cells in both Raji-DC-SIGN and Raji-DC-SIGNR compared to WT virus.

E glycosylation at position N67 does not functionally complement the loss of glycosylation at position N154 for ZIKV replication in mice.

We next tested whether glycosylation at N67 of E can functionally complement the loss of glycosylation at position N154 in wild-type mice pre-treated with an IFNAR1-blocking MAb. We injected 5-to-6-week-old mice with 2mg of MAb MAR1-5A3 intraperitoneally and infected one day later with 1 x 10^3 FFU of H/PF/2013 WT clone, N154Q, D67N/N154Q, or D67N viruses via a subcutaneous route in the footpad and measured viral loads in the serum at 2 dpi by qRT-PCR (Fig 2.11A). Compared to the WT virus, ZIKV N154Q produced ~10-100-fold lower viral loads in the serum, while D67N/N154Q and D67N were further attenuated by an additional ~10-fold. These data indicate the addition of a glycosylation site at position N67 of E does not functionally

complement the loss at N154, and, in mice, attenuates the virus more than having no E glycosylation.

Altogether, our results demonstrate that it is not the case that ZIKV simply requires a glycan anywhere on E, but rather that glycosylation at position 154 of E is important for ZIKV infection in a cell type-specific manner, which may result from augmented infection of cells expressing certain cell-surface lectins.

2.5 Discussion

The emergence of ZIKV in the Western Hemisphere has been associated with new clinical manifestations including Guillain-Barre syndrome and congenital Zika syndrome (2). Phylogenetic analyses of ZIKV isolates from past and recent outbreaks have revealed amino acid differences between historic African-lineage strains and the contemporary Asian-lineage strains that are currently circulating in the Western Hemisphere (41, 155, 179). Several of these amino acid differences have been implicated in transmission, immune suppression, and enhanced disease. A single amino acid substitution (A188V) in NS1 has been shown to enhance ZIKV antigenemia in mice and infectivity of *Aedes aegypti* mosquitoes (157) and also inhibits IFN-β production *in vitro* (158). A single amino acid substitution in prM (S139N) has been shown to increase ZIKV replication in human neural progenitor cells and may contribute to a more severe microcephalic phenotype in mice (159), although others found that this mutation is not essential for fetal pathology in a mouse transplacental transmission model (180).

Nearly all contemporary Asian-lineage strains possess an intact E glycosylation motif at N154. However, in 2016, a non-glycosylated (4 AA Δ) Asian-lineage ZIKV strain

(AFMC-U; accession no. KY553111), was isolated from the urine of a male recruit in a Korean Army training center in the Republic of Korea (181). In contrast, many historic African-lineage ZIKV strains lack this motif (29, 174), though limited sampling of African ZIKV strains precludes robust conclusions about how common non-glycosylated viruses are in nature. E glycosylation plays a role in attachment and infectivity for DENV (83), WNV (67, 81, 96), and JEV (84) and has been associated with enhanced mosquito transmission and/or increased virulence and neuroinvasion in vertebrates for other flaviviruses (82, 95, 105, 107, 114, 116–118, 161, 162). We investigated the role of the ZIKV E glycosylation in tissue tropism and pathogenesis in an immunocompromised mouse model. Our results indicate that both Asian and African lineage ZIKV strains lacking E glycosylation sustained lower tissue viral loads compared to WT virus. These results are consistent with other reports of a role for E glycosylation in mediating ZIKV virulence. Annamalai et al. showed that ZIKV strain MR766 lacking E glycosylation due to a 4 amino acid deletion or a N154A substitution produced lower viral loads in serum and brains of A129 mice compared to glycosylated virus (98). Similarly, Fontes-Garfias et al. showed that a Cambodian ZIKV strain lacking E glycosylation due to a N154Q substitution also resulted in decreased viral loads in serum of A129 mice compared to the WT glycosylated virus (99). Notably, even though we found that ZIKV lacking E glycosylation resulted in lower viral loads in the serum, eyes, and brains compared to glycosylated virus, we observed similar viral loads in the spleen and testes, consistent with a previous report that glycosylated and non-glycosylated ZIKV strain MR766 sustained similar viral loads in the spleen and liver (98). Likewise, a non-glycosylated mutant of Tembusu virus produced equivalent viral loads in the spleens of infected

ducks, despite reduced viral loads in other tissues (114). Furthermore, our observation that the ZIKV H/PF/2013 N154Q mutation was maintained upon intracranial inoculation, but selected against after subcutaneous inoculation, suggests that glycosylation provides a selective advantage to ZIKV in peripheral tissues but not within the brain. Altogether, these observations suggest E glycosylation facilitates infection of ZIKV, and perhaps other flaviviruses, in a tissue or cell type-specific manner.

E glycosylation likely facilitates attachment to and infection of lectin-expressing cells, including CD14+ monocytes cells that are targets of ZIKV in humans (182–185). DC-SIGN and DC-SIGNR are among several attachment factors described for flaviviruses such as DENV (83, 177, 186), JEV (82, 84), and WNV (67, 81, 96) as well as for ZIKV (85, 187, 188), though it is less clear which lectins or other attachment factors actually mediate ZIKV infection in mice or humans (189–191). Though mice do not have clear DC-SIGN or DC-SIGNR orthologs, they have eight DC-SIGN homologs clustered within the same genomic region (182). According to their glycan specificity, murine SIGNR1 and SIGNR3 are the closest candidates to fulfill DC-SIGN function in mice, but their ability to facilitate flavivirus infection is unclear. Unexpectedly, we found DC-SIGNR was able to augment infection by the N154Q mutant, even in the absence of E glycosylation, which was unlike the T156I mutant. The different infection efficiencies of the two non-glycosylated mutants on Raji DC-SIGNR cells could result from less efficient maturation of N154Q virions compared to T156I virions; in this case, glycosylated prM on immature N154Q virions may partially complement the loss of E glycosylation (188). Cleavage of prM is required to produce mature infectious virions, because interactions between prM and E prevent the conformational changes required

to drive pH-dependent membrane fusion, but partially mature virions also can be infectious (20). The cleaved portion of prM is glycosylated and uncleaved prM on partially mature virions can facilitate attachment and entry in a DC-SIGNR-dependent manner (81, 188). Alternatively, the difference in infection efficiencies in DC-SIGNR cells could indicate a specific role for Gln 154 or Thr 156 independent of glycosylation, perhaps through modulation of the glycan loop and resulting effects on attachment and fusion (188, 191). For example, different amino acid substitutions at E154/156 of WNV conferred distinct avian host and vector competence phenotypes independent of E-protein glycosylation status (101).

The location and number of glycosylation sites on E have been shown to impact attachment and infection for WNV and JEV (79, 82). We show that the addition of a glycan at position N67 of ZIKV E impacts attachment, infectivity, and replication in lectin-expressing leukocytes and A549 cells, but had minimal impact in Vero cells. The addition of a glycan at position N67 was unable to functionally complement the loss of the glycan at position N154. Distinct glycosylation profiles also could have an impact on the host Ab response. This is significant because ZIKV is circulating in DENV endemic regions, and the similarity between the two flavivirus could impact cross-reactive Ab responses. Overall, our findings demonstrate a role for E glycosylation, specifically at position N154, in ZIKV pathogenesis, possibly by facilitating attachment and infection of lectin-expressing leukocytes.

2.6 Materials and methods

Cells and viruses. Vero and A549 cells were maintained in Dulbecco's modified Eagle medium (DMEM) containing 10% heat-inactivated fetal bovine serum (FBS) and

L-glutamine at 37°C with 5% CO_2. Raji, Raji-DC-SIGN, and Raji-DC-SIGNR cells were obtained from Dr. Ted Pierson (NIH). Raji cells were maintained in RPMI 1640 media supplemented with 10% FBS and penicillin/streptomycin. ZIKV strains H/PF/2013 and PRVABC59 were provided by the U.S. Centers for Disease Control and Prevention (172, 173). The ZIKV MR766 strains were obtained from the World Reference Center for Emerging Viruses and Arboviruses (24, 50, 176). DENV-3 WHO Reference strain (CH54389) was obtained from Dr. Aravinda de Silva (UNC) (192). Virus stocks were grown in Vero (African green monkey kidney epithelial) cells. Virus stocks were titered on Vero cells by focus-forming assay (FFA) (193). For multi-step growth analysis, cells were infected at a MOI of 0.01 and incubated at 37°C with 5% CO_2. Samples of infected cell culture supernatant were collected at 4, 24, 48 and 72 hpi and stored at -80°C for virus titration. Virus quantification was performed by FFA on Vero cells. Duplicates of serial 10-fold dilutions of virus in viral growth medium (DMEM containing 2% FBS and 20 mM HEPES) were applied to Vero cells in 96-well plates and incubated at 37°C with 5% CO_2 for 1 hr. Cells were then overlaid with 1% methylcellulose in minimum essential medium Eagle (MEM). Infected cell foci were detected 42-46 hpi. Following fixation with 2% paraformaldehyde for 1 hr at room temperate, plates were incubated with 500 ng/ml of flavivirus cross-reactive mouse MAb E60 (194) for 2 hr at room temperature or overnight at 4°C. After incubation at room temperate for 2 hr with a 1:5,000 dilution of horseradish peroxidase (HRP)-conjugated goat anti-mouse IgG (Sigma), foci were detected by addition of TrueBlue substrate (KPL). Foci were quantified with a CTL Immunospot instrument. To prepare UV-inactivated virus**,** 20ml of PRVABC59 WT clone virusat 1 $x10^5$ FFU/mL was placed in a petri dish and exposed to UV light at 0.9 J/cm^2

for 10 minutes in a HL-2000 HybriLinker (UVP Lab Products); inactivation was confirmed by FFA.

ZIKV infectious clone design and mutagenesis. We used a quadripartite unidirectional molecular clone strategy as previously described (164), to generate a new infectious clone of ZIKV strain PRVABC59. Due to the high sequence similarity between H/PF/2013 and PRVABC59 we were able to use the same naturally occurring class IIG nonpalindromic restriction endonuclease sites within the full-length genome as previously described for ZIKV strain H/PF/2013 (164). NotI and EcoRV restriction endonuclease sites followed by a T7 promoter sequence, for *in vitro* transcription, were added to the immediate 5' end of the genome. A hepatitis delta virus (HDV) ribozyme sequence, to generate an intact 3' UTR, followed by a SmaI restriction endonuclease site were added directly after the last nucleotide of the genome. The four subgenomic fragments were synthesized into the pUC-57 vector (BioBasic) and amplified in One Shot TOP10 Chemically Competent *E. Coli.* cells (Thermo) grown on LB plates with carbenicillin at 37^{o}C for ~16 hrs. Individual colonies were picked, grown to high concentrations in selective LB, purified (Qiagen Mini-spin kit), and sequenced. The resulting purified plasmids were digested, ligated, *in vitro* transcribed, and electroporated into Vero cells as previously described (195). Supernatants from electroporated Vero or C6/36 cells were harvested after 6 to 7 days and passaged once on Vero cells or C6/36 cells to generate virus stocks. Virus stocks were titered by FFA on Vero cells. Site-directed mutagenesis was used to introduce a single amino acid substitution (N154Q, T156I, or D67N) in the envelope protein to ablate the glycosylation motif. Restriction enzymes and Phusion High Fidelity PCR kit were obtained from New England BioLabs. SuperScript III First Strand

Synthesis kit was obtained from Invitrogen. Oligonucleotide primers and probes for DNA amplification, qRT-PCR, and sequencing were obtained from Sigma and IDT. The mMachine T7 Ultra transcription kit was obtained from Ambion.

Glycosylation assays. Anti-flavivirus MAbs E60, 1M7, and 4G2 were produced by the UNC Protein Expression and Purification Core Facility (194, 196, 197). E protein was immunoprecipitated from infected Vero cell lysates using MAb 1M7 (1µg) and magnetic protein A/G beads (Pierce). Immunoprecipitated E protein was digested with peptide N- glycosidase F (PNGaseF; New England BioLabs) according to the manufacturer's protocol with a minor modification. Instead of denaturation in the provided glycoprotein denaturation buffer containing dithiothreitol, immunoprecipitates were denatured in 0.5% SDS, because the epitope recognized by MAb 4G2 is sensitive to reducing state (198). PNGaseF digestions were separated by SDS-PAGE (7.5% precast polyacrylamide gels, BioRad) under non-reducing conditions and analyzed by western or lectin blot. Proteins were transferred to a nitrocellulose membrane using a Trans-Blot Turbo Transfer System (BioRad). In western blots, E protein was detected using MAb 4G2 as a primary antibody and HRP-conjugated goat anti-mouse IgG as a secondary antibody. For lectin blots, glycosylated E was detected with the biotinylated lectin concanavalin A (ConA) (Vector Laboratories), followed by HRP-conjugated streptavidin. Pierce ECL western blotting substrate was used to detect HRP (Thermo). Western and lectin blots were imaged on a ChemiDoc XRS+ system (BioRad).

Mouse experiments. Animal husbandry and experiments were performed under the approval of the University of North Carolina at Chapel Hill Institutional Animal Care and Use Committee. Five - to six-week old or 8- to10-week-old male and female wild-

type or *Ifnar1*$^{-/-}$ mice on a C57BL/6 background were used. MAR1-5A3 (134, 199) was administered intraperitoneally in a volume of 300µl. Mice were inoculated with 1x10^3 FFU of ZIKV in a volume of 50µl subcutaneously (footpad) or 25µl intracranially. Survival and weight loss were monitored for 14 or 21 days. Animals that lost >30% of their starting weight or that became moribund were euthanized.

Measurement of viral loads. ZIKV-infected mice were sacrificed at 4 or 6 dpi and perfused with 20 ml of PBS. Spleen, kidney, testes, brain, and eyes were harvested and homogenized with zirconia beads (BioSpec) in a MagNA Lyser instrument (Roche Life Science) in 500µl (eyes) or 1ml (all other tissues) of buffer RLT (Qiagen). Blood was collected at 2 and 4 dpi by submandibular bleeds with a 5mm Goldenrod lancet and by cardiac puncture at 6 dpi. Blood was collected in serum separator tubes (BD) and serum was separated by centrifugation at 8000rpm for 5 min. Tissues and serum from infected animals were stored at -80ºC until RNA isolation. RNA was extracted with the RNeasy Mini Kit (tissues) or Viral RNA Mini Kit (serum) (Qiagen). ZIKV RNA levels were determined by TaqMan one-step quantitative reverse transcription PCR (qRT-PCR) on a CFX96 Touch Real-Time PCR Detection System (BioRad) using standard cycling conditions. Viral burden is expressed on a Log_{10} scale as either viral RNA equivalents per ml after comparison with a standard curve produced using serial 10-fold dilutions of RNA extracted from a ZIKV stock or genome copies per ml after comparison with a standard curve produced using serial 100-fold dilutions of ZIKV A plasmid. A previously published primer set was used to detect ZIKV H/PF/2013 and PRVABC59 RNA: forward, CCGCTGCCCAACACAAG; reverse, CCACTAACGTTCTTTTGCAGACAT; probe, /56-FAM/AGCCTACCT/ZEN/TGA CAAGCAATCAGACACTCAA/3IABkFQ/

(Integrated DNA Technologies) (200). ZIKV MR766 RNA was detected using the following primers: forward, GGGCGTGTCATATTCCTTGT; reverse, TCCATCTGTCCCTGCATACT; probe, /56-FAM/AGCCTACCT/ZEN/TGACAAGCAATCAGACACTCAA/3IABkFQ/ (Integrated DNA Technologies).

Flow cytometry. Cells ($2x10^4$) were infected with ZIKV at a MOI of 5 for 1hr at 37°C in RPMI 1640 or DMEM supplemented with 2% FBS. The cells subsequently were washed with FACS buffer (PBS + 1% FBS) to remove excess virus and incubated at 37°C for 24 hrs. Following incubation, cells were washed with FACS buffer and fixed by adding 100ul 1% PFA and incubating at 4°C for 10 min. Cells were subsequently washed and permeabilized with permeabilization buffer (BSA + saponin). The permeabilized cells were stained for ZIKV E protein using monoclonal antibody 4G2 conjugated to Alexa Fluor-488, diluted 1:200, for 30 min at 4°C. For extracellular staining, cell surface DC-SIGN and DC-SIGNR were stained using monoclonal antibody clone 9E9A8 for DC-SIGN (BioLegend) and MAB162 for DC-SIGNR (R&D Systems) at 4°C for 30 min. After washing with FACS buffer, cells were fixed and permeabilized as above. The permeabilized cells were stained with secondary anti-IgG-PerCP, diluted 1:100. The stained cells were subsequently washed and analyzed by flow cytometry using a Guava EasyCyte HT flow cytometer (Millipore).

Data analysis. All data were analyzed with GraphPad Prism software. Flow cytometry data were analyzed with FlowJo V10 software. Kaplan-Meier survival curves were analyzed by the log rank test, and weight losses were compared using two-way

ANOVA. For viral burden analysis, the log-transformed titers were analyzed by the Mann-Whitney test. A p value of < 0.05 indicated statistically significant differences.

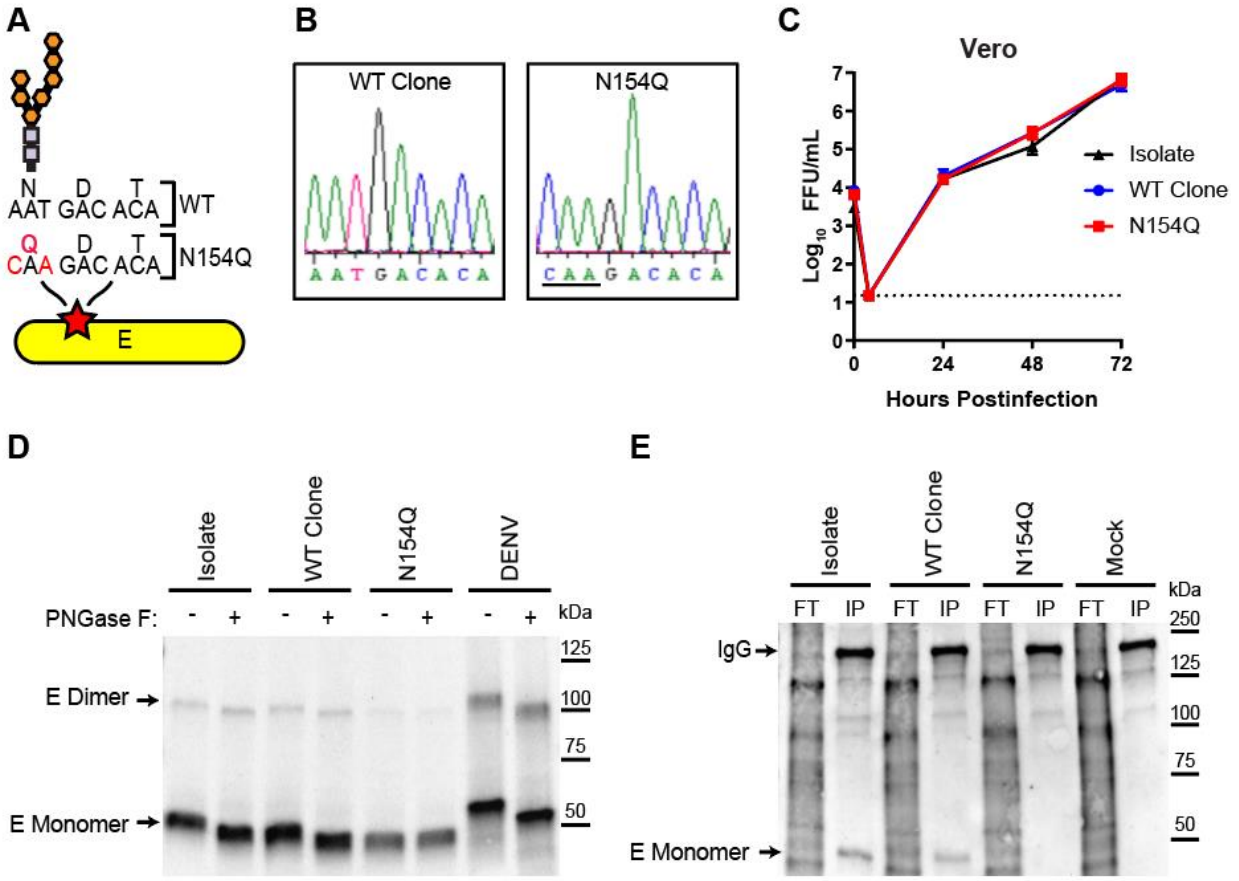

Figure 2.1. E glycosylation is not required for ZIKV replication. **A**. ZIKV envelope protein, depicting the nucleotide and amino acid residues of the glycosylation site, and N154Q mutation. **B**. Sequence chromatograms of E protein glycosylation site of wild-type (WT) and N154Q viruses. **C**. Vero cells were infected at a MOI of 0.01 with ZIKV H/PF/2013 isolate, WT clone, or N154Q mutant. Virus in culture supernatant was titered by focus-forming assay. Data shown are the means ± SEM of 9 samples from 3 independent experiments. **D** and **E**. E proteins were immunoprecipitated with MAb 1M7 from lysates of Vero cells infected with ZIKV H/PF/2013 isolate, WT clone, N154Q mutant, or DENV. **D**. Lysates were treated with PNGase F, separated by non-reducing SDS-PAGE, and probed with MAb 4G2. **E**. Lysates were separated by non-reducing SDS-PAGE and probed with biotinylated concanavolin A to detect glycans.

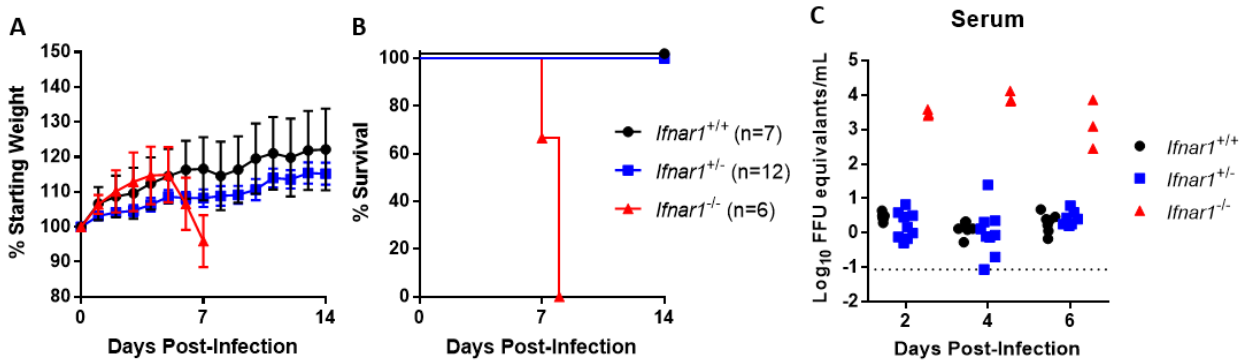

Figure 2.2. **One copy of *Ifnar1* is sufficient to protect mice against ZIKV disease**. *Ifnar1* heterozygous mice were crossed to generate mixed litters of wild-type (*Ifnar1*$^{+/+}$), heterozygous (*Ifnar1*$^{+/-}$), and homozygous knockout mice (*Ifnar1*$^{-/-}$). Four- to six-week-old mice were inoculated with 1x10^{3} FFU of ZIKV strain H/PF/2013 isolate by a subcutaneous route in the footpad. **A**. Mice were weighed daily and weights are expressed as percentage of body weight prior to infection. Results shown are the mean ± SEM of the indicated number of mice per group. Weights were censored once one mouse in the group died. **B**. Lethality was monitored for 14 days. **C**. Blood was collected at 2, 4, and 6 days after infection by submandibular bleed and ZIKV RNA in serum was measured by qRT-PCR. Mice per group were combined from 3 (A and B) and 2 independent experiments (C).

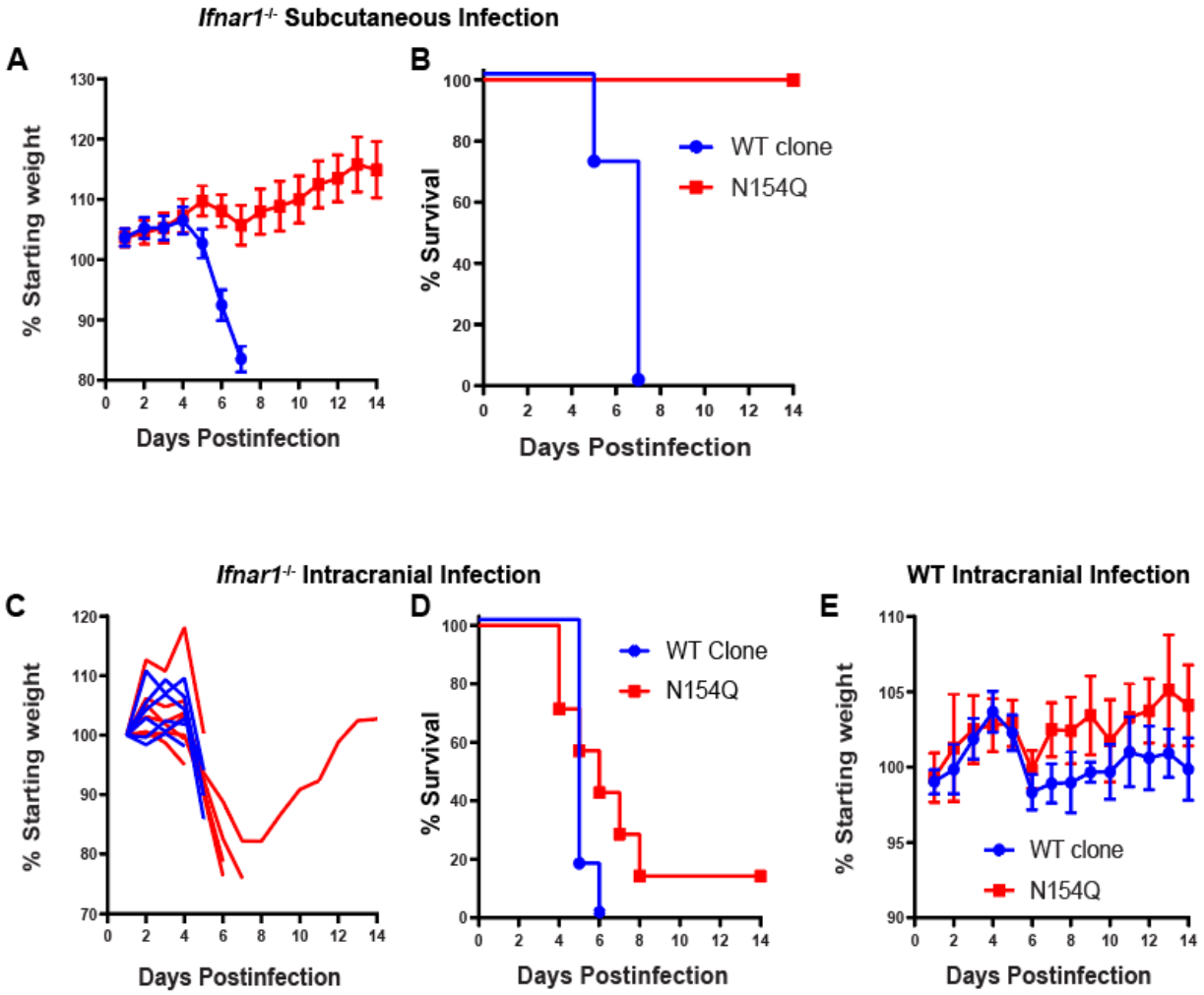

Figure 2.3. ZIKV E N154Q is attenuated upon subcutaneous but not intracranial inoculation. Five- to six –week old *Ifnar1*$^{-/-}$ or wild-type (WT) mice were inoculated with 1x10^{3} FFU of ZIKV strain H/PF/2013 WT clone or N154Q mutant by a subcutaneous (**A** and **B**) or intracranial (**C-E**) route. Mice were weighed daily and weights are expressed as percentage of body weight prior to infection. Results shown are the mean ± SEM of 6-8 *Ifnar1*$^{-/-}$ mice or 3 WT mice per virus from two or three independent experiments. Lethality was monitored for 14 days.

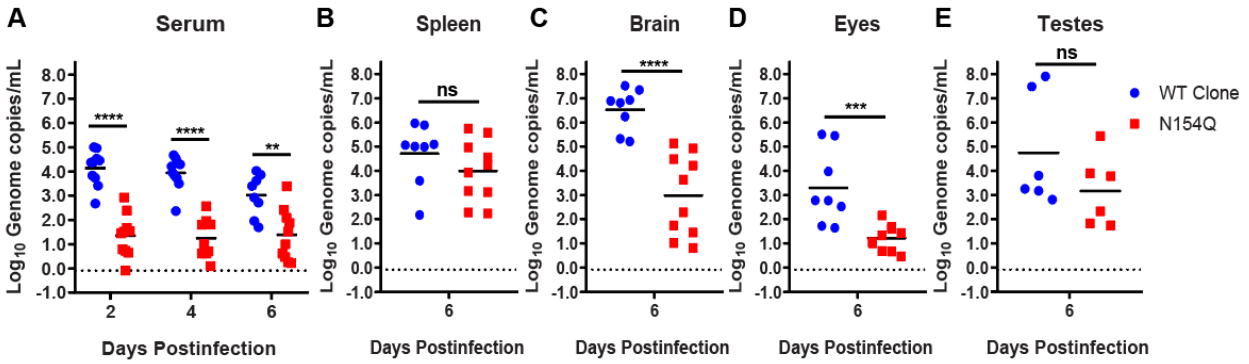

Figure 2.4. N154 glycosylation mediates ZIKV infection in mice. Five- to six –week old *Ifnar1*$^{-/-}$ mice were inoculated with 1x10^{3} FFU of ZIKV strain H/PF/2013 WT clone or N154Q mutant by a subcutaneous route in the footpad. **A**. Blood was collected at 2, 4, and 6 days after infection and ZIKV RNA in serum was measured by qRT-PCR. **B-E**. Mice were euthanized 6 days after infection, perfused, and tissues were harvested. ZIKV RNA in tissue was measured by qRT-PCR. **, P < 0.01; ***, P < 0.001; ****, P < 0.0001; ns, not significant (unpaired 2-tailed t test).

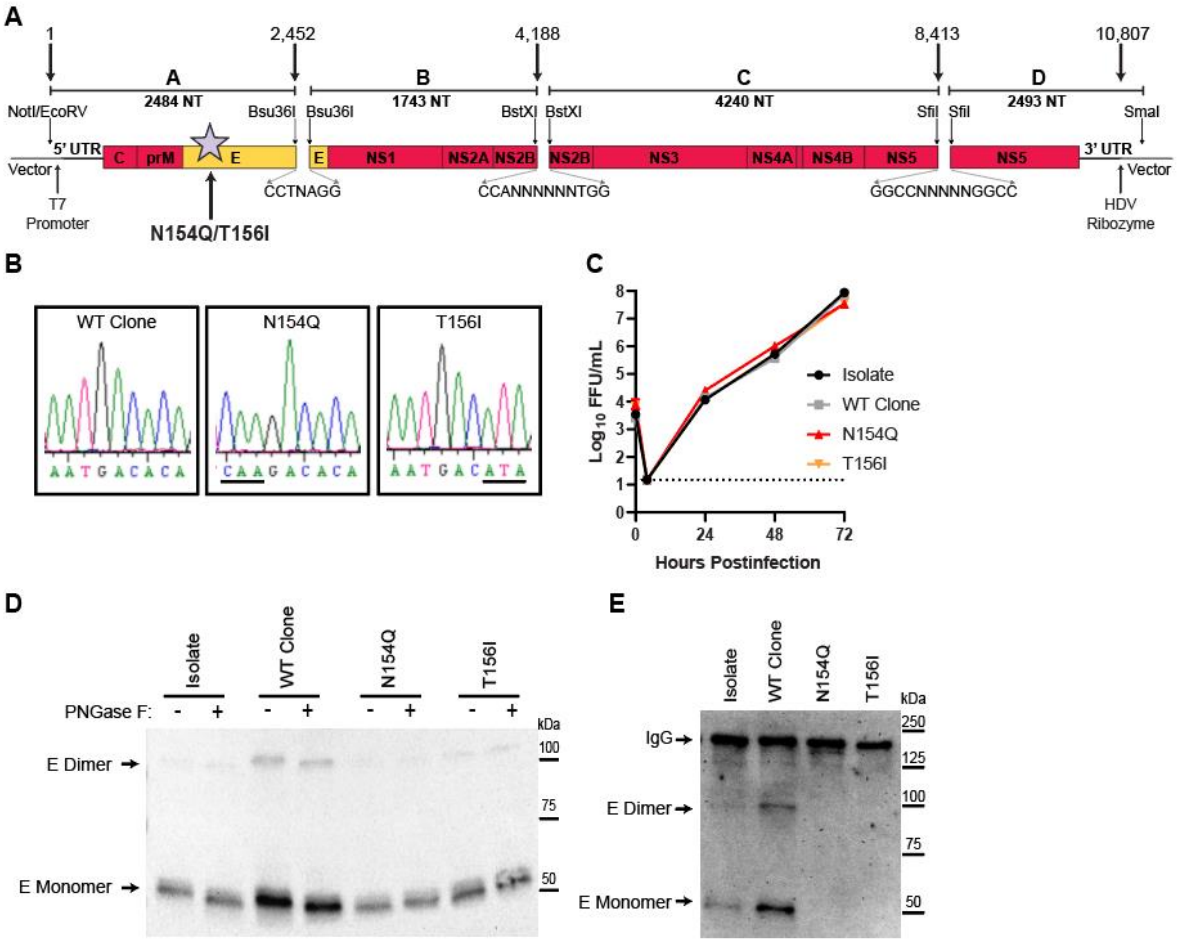

Figure 2.5. Generating an infectious clone of ZIKV PRVABC59 and non-glycosylated mutants. **A**. An infectious clone of ZIKV strain PRVABC59 was generated using a system that divides the viral genome into 4 fragments flanked by the indicated restriction endonucleases sites. Numbers above fragments indicate nucleotide position in the viral genome. T7 promoter and a hepatitis delta virus (HDV) ribozyme sequences flank the genome. **B**. Sequence chromatograms of E protein glycosylation site of WT, N154Q, or T156I clones. **C.** Vero cells were infected at a MOI of 0.01 with ZIKV PRVABC59 isolate, WT clone, N154Q mutant, or T156I mutant. Virus in culture supernatant was titrated by focus-forming assay. Data shown are the mean ± SEM of 9 samples from 3 independent experiments. **D** and **E**. E proteins were immunoprecipitated with MAb 1M7 from lysates of Vero cells infected with ZIKV PRVABC59 isolate, WT clone, N154Q mutant, and T156I mutant. **D.** Lysates were treated with PNGase F, separated by non-reducing SDS-PAGE, and probed with MAb 4G2. **E.** Lysates were separated by non-reducing SDS-PAGE, and probed with biotinylated lectin concanavalin A.

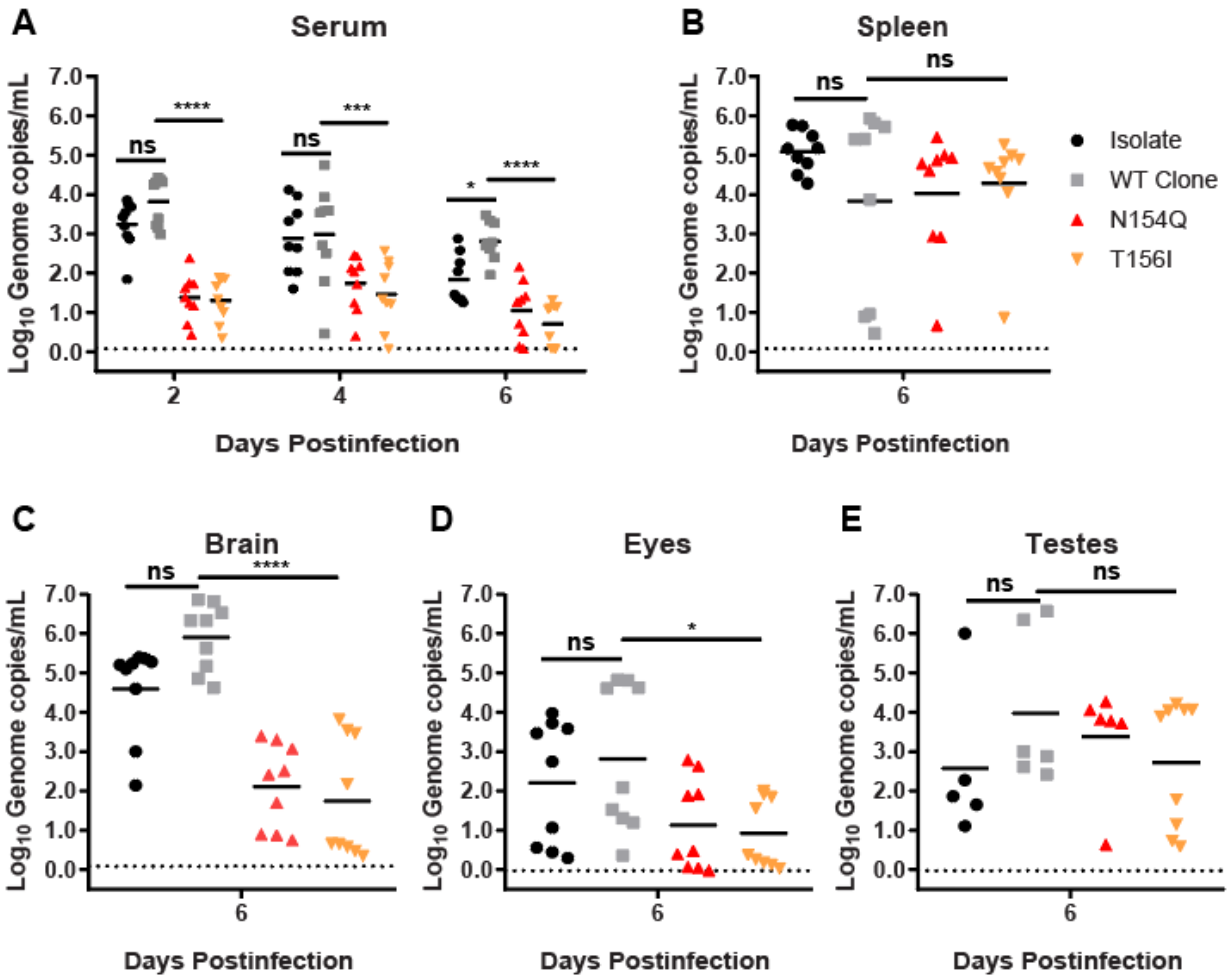

Figure 2.6. E glycosylation mediates ZIKV PRVABC59 infection in mice. Five- to six –week old *Ifnar1*$^{-/-}$ mice were inoculated with 1x10^{3} FFU of ZIKV strain PRVABC59 isolate, WT clone, N154Q mutant, or T156I mutant by a subcutaneous route in the footpad. **A**. Blood was collected at 2, 4, and 6 days after infection and ZIKV RNA in serum was measured by qRT-PCR. **B-E**. Mice were euthanized 6 days after infection, perfused, and tissues were harvested. ZIKV RNA in tissues was measured by qRT-PCR. Data are combined from 2 independent experiments. **, P < 0.01; ***, P < 0.001; ****, P < 0.0001; ns, not significant (unpaired 2-tailed t test).

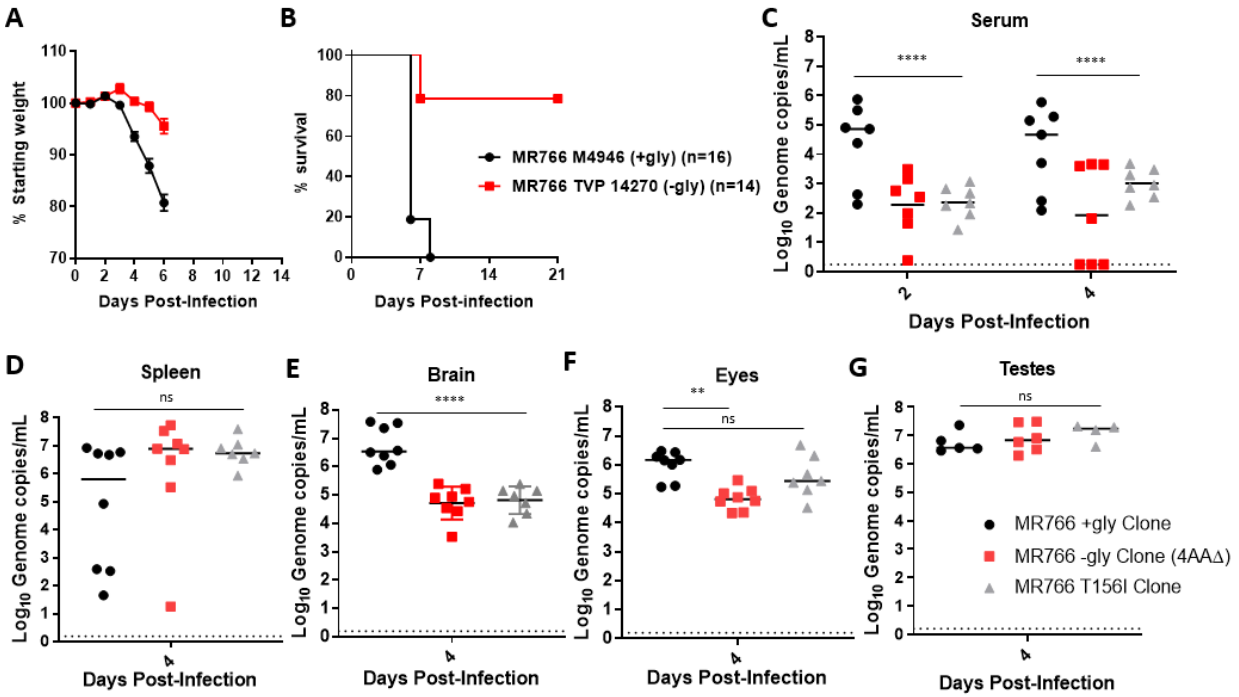

Figure 2.7. E glycosylation mediates ZIKV MR766 infection in mice. **A-B**. Seven- to ten-week old *Ifnar1*$^{-/-}$ mice were inoculated with 1x10^{3} FFU of ZIKV strain MR766 isolate containing the E glycan (+gly) or lacking the E glycan (-gly [4AAΔ)] by a subcutaneous route in the footpad. Mice were weighed daily and weights are expressed as percentage of body weight prior to infection and censored once one mouse in a group died. Results shown are the mean ± SEM of 14 to 16 *Ifnar1*$^{-/-}$ mice per virus. Lethality was monitored for 21 days. **C-G**. Five-week-old *Ifnar1*$^{-/-}$ mice were inoculated with 1x10^{3} FFU of ZIKV strain MR766 +gly clone, -gly clone (4AAΔ), or T156I clone by a subcutaneous route in the footpad. **C**. Blood was collected at 2 and 4 days after infection and ZIKV RNA in serum was measured by qRT-PCR. **D-G**. Mice were euthanized 4 days after infection, perfused, and tissues were harvested. ZIKV RNA in tissues was measured by qRT-PCR. **, P < 0.01; ***, P < 0.001; ****, P < 0.0001; ns, not significant (unpaired 2-tailed t test).

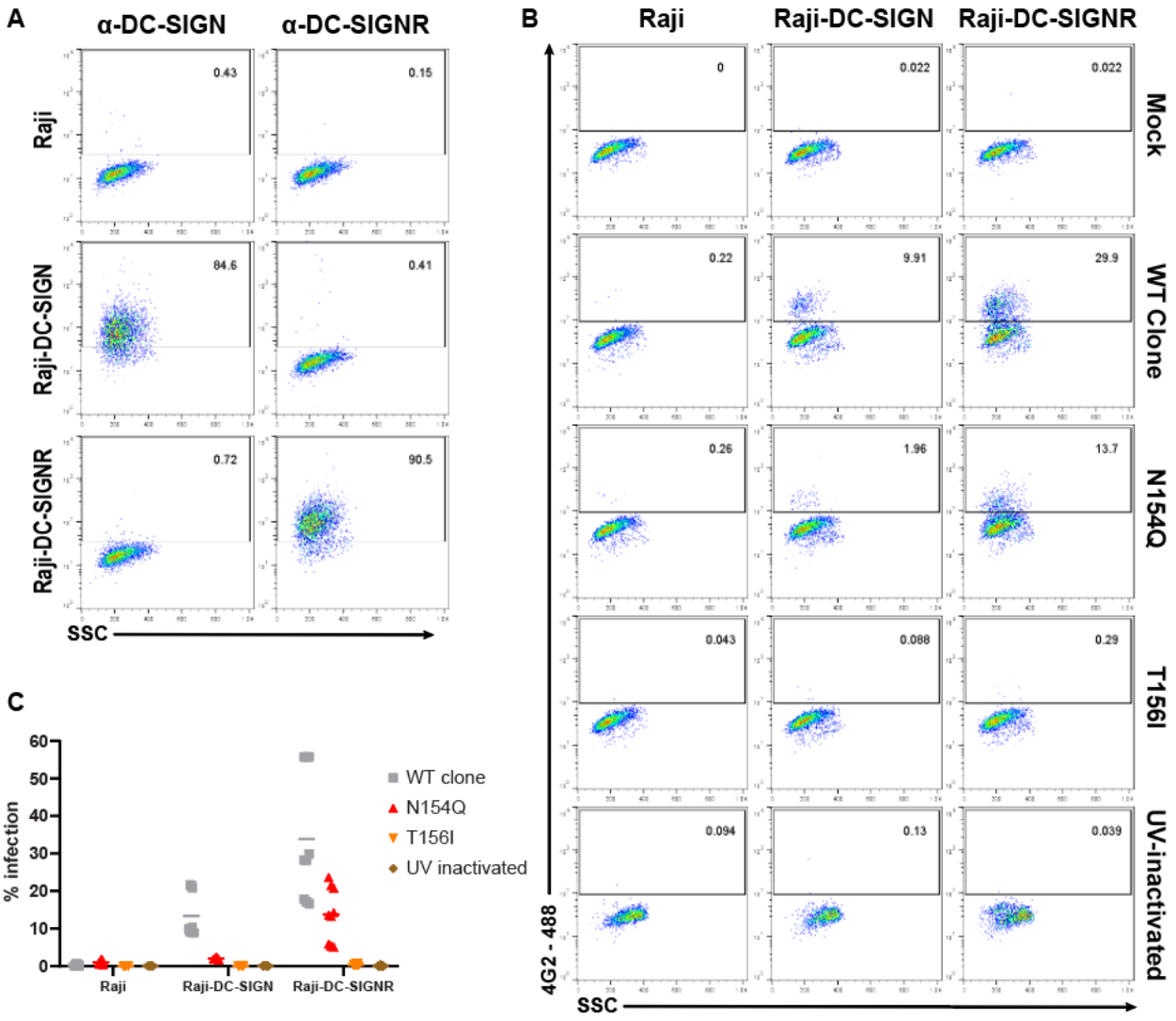

Figure 2.8. E glycosylation facilitates ZIKV infection of DC-SIGN and DC-SIGNR expressing cells. **A**. Representative flow plots of Raji, Raji-DC-SIGN and Raji-DC-SIGNR cells stained for cell surface DC-SIGN and DC-SIGNR. **B**. Representative flow plots of Raji, Raji-DC-SIGN, and DC-SIGNR cells infected at a MOI of 5 with ZIKV PRVABC59 WT, N154Q, T156I, or UV-inactivated WT virus. Cells were stained at 24 hpi with Alexa Fluor 488-conjugated ZIKV MAb 4G2 to detect intracellular E protein. Values indicate the proportion of cells staining positive. **C**. Percentage of infected (E positive) Raji, Raji-DC-SIGN, or DC-SIGNR cells combined from 3 independent experiments performed in triplicate.

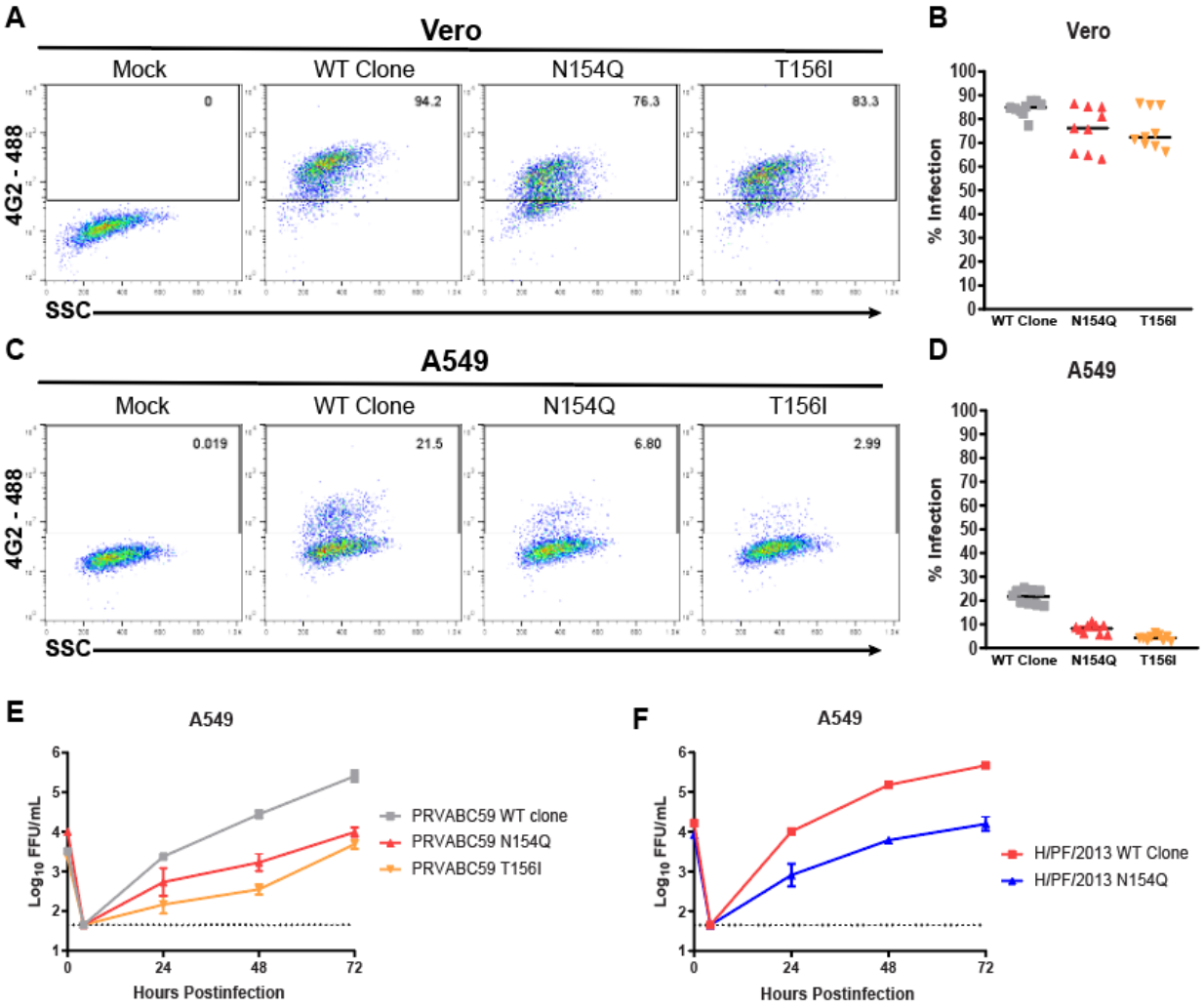

Figure 2.9. E glycosylation facilitates ZIKV infection of A549 but not Vero cells. **A-D.** Vero and A549 cells were infected at a MOI of 5 with ZIKV PRVABC59 WT, N154Q, or T156I clones. Cells were stained at 24 hpi with Alexa Fluor 488-conjugated ZIKV MAb 4G2 to detect intracellular E protein. **A** and **C.** Representative flow plots of infected Vero or A549 cells. **B** and **D.** Percentage of infected (E positive) Vero or A549 cells combined from 3 independent experiments performed in triplicate. **E and F.** A549 cells were infected at a MOI of 0.01 with ZIKV PRVABC59 WT clone, N154Q mutant, and T156I mutant or ZIKV H/PF/2013 WT clone and N154Q mutant. Virus in culture supernatant was titrated by focus-forming assay. Data shown are the mean ± SEM of 9 samples from 3 independent experiments.

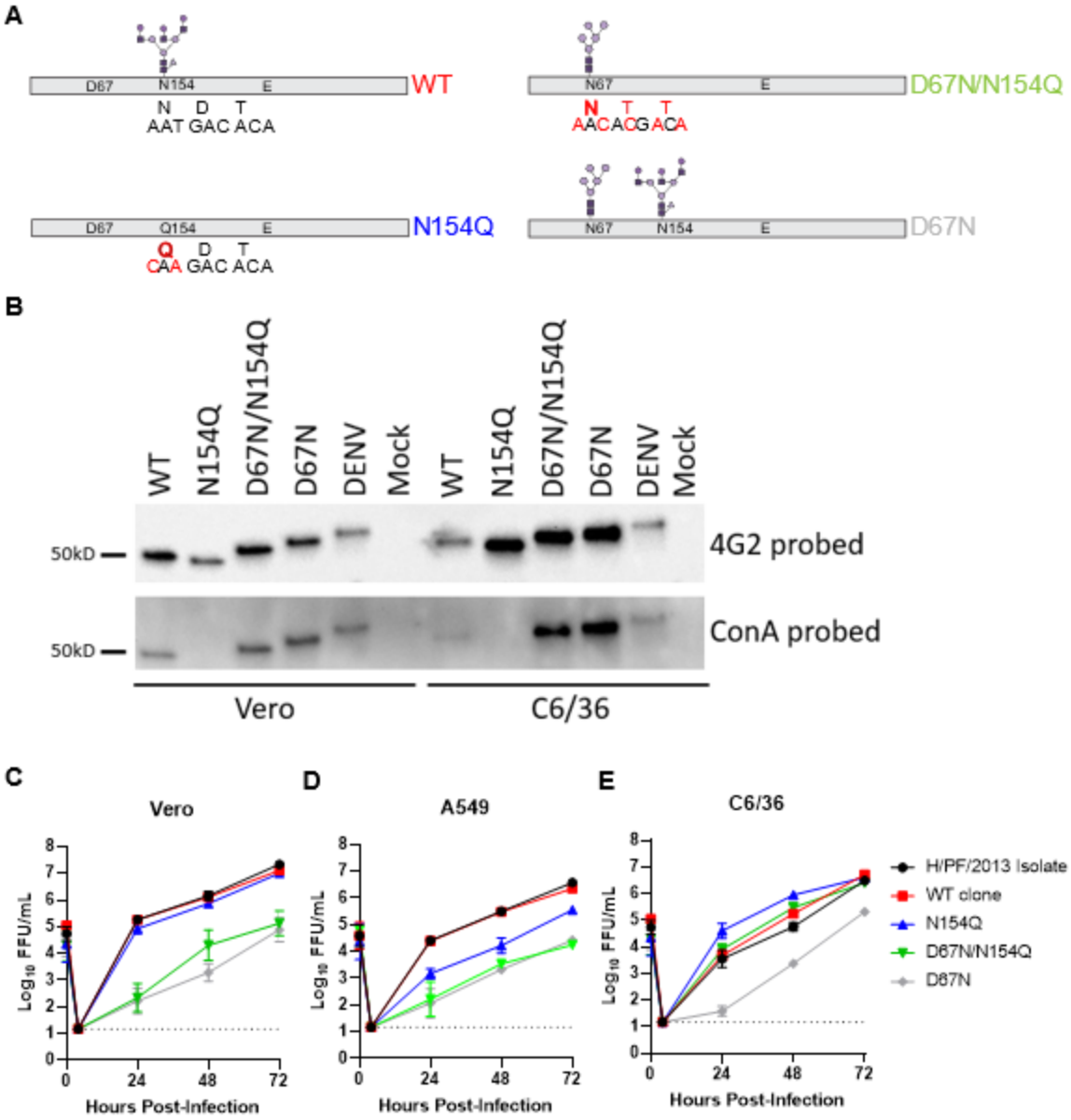

Figure 2.10. The number and location of ZIKV E glycosylation sites affects replication in cell culture. A. Predicted glycosylation of ZIKV envelope protein mutants (red letters). **B**. E proteins were immunoprecipitated with MAb 1M7 from lysates of Vero or C6/36 cells infected with ZIKV H/PF/2013 WT clone, N154Q mutant, D67N/N145Q mutant, D67N mutant, or DENV. Lysates were separated by nonreducing SDS-PAGE, and probed with MAb 4G2 or ConA. **C-E**. Vero, A549, and C6/36 cells were infected at a MOI of 0.01 with ZIKV H/PF/2013 isolate, WT clone, N154Q mutant, D67N/N154Q mutant, or D67N mutant virus. Viruses in culture supernatants were titrated by focus-forming assay. Data shown are the mean values ± standard errors of the means (SEM) of 9 samples from 3 independent experiments

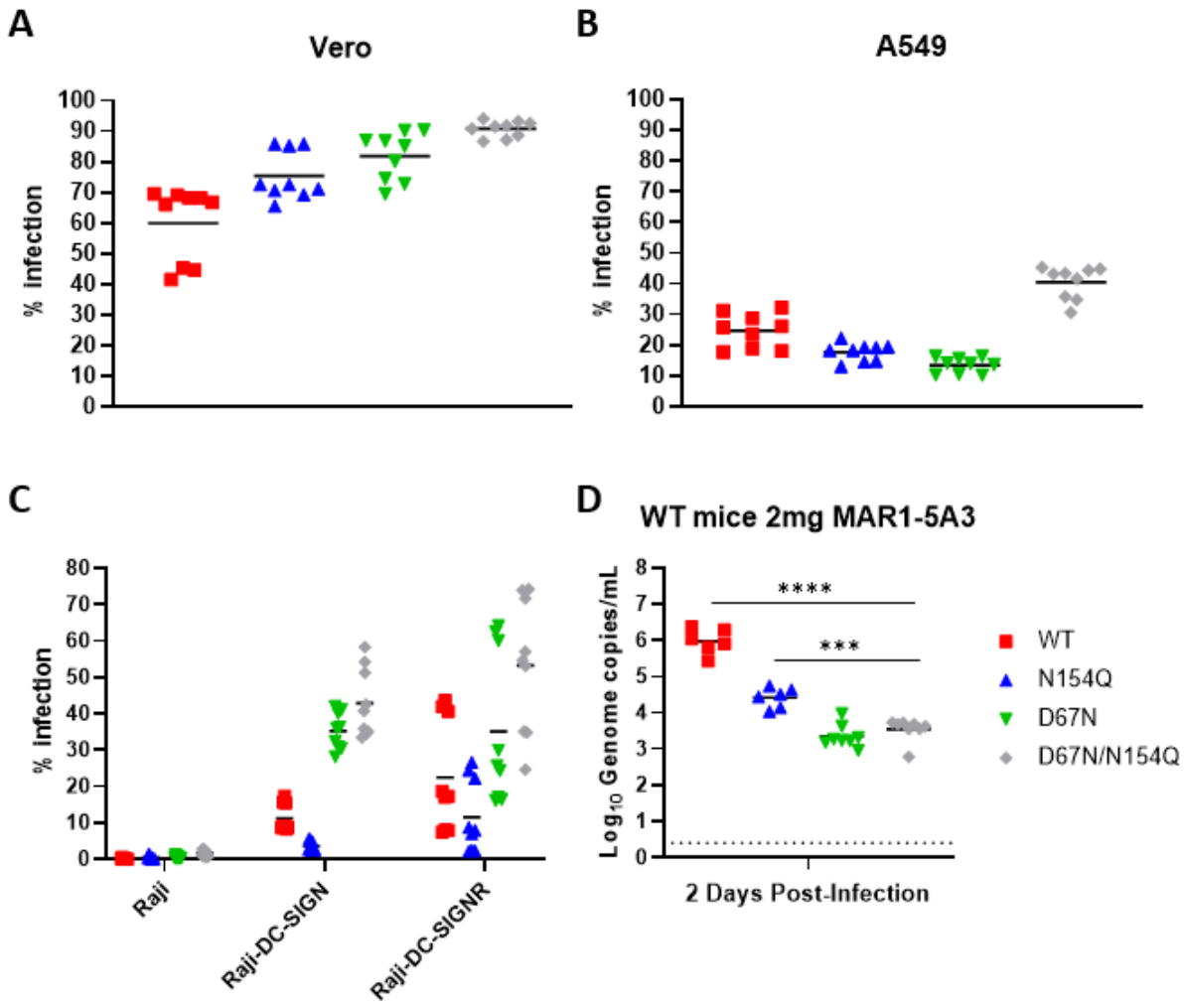

Figure 2.11. The location and number of glycans on E effect ZIKV replication *in vitro* and *in vivo*. A-C Percentage of infected (E positive) Vero, A549, or Raji, Raji-DC-SIGN, and DC-SIGNR cells from 3 independent experiments performed in triplicate. Cells were infected at a MOI of 1 with ZIKV H/PF/2013 WT, N154Q, D67N/N154Q, or D67N virus. Cells were stained at 24 hpi with Alexa Fluor 488-conjugated ZIKV MAb 4G2 to detect intracellular E protein. Values indicate the proportion of cells staining positive. **D** Five- to six –week old WT mice were pre-treated with 2mg MAR1, then inoculated with $1x10^3$ FFU of ZIKV strain H/PF/2013 WT clone, N154Q mutant, D67N/N154Q mutant, or D67N mutant by a subcutaneous route in the footpad. Blood was collected at 2 days after infection and ZIKV RNA in serum was measured by qRT-PCR. ***, $P < 0.001$; ****, $P < 0.0001$; (unpaired 2-tailed t test).

CHAPTER 3 – TWO GENETIC DIFFERENCES BETWEEN CLOSELY-RELATED ZIKA VIRUS STRAINS DETERMINE PATHOGENIC OUTCOME IN MICE[1]

3.1 Summary

Recent Zika virus (ZIKV) outbreaks and unexpected clinical manifestations of ZIKV infection have prompted an increase in ZIKV-related research. Here we identify two strain-specific determinants of ZIKV virulence in mice. We found that H/PF/2013 caused 100% lethality in *Ifnar1*$^{-/-}$ mice, whereas PRVABC59 caused no lethality; both strains caused 100% lethality in *Ifnar1*$^{-/-}$ *Ifngr1*$^{-/-}$ DKO mice. Deep sequencing revealed a high-frequency variant in PRVABC59 not present in H/PF/2013: a G to T change at nucleotide 1965 producing a Val to Leu substitution at position 330 of the viral envelope (E) protein. We show that the V330 variant is lethal on both strains, whereas the L330 variant is attenuating only on the PRVABC59 background. These results identify a balanced polymorphism in the E protein that is sufficient to attenuate the PRVABC59 strain, but not H/PF/2013. The consensus sequences of H/PF/2013 and PRVABC59 differ by 3 amino acids, but these were not responsible for the difference in virulence between the two strains.

[1]Parts of this work are in revision for publication in *Journal of Virology.*

H/PF/2013 and PRVABC59 differ by an additional 31 non-coding or silent nucleotide changes. We made a panel of chimeric viruses with identical amino acid sequences, but nucleotide sequences derived from H/PF/2013 or PRVABC59. We found that 6 nucleotide differences in the 3' quarter of the H/PF/2013 genome were sufficient to confer virulence in *Ifnar1*$^{-/-}$ mice. Altogether, our work identifies a large and previously unreported difference in virulence between two commonly used ZIKV strains, in two widely used mouse models of ZIKV pathogenesis (*Ifnar1*$^{-/-}$ and *Ifnar1*$^{-/-}$ *Ifngr1*$^{-/-}$ DKO mice).

3.2 Importance

Contemporary ZIKV strains are closely related and often used interchangeably in laboratory research. Here we identify two strain-specific determinants of ZIKV virulence which are evident only in *Ifnar1*$^{-/-}$ mice, not *Ifnar1*$^{-/-}$ *Ifngr1*$^{-/-}$ DKO mice. These results identify a balanced polymorphism in the E protein that is sufficient to attenuate the PRVABC59 strain, but not H/PF/2013. We further identify a second virulence determinant in the H/PF/2013 strain, which is driven by the viral nucleotide sequence, not the amino acid sequence. Altogether, our work identifies a large and previously unreported difference in virulence between two commonly used strains of ZIKV, in two widely used mouse models of ZIKV pathogenesis. Our results highlight that even very closely related virus strains can produce significantly different pathogenic phenotypes in common laboratory models.

3.3 Introduction

Zika virus (ZIKV) is a mosquito-transmitted flavivirus belonging to the *Flaviviridae* family of positive-sense single-stranded RNA viruses. ZIKV is related to other pathogenic flaviviruses, including dengue (DENV), yellow fever (YFV), West Nile (WNV), Japanese encephalitis (JEV), and tick-borne encephalitis (TBEV) viruses. Historically, ZIKV has been associated with a self-limiting rash and febrile illness that resolves within a few days, and these symptoms only occur in ~20% of infected individuals (2, 201). However, new clinical manifestations associated with recent ZIKV outbreaks, including Guillain-Barré syndrome and congenital Zika syndrome, have stimulated a surge in ZIKV research (2, 34, 39, 40).

Since the spread of ZIKV to the Western Hemisphere, numerous ZIKV strains have been isolated from patients and mosquitoes and distributed to laboratories across the world. Some widely-used strains include FSS13025 which was isolated in 2010 from patient serum in Cambodia, H/PF/2013 which was isolated in 2013 from patient serum in French Polynesia, PRVABC59 which was isolated in 2015 from patient serum in Puerto Rico, Paraiba_01/2015 which was isolated in 2015 from patient serum in Brazil, and Mex-2-81 which was isolated in 2016 from an *Aedes* mosquito in Mexico (31, 170, 173, 202). All of these strains share high nucleotide identity (at least 98.6% identity between any two strains), and minimal amino acid differences throughout their genomes. Thus, these closely related contemporary strains have been used largely interchangeably, and results from studies using various strains have been compared and combined to draw overall conclusions about the pathogenesis of contemporary ZIKV strains. Furthermore, various immunodeficient mouse models are used to study ZIKV pathogenesis, and the two most

commonly used systems (*Ifnar1*$^{-/-}$ mice and *Ifnar1*$^{-/-}$ *Ifngr1*$^{-/-}$ DKO mice) largely have been assumed to yield comparable results. *Ifnar1*$^{-/-}$ mice lack the type I interferon (IFN-αβ) receptor, whereas *Ifnar1*$^{-/-}$ *Ifngr1*$^{-/-}$ DKO mice lack both the IFN-αβ receptor and the type II interferon (IFN-γ) receptor. (203).

In this study we identified two strain-specific determinants of ZIKV virulence that are evident only in *Ifnar1*$^{-/-}$ mice, not *Ifnar1*$^{-/-}$ *Ifngr1*$^{-/-}$ DKO mice. We identified a balanced polymorphism in the E protein that is sufficient to attenuate the PRVABC59 strain, but not H/PF/2013. Furthermore, we identified a second virulence determinant in the H/PF/2013 strain that is driven by the viral nucleotide sequence, not the amino acid sequence.

3.4 Results

ZIKV strains H/PF/2013 and PRVABC59 have distinct lethality phenotypes in *Ifnar1-/-* mice.

ZIKV strain H/PF/2013 was isolated from patient serum from a 2013 outbreak in French Polynesia and ZIKV strain PRVABC59 was isolated from patient serum from a 2015 outbreak in Puerto Rico (170, 173). Deposited consensus sequences for these ZIKV strains (Genbank accession numbers KJ776791, KU501215) as well as Sanger sequencing of our lab stocks of H/PF/2013 and PRVABC59 (52, 164) show that these two strains are very similar: they share >99% nucleotide identity (34 nucleotide differences across the genome) and have only 3 amino acid differences (one in capsid and two in NS5). Both strains have been used widely and largely interchangeably by many research groups studying ZIKV virology and pathogenesis (52, 85, 138, 164, 188, 204–208). However, we found that H/PF/2013 and PRVABC59 have distinct lethality

phenotypes in *Ifnar1*$^{-/-}$ mice (Fig. 3.1). We infected 5- to 6-week-old *Ifnar1*$^{-/-}$ mice with 1 x 10^3 focus-forming units (FFU) of ZIKV H/PF/2013 or PRVABC59 by a subcutaneous route in the footpad and evaluated weight loss and lethality (Fig. 3.1A and B). These experiments used isolate virus stocks, originally derived from patient serum samples propagated through several passages on Vero cells. ZIKV H/PF/2013 was lethal in *Ifnar1*$^{-/-}$ mice, with mice beginning to lose weight at 6 days post-infection (dpi) and all mice succumbing by 11 dpi. In contrast, PRVABC59 was attenuated, causing no morbidity or mortality.

The attenuation of PRVABC59 was unexpected, given its high similarity to H/PF/2013 and because other groups have shown the PRVABC59 isolate to be lethal in *Ifnar1*$^{-/-}$ *Ifngr1*$^{-/-}$ DKO mice (137, 138). To test this, we infected 5- to 6-week-old *Ifnar1*$^{-/-}$ *Ifngr1*$^{-/-}$ DKO mice, as well as *Ifng*$^{-/-}$ mice (which do not produce IFN-γ), with 1 x 10^3 FFU of PRVABC59 or H/PF/2013 isolate virus by a subcutaneous route in the footpad and evaluated weight loss and lethality (Fig. 3.1 C and D). *Ifnar1*$^{-/-}$ *Ifngr1*$^{-/-}$ DKO mice began losing weight at 5 dpi, and all mice succumbed to either H/PF/2013 or PRVABC59 virus by 10 dpi. These results indicate that despite its attenuation in *Ifnar1*$^{-/-}$ mice, the PRVABC59 isolate can be lethal in a more susceptible mouse model (mice lacking both IFN-α/β and IFN-γ signaling). Unsurprisingly, since *Ifng*$^{-/-}$ mice retain interferon (IFN)-α/β signaling, no *Ifng*$^{-/-}$ mice lost weight or succumbed to either virus, showing that loss of IFN-γ signaling is not sufficient to render mice susceptible to ZIKV. To test whether PRVABC59 attenuation in *Ifnar1*$^{-/-}$ mice could be overcome with a higher inoculation dose, we infected 5- to 6-week-old *Ifnar1*$^{-/-}$ mice with 1 x 10^5 FFU of PRVABC59 isolate virus by a subcutaneous route in the footpad and evaluated weight loss and lethality (Fig. 3.1

E and F). Mice began losing weight at 5 dpi, but 5 of 7 mice recovered. One mouse began losing weight at 5 dpi and continued to lose weight until it succumbed at 11 dpi, while another mouse lost weight from 5 to 9 dpi, began to recover, gaining weight until 16 dpi, then succumbed at 20 dpi. Thus, even at 100-fold greater inoculation dose, the PRVABC59 isolate virus did not cause the ~100% lethality characteristic of the H/PF/2013 strain in *Ifnar1*$^{-/-}$ mice. Altogether, these data reveal profoundly different virulence phenotypes between ZIKV strain PRVABC59 and H/PF/2013 in *Ifnar1*$^{-/-}$ mice, despite their similar phenotypes in *Ifnar1*$^{-/-}$ *Ifngr1*$^{-/-}$ DKO mice. Given the high genetic similarity between PRVABC59 and H/PF/2013, we further investigated the viral determinants of these distinct virulence phenotypes.

PRVABC59 isolate contains high frequency variants.

Although the consensus sequences of PRVABC59 and H/PF/2013 were highly similar, isolate viruses typically contain a mixture of genetic variants either present in the original patient sample or generated during passage in cell culture. To determine whether these two strains included distinct variants compared to their reference genomes, we sequenced RNA isolated from concentrated virus stocks using a deep sequencing protocol. Most of the variants found in the two virus strains were present at relatively low frequencies (<10%), with the variants distributed across the genome. However, the PRVABC59 isolate contained 10 variants at >10% frequency, whereas H/PF/2013 contained 1 variant at >10% frequency, which was not shared between the two viruses. (Fig. 3.2A and B). The PRVABC59 variant present at the highest frequency was a G to T mutation at nucleotide 1965, resulting in a Val to Leu substitution at amino acid position 330 in domain III of the envelope protein. This data is consistent with deep sequencing

results of the PRVABC59 strain by other groups, who also identified the V330L substitution (137, 138, 209), suggesting that this polymorphism is maintained through independent passage of this strain in separate labs. To quantify more accurately the frequency of G1965T variation in ZIKV stocks, we next used the Primer ID sequencing strategy. Primer ID is a deep sequencing technique that incorporates an eleven nucleotide degenerative index into the cDNA synthesis primer, thereby uniquely identifying each template sequence and allowing resampled sequencing reads to be identified and pooled to create a highly accurate consensus sequence for each template (210). Primer ID confirmed an approximately 70% frequency of the G1965T variant in the PRVABC59 isolate, whereas no variation was detected at position 1965 of strain H/PF/2013 (Fig. 3.2 C and D). To investigate whether this variant was unique to ZIKV strain PRVABC59, we performed Primer ID on seven ZIKV strains propagated in either Vero or C6/36 cells, including two African lineage strains (Dakar 41662 and Dakar 41671) and five Asian-lineage strains (H/PF/2013, PRVABC59, FSS13025, Paraiba_01/2015, and Mex-2-81). We also tested two related flaviviruses, Spondweni virus (SPOV) and DENV (Table 3.1). The published consensus sequences for all of these viruses encode a Val at position 330, except SPOV, which encodes a Leu. We found that only the PRVABC59 strain has variation at position 1965, in virus grown in either Vero (69%T) or C6/36 cells (72%T). These results indicate the PRVABC59 isolate maintains T/G variation at position 1965 of the genome through multiple independent passages, suggesting a balanced polymorphism that is not found in other ZIKV strains or in either of two related flaviviruses. We next asked whether this variant was responsible for attenuating the PRVABC59 isolate in *Ifnar1*$^{-/-}$ mice.

PRVABC59 V330 is lethal in *Ifnar1*-/- mice, whereas L330 is attenuated.

To test whether the G/T1965 variant affected ZIKV virulence, we generated infectious clones of PRVABC59 or H/PF/2013 with either a G at position 1965 (V330) or a T at position 1965 (L330) of the genome (Table 3.2). The PRVABC59 and H/PF/2013 L330 or V330 viruses replicated equivalently to the isolates in Vero, A549, and C6/36 cells (Fig. 3.3).

To evaluate virulence, we infected 5- to 6-week-old *Ifnar1*$^{-/-}$ mice with 1 x 10^3 FFU of PRVABC59 or H/PF/2013 V330 or L330 clone viruses by a subcutaneous route in the footpad and evaluated weight loss and lethality (Fig. 3.4). Mice infected with PRVABC59 L330 lost weight from 6 to 9 dpi, with only 1 of 7 mice succumbing, whereas mice infected with PRVABC59 V330 virus began losing weight at 6 dpi and all mice succumbed by 11 dpi (Fig. 4A and B). All mice infected with either H/PF/2013 V330 or L330 virus began losing weight at 6 dpi and succumbed by 8 dpi (Fig. 3.4C and D). To determine whether the PRVABC59 L330 virus could be lethal in a more susceptible mouse model, we infected 8-week-old *Ifnar1*$^{-/-}$ *Ifngr1*$^{-/-}$ DKO mice with 1 x 10^3 FFU by a subcutaneous route in the footpad. Mice began to lose weight at 4 dpi and all mice succumbed by 10 dpi (Fig 3.4A and B). These results show that the L330 variant is attenuating on the PRVABC59 genetic background (with a phenotype similar to the PRVABC59 isolate virus), but did not impact virulence on the H/PF/2013 genetic background, altogether implying an epistatic effect of L330 on virulence.

Since the PRVABC59 V330 and L330 viruses produced distinct lethality phenotypes in *Ifnar1*$^{-/-}$ mice, we next compared viral loads in serum and tissues (Fig. 3.5).

We infected 5- to 6-week-old *Ifnar1*$^{-/-}$ mice with 1 x 10^3 FFU of PRVABC59 V330 or L330 virus by a subcutaneous route in the footpad and measured viral loads in the serum at 2, 4, and 6 dpi (Fig. 3.5A) and viral loads in the tissues (spleen, brain, eyes, and testes) at 6 dpi by reverse transcription-quantitative PCR (qRT-PCR) (Fig. 3.5B-E). Compared to the V330 virus, the L330 virus produced similar viral loads at 2 and 4 dpi, but significantly lower viral loads at 6 dpi in serum (10-fold reduction). There was no significant difference between the PRVABC59 V330 or L330 viral loads in any tissues tested. However, since the last PRVABC59 V330 infected mouse succumbed at 11 dpi, viral loads may differ at a later time post-infection. To test differences in viral tissue loads between PRVABC59 V330 and L330 infected mice later after infection, we infected 5- to 6-week-old *Ifnar1*$^{-/-}$ mice with 1x10^3 FFU of PRVABC59 V330 or L330 virus by a subcutaneous route in the footpad and harvested tissues from V330 infected mice when the mice were moribund and harvested tissues from L330 infected mice when the last V330 infected mouse was harvested (L330-infected mice did not exhibit disease signs). Brain viral loads were measured by qRT-PCR (Fig 5F). One PRVABC59 V330 infected mouse was moribund and harvested at 8dpi, and all other V330 infected mice were harvested at 9dpi, along with all L330 infected mice. At 9dpi, all PRVABC59 L330 mice had significantly lower viral loads (1000-fold) in the brain compared to V330 infected mice. Sanger sequencing of virus isolated from brains 9dpi confirmed the viruses maintained their original V330 or L330 genotype, with no additional mutations throughout E. Altogether, these data show that attenuation of the L330 virus corresponds to lower viremia at 6dpi and lower viral loads in the brain late in infection, suggesting the L330 virus may be cleared more efficiently than V330 virus.

Since the PRVABC59 isolate virus is a mix of V330 and L330 virus, we next tested whether the attenuated phenotype of the L330 virus was dominant over the virulent phenotype of the V330 virus. We infected 5- to 6-week-old *Ifnar1*$^{-/-}$ mice with a total of 1 x 10^3 FFU of PRVABC59 V330:L330 at 1:1, 1:10, 1:100, or 1:1000 ratios of V330:L330 clone viruses by a subcutaneous route in the footpad and evaluated weight loss and lethality (Fig. 3.6). Mice infected with either a 1:1 or 1:10 ratio began losing weight at 5 days post-infection with all mice succumbing by 10 dpi, similar to mice infected with PRVABC59 V330 alone. In contrast, mice infected with a 1:100 or 1:1000 ratio lost weight from 6 to 11 dpi with all mice recovering except for one, similar to PRVABC59 L330 alone. These data indicate a ratio of 1:100, where the majority of the virus is L330, is able to attenuate the V330 virus, consistent with the attenuated phenotype of the PRVABC59 isolate virus.

Though the G1965T nucleotide change results in a Val to Leu amino acid substitution, the coding change may not be responsible for the difference in virulence between PRVABC59 V330 and L330 in *Ifnar1*$^{-/-}$ mice. Evaulating the nucleotide sequence of the PRVABC59 virus with either G1965 or T1965 using a web server for RNA secondary structure prediction (https://rna.urmc.rochester.edu/RNAstructureWeb/Servers/Fold/Fold.html) showed that the nucleotide change may alter the RNA secondary structure at this site (Fig 3.7A). We used the same RNA secondary structure prediction server to identify a nucleotide change (G1908T) that was predicted to restore the RNA secondary structure of the T1965 virus to the G1965 structure (Fig 3.7A). We generated the T1965 + T1908 virus (V034), which is predicted to have the same RNA secondary structure as the V330 virus, while encoding

a Leu at position 330 (the G1908T mutation also produces an Ala to Pro change at AA 311 of E). We infected 5- to 6-week-old *Ifnar1*$^{-/-}$ mice with 1 x 10^3 FFU of PRVABC59 L330 or V034 clone viruses by a subcutaneous route in the footpad and evaluated weight loss and lethality (Fig. 3.7B and C). Mice infected with V034 did not lose weight and no mice succumbed to the virus, whereas mice infected with PRVABC59 L330 lost weight from 7 to 11 dpi with all mice recovering, similar to prior experiments. These data suggest the predicted RNA secondary structure changes due to the G1965T nucleotide change are not responsible for the attenuation of the PRVABC59 L330 virus, although we cannot exclude that the Ala to Pro change independently attenuates V034, or that G1965T causes RNA structure changes distinct from this predicted structure.

Nucleotide differences near the 3' end of the H/PF/2013 genome confer virulence.

Since the variation at position 330 of the envelope protein only affected virulence on the PRVABC59 background, not H/PF/2013, other differences between the two viruses must contribute to virulence in *Ifnar1*$^{-/-}$ mice. The consensus sequences of PRVABC59 and H/PF/2013 differ by only 34 nucleotides throughout the entire genome. These include 30 silent changes, 1 non-coding change, and 3 coding changes (one in capsid (I/T75) and two in the methyltransferase domain of NS5 (V/A37 and V/M60)). To test whether any of the three amino acids that differ between the two viruses were responsible for their differential lethality in *Ifnar1*$^{-/-}$ mice, we used site directed mutagenesis to generate a PRVABC59 L330 virus (V020) with an amino acid sequence identical to H/PF/2013 L330 but maintaining the 31 silent and non-coding nucleotides from the PRVABC59 genome (Table 3.2) (Fig. 3.8A). V020 replicated equivalently to PRVABC59 L330 in Vero cells (Fig. 3.8B). We infected five- to six-week-old *Ifnar1*$^{-/-}$ mice

with 1 x 10^3 FFU of PRVABC59 L330 or V020 by a subcutaneous route in the footpad and evaluated weight loss and lethality (Fig. 3.8C and D). Mice infected with PRVABC59 L330 began losing weight from 7 to 10 dpi, with only 1 of 7 mice succumbing to the infection, similar to previous experiments (Fig 3.4). Mice infected with V020 did not lose weight and no mice succumbed to the infection. These results indicate that the three amino acids that differ between the consensus sequences of PRVABC59 and H/PF/2013 viruses are not responsible for their differential lethality in *Ifnar1*$^{-/-}$ mice.

Since amino acid changes did not explain the observed differences in virulence between the PRVABC59-L330 and H/PF/2013-L330 viruses, we next investigated whether the remaining 31 nucleotide differences between the two strains were responsible. The infectious clone system used to generate PRVABC59 and H/PF/2013 viruses divides the viral genome over four plasmids (fragments A, B, C, and D) (52, 164). The high sequence identity between PRVABC59 and H/PF/2013 preserves the restriction sites used to ligate each genomic fragment, making it straightforward to generate chimeras of the two strains. We generated chimeric viruses encoding the PRVABC59-L330 amino acid sequence, but the nucleotide sequence of either PRVABC59 or H/PF/2013 and evaluated their virulence in *Ifnar1*$^{-/-}$ mice (Table 3.2) (Fig. 3.9A). All viruses tested replicated equivalently in Vero cells (Fig. 3.9B). We first tested viruses with the 5' half (fragments A and B) derived from the PRVABC59 nucleotide sequence and the 3' half (fragments C and D) from the H/PF/2013 nucleotide sequence (V024) or vice versa (V025) (Fig. 3.9A). We infected 5- to 6-week-old *Ifnar1*$^{-/-}$ mice with 1 x 10^3 FFU of V024 or V025 virus by a subcutaneous route in the footpad and evaluated weight loss and lethality (Fig. 9C and D). Mice infected with V024 began losing weight at 7 dpi and 6

of 8 mice succumbed to the virus by 11 dpi, whereas mice infected with V025 did not lose weight and no mice succumbed to the virus. Since both viruses encoded the same amino acid sequence, these data indicate that nucleotides on the 3' half of H/PF/2013 genome confer virulence in *Ifnar1*$^{-/-}$ mice. To further define which of these 18 nucleotide differences contribute to the virulent phenotype, we generated chimeric viruses still encoding the PRVABC59-L330 amino acid sequence but with either the C fragment (V026) or D fragment (V027) having the nucleotide sequence of H/PF/2013. The C fragment contains 12 nucleotide differences between the two strains, and the D fragment contains 6. We infected 5- to 6-week-old *Ifnar1*$^{-/-}$ mice with 1 x 10^3 FFU of V026 or V027 virus by a subcutaneous route in the footpad and evaluated weight loss and lethality (Fig. 3.7E and F). Mice infected with V026 lost weight from 6 to 12 dpi, with 7 of 9 mice recovering, whereas mice infected with V027 began losing weight at 6 dpi and all mice succumbed to the virus by 11 dpi. These results implicate one or more of the 6 nucleotide differences in the D fragment as virulence determinants for ZIKV H/PF/2013.

To test if the differential virulence of V026 and V027 corresponded to higher viral loads in V027 infected mice, we infected 5- to 6-week-old *Ifnar1*$^{-/-}$ mice with 1x10^3 FFU of V026 or V027 virus by a subcutaneous route in the footpad and harvested tissues when V027 infected mice were moribund (9dpi for all mice). Brain viral loads were measured by qRT-PCR (Fig 7G). All V026 infected mice had lower viral loads than V027 infected mice at 9dpi, with the exception of one V026 infected mouse, which was the only V026 infected mouse to show disease signs. These results suggest small differences in CNS viral loads can correspond to profound differences in virulence. Sanger sequencing of

virus isolated from the brains of infected mice confirmed the viruses maintained the six nucleotides that differ in the D fragment, with no additional mutations in the D fragment.

One of the six nucleotides that differ on the D fragment is in the 3' UTR, 6 nucleotides upstream of the first stem loop. This stem loop plays an important role in ZIKV virulence, as it inhibits the host 5'-to-3' exonuclease Xrn1, resulting in a stable subgenomic RNA (sfRNA) that facilitates ZIKV replication and pathogenesis by a variety of mechanisms (144). To test if this single base change in the 3' UTR was sufficient to confer virulence, we generated a virus (V030) with the single nucleotide change (A10392G) on the V020 background (Table 3.2). We infected 5- to 6-week-old *Ifnar1*$^{-/-}$ mice with 1 x 10^3 FFU of V030 virus by a subcutaneous route in the footpad and evaluated weight loss and lethality (Fig 3.9E and F). Mice infected with V030 did not lose any weight and no mice succumbed to the virus, indicating that this single nucleotide change is not sufficient to confer the virulent phenotype of the V027 virus. These data suggest that one of the other five bases or some combination of the six nucleotides that differ between the two viruses on the D fragment are responsible for the virulent phenotype of the H/PF/2013 strain.

PRVABC59 is not more sensitive to IFN-γ, nor does it induce more IFN-γ than H/PF/2013.

We found that PRVABC59 is not lethal in *Ifnar1*$^{-/-}$ mice, but equally as lethal as H/PF/2013 in *Ifnar1*$^{-/-}$ *Ifngr1*$^{-/-}$ DKO mice, suggesting that IFN-γ differentially controls the pathogenesis of these two ZIKV strains. We first investigated whether PRVABC59 is more sensitive to IFN-γ than is H/PF/2013. We pre-treated *Ifnar1*$^{-/-}$ mouse embryonic fibroblasts (MEF) with 0, 0.5, 1, 5, or 10ng of mouse IFN-γ for 24hrs, washed with PBS, then infected

with ZIKV strain H/PF/2013 or PRVABC59 isolate viruses at a MOI of 0.1. Viruses in culture supernatants were titrated 24 hours-post infection by focus-forming assay (Fig 3.10A). We saw a dose-dependent inhibition of both viruses with IFN-γ treatment, however there were no significant differences in viral titers between H/PF/2013 and PRVABC59 isolate at any IFN-γ concentration. Although we observed no differential inhibition in cell culture, we next tested whether the PRVABC59 isolate induces more IFN-γ than H/PF/2013, possibly leading to attenuation in *Ifnar1*$^{-/-}$ mice. Five- to six-week-old wild-type mice pretreated with 2mg IFNAR1-blocking monoclonal antibody MAR1-5A3 (134, 199) then inoculated with 1 x 10^3 FFU of ZIKV strain H/PF/2013 or PRVABC59 and serum was collected at 2, 4, 6 and, 8 dpi. We also infected *Ifnar1*$^{-/-}$ mice and harvested serum at 6 dpi. Serum IFN-γ levels were measured by ELISA (Fig 3.10B and C). In wild-type MAR1 treated mice, IFN-γ levels peaked at 6 dpi, with no significant difference between the two viruses. The level of IFN-γ induction was much higher in *Ifnar1*$^{-/-}$ mice, which may be due to increased viral replication compared to MAR1-treated mice, or to dysregulated IFN-γ signaling in *Ifnar1*$^{-/-}$ mice (211). Nonetheless, we did not detect a significant difference in IFN-γ levels between the two viruses.

Macrophages and dendritic cells (DCs) are two key cell types that regulate innate immunity in response to viral infections and are cellular targets of ZIKV infection (212). To test if macrophages or DCs are differentially susceptible to ZIKV H/PF/2013 or PRVACB59, we measured the growth kinetics of each virus in *Ifnar1*$^{-/-}$ bone marrow derived macrophages (BMDM) or DCs (BMDC). BMDM or BMDC were infected at a MOI of 0.01 with ZIKV H/PF/2013 isolate, PRVABC59 isolate, or a Kunjin virus clone as a positive control (213–215) and viral supernatants were titered by FFA (Fig 3.11A and B).

As expected, Kunjin virus replicated to high titers in both BMDM (8 Log_{10} FFU/mL at 96 hpi) and BMDCs (5.5 Log_{10} FFU/mL). H/PF/2013 replicated to between 3-4 Log_{10} FFU/mL in both cell types, though much slower and to lower levels than Kunjin virus. PRVABC59 did not replicate in BMDM, but did replicate in BMDC, though to lower viral titers than H/PF/2013 (peak titer ~ 2 Log_{10} FFU/mL). We next tested whether virulence in *Ifnar1*$^{-/-}$ mice corresponded to replication in BMDC. We infected *Ifnar1*$^{-/-}$ BM DC at a MOI of 0.01 with H/PF/2013 isolate, PRAVABC59 isolate, H/PF/2013 V330 or L330, PRVABC59 V330 or L330, V024 or V025 viruses and viral supernatants were titered by FFA (Fig 3.11C). There was variable replication among the viruses, plateauing at 48-72 hpi, with H/PF/2013 isolate reaching a peak titer of 4.65 Log_{10} FFU/mL at 48 hpi, followed by V025 (4.27 Log_{10} FFU/mL), H/PF/2013 V330 (4.11 Log_{10} FFU/mL), PRVABC59 V330 (3.42 Log_{10} FFU/mL), PRVABC59 L330 (3.42 Log_{10} FFU/mL), PRVABC59 isolate (3.20 Log_{10} FFU/mL), H/PF/2013 L330 (3.03 Log_{10} FFU/mL). V024 did not replicate above the limit of detection, most likely due to a much lower starting inoculum concentration. Regardless, replication in BMDC did not correspond to virulence in *Ifnar1*$^{-/-}$ mice.

Altogether, this work identifies a large and previously unreported difference in virulence between two commonly used ZIKV strains. Our data further define the effect of a previously reported variant in the PRVABC59 strain. We also identify a novel role for non-coding changes as ZIKV virulence determinants, suggesting possible effects on RNA properties, such as RNA structure or post-transcriptional modifications.

3.5 Discussion

The new clinical manifestations associated with ZIKV after its emergence in the Western Hemisphere, particularly congenital Zika syndrome, led to a surge in ZIKV

research. Many different ZIKV strains have been isolated during the recent outbreaks and distributed to research labs around the world (e.g. ~12 contemporary strains available from BEI resources and ~20 from the World Reference Center for Emerging Viruses and Arboviruses). All contemporary ZIKV strains share high nucleotide identity and minimal amino acid differences throughout their genomes and thus have been used largely interchangeably to draw conclusions about the pathogenesis of contemporary ZIKV strains. However, not all contemporary ZIKV strains share the same pathogenic outcome in mice. A ZIKV strain isolated in 2013 from French Polynesia (H/PF/2013) and a strain isolated in 2015 from Brazil (Paraiba_01/2015) have been shown to cause 100% and 80% lethality in *Ifnar1*$^{-/-}$ mice, respectively (134, 135). In contrast, a ZIKV strain isolated in 2010 from Cambodia (FSS13025) was only 20-30% lethal in *Stat2*$^{-/-}$ or *Ifnar1*$^{-/-}$ mice, and a strain isolated in 2015 from Puerto Rico (PRVABC59) was not lethal in either mouse model (136). However, the H/PF/2013, FSS13025, and PRVABC59 strains were uniformly lethal in *Ifnar1*$^{-/-}$ *Ifngr1*$^{-/-}$ DKO mice (137–140). These data indicate ZIKV strain-specific contributions to virulence in mice, and highlight that differences in pathogenesis may not be evident in highly susceptible models, such as *Ifnar1*$^{-/-}$ *Ifngr1*$^{-/-}$ DKO mice. Strain characteristics such as virus source (human versus mosquito), disease outcome, geographic origin, or year of isolation, do not obviously correlate with pathogenic phenotype in mice, though such relationships might be revealed by comparing a larger number of strains under identical experimental conditions (136, 166, 216). In this study, we describe two distinct genetic determinants of ZIKV strain-specific virulence; notably, both phenotypes were evident in *Ifnar1*$^{-/-}$ mice but masked in *Ifnar1*$^{-/-}$ *Ifngr1*$^{-/-}$ DKO mice. Our results further define the effect of a previously reported variant in the PRVABC59

strain (138), identify a novel role for non-coding changes as ZIKV virulence determinants, and highlight that even very closely related virus strains can produce significantly different pathogenic phenotypes in common laboratory models.

Duggal et al. previously reported variants in the PRVABC59 isolate virus that led to attenuated pathogenesis in *Ifnar1*$^{-/-}$ *Ifngr1*$^{-/-}$ DKO mice (138). Their deep sequencing revealed the presence of a Val to Leu substitution at position 330 of the E protein, as well as a Trp to Gly substitution at position 98 of non-structural protein 1 (NS1). These authors concluded that the substitutions were tissue culture adaptations, as these variants were found at very low levels upon deep sequencing of the original patient sera, and were found to increase in frequency over three passages in Vero cells. However, while these substitutions increased in frequency with passage, it is not clear whether they are truly adaptive. Notably, we did not detect the L330 substitution in the H/PF/2013 strain, even though our stock of this strain has been passaged more extensively in Vero cells than the PRVABC59 strain, nor was this substitution detected in other ZIKV strains we tested (though many of these have less certain passage history). Furthermore, the frequency of the V330 and L330 variants remains constant (~70% L330) in independent passages of the PRVABC59 strain grown on different cell types (Vero versus C6/36) and by different laboratories. The stability of this variation could suggest a balanced polymorphism at this site, though the selective advantage of this or why it would be advantageous only on the PRVABC59 genetic background is unclear. Our mixed inoculum experiments suggest that a ratio of 1:100, where the majority of the virus is L330, is able to attenuate the V330 virus, consistent with the attenuated phenotype of the PRVABC59 isolate virus.

Duggal et al. found that the L330 substitution attenuated the virus in 12- to 16 – week - old *Ifnar1*$^{-/-}$ *Ifngr1*$^{-/-}$ DKO mice, increasing the mean time to death, and the addition of the NS1 G98 substitution further attenuated the virus, highlighting the ability of this variant to act epistatically to modulate virulence. We also identified the E L330 and NS1 G98 variants in our PRVABC59 isolate, which were not present in our H/PF/2013 stock. We found that the L330 substitution was sufficient to attenuate the PRVABC59 virus in *Ifnar1*$^{-/-}$ mice (recapitulating the phenotype of the isolate virus), so we did not further investigate the NS1 G98 variant.

ZIKV replicates poorly in mice with intact IFN-αβ signaling, due to an inability to antagonize murine STAT2 and STING (131, 132, 217, 218). Thus, mouse pathogenesis studies typically use mice deficient in IFN-αβ signaling and both *Ifnar1*$^{-/-}$ and *Ifnar1*$^{-/-}$ *Ifngr1*$^{-/-}$ DKO mice are widely used in the field (137, 139, 166, 219–221). However, *Ifnar1*$^{-/-}$ *Ifngr1*$^{-/-}$ DKO mice develop more severe disease and succumb more rapidly to ZIKV infection, independent of the inoculation route, compared to *Ifnar1*$^{-/-}$ mice (139, 222). Consistent with the phenotype of the PRVABC59 isolate virus, our PRVABC59-L330 virus caused 100% lethality in *Ifnar1*$^{-/-}$ *Ifngr1*$^{-/-}$ DKO mice but only 10% lethality in *Ifnar1*$^{-/-}$ mice.

We found that the L330 substitution was sufficient to attenuate on the PRVABC59 genetic backbone (10% lethality with PRVABC59 L330, compared to 100% lethality with PRVABC59 V330 in *Ifnar1*$^{-/-}$ mice). So, it was surprising that this same substitution had no effect on the H/PF/2013 backbone (the L330 virus remained 100% lethal). The mechanism by which a Val to Leu substitution in domain III of the envelope protein would attenuate virulence, and why this would be specific to the PRVABC59 strain remains unclear. Apart from V330L variation, the PRVABC59 and H/PF/2013 strains have

identical E protein amino acid sequences, so the L330 substitution would be expected to have a similar effect on both strains. An alternative explanation is that the distinct virulence phenotypes are determined not by the V330L change in the E protein, but by the effect of the G1965T nucleotide change on RNA structure or other RNA functions. Unfortunately, the codons in this position preclude generating mutants that would distinguish the effects of nucleotide and amino acid changes at this site. Our compensatory mutant virus data suggest the predicted RNA secondary structure changes due to the G1965T nucleotide change are not responsible for the attenuation of the PRVABC59 L330 virus, although we cannot exclude that the Ala to Pro change independently attenuates V034, or that G1965T causes RNA structure changes distinct from this predicted structure.

Since the L330 substitution was not attenuating on the H/PF/2013 background, and the other three amino acids that differ between the two strains did not have an effect on virulence, we sought to identify which of the other 31 nucleotide differences between the two strains were responsible for the differential lethality. Using chimeric viruses, we were able to narrow down the virulence determinant to 6 nucleotide differences in the 3' region of the H/PF/2013 genome (including NS5 and the 3'UTR), though the mechanism by which these nucleotide changes modulate virulence remains unclear. Possible mechanisms could include effects on RNA structure and/or post-transcriptional modifications, though these changes did not obviously disrupt predicted RNA structures or predicted m6A modification sites. Though the one nucleotide differences that falls 6 nucleotides upstream of the first stem loop structure in the 3' UTR was not sufficient to confer virulence, it is plausible that one or more of the other nucleotide changes between

PRVABC59 and H/PF/2013 could impact the production, stability, or function of sfRNA and thereby modulate ZIKV replication and/or virulence.

Though PRVABC59 is not lethal in *Ifnar1*$^{-/-}$ mice, this strain is equally as lethal as H/PF/2013 in *Ifnar1*$^{-/-}$ *Ifngr1*$^{-/-}$ DKO mice, suggesting that IFN-γ differentially controls the pathogenesis of these two ZIKV strains. However, we were not able to detect a significant difference in IFN-γ levels between the two viruses in mice, nor a significant difference in inhibition by IFN-γ between the two viruses in cell culture.

Altogether, our work identifies a large and previously unreported difference in virulence between two commonly used ZIKV strains, in two widely used mouse models of ZIKV pathogenesis (*Ifnar1*$^{-/-}$ and *Ifnar1*$^{-/-}$ *Ifngr1*$^{-/-}$ DKO mice). Our data further describe the effect of a previously reported variant in the PRVABC59 strain that appears to be attenuating only on the PRVABC59 genetic background. We also identified a novel role for non-coding changes as ZIKV virulence determinants, suggesting possible effects on RNA structure or post-transcriptional modifications. Our results highlight that even very closely related virus strains can produce significantly different pathogenic phenotypes in common laboratory models.

3.6 Materials and methods

Viruses and cells. ZIKV strains H/PF/2013 and PRVABC59 were provided by the U.S. Centers for Disease Control and Prevention (172, 173). ZIKV strains Dakar 41662, Dakar 41671, FSS13025, and Mex-2-81, as well as SPOV, were provided by the World Reference Center for Emerging Viruses and Arboviruses (31, 170, 173). Paraiba_01/2015 was obtained from Dr. Michael Diamond (Washington University in St. Louis) and DENV4

(KC963424.1) was obtained from Dr. Aravinda de Silva (UNC) (202, 223). Virus stocks were grown in Vero (African green monkey kidney epithelial) cells. Virus stocks were titered on Vero cells by focus-forming assay (FFA) (193). Vero and A549 cells were maintained in Dulbecco's modified Eagle medium (DMEM) containing 5% heat-inactivated fetal bovine serum (FBS) and L-glutamine at 37ºC with 5% CO_2. C6/36 cells were maintained in DMEM containing 6% FBS, NEAA, and P/S at 32ºC with 5% CO_2. Macrophages and dendritic cells were generated after cell isolation from the bone marrow of *Ifnar1*$^{-/-}$ mice and culturing for 7 days either in the presence of 40 ng/ml macrophage colony-stimulating factor (MCSF; BioLegend) to generate macrophages or with 20 ng/ml granulocyte-macrophage CSF (GM-CSF; BioLegend) and 20 ng/ml interleukin-4 (IL-4; BioLegend) to generate dendritic cells. For multi-step growth analysis, cells were infected at a multiplicity of infection of 0.01 and incubated at 37ºC or 32ºC with 5% CO_2 for one hour. Then, inoculum was aspirated and cells were washed with PBS and media was replenished. Samples of infected cell culture supernatant were collected at 4, 24, 48, 72, and 96 hrs post-infection and stored at -80ºC for virus titration. Virus quantification was performed by FFA on Vero cells. Duplicates of serial 10-fold dilutions of virus in viral growth medium (DMEM containing 2% FBS and 20 mM HEPES) were applied to Vero cells in 96-well plates and incubated as described above for 1 hr. Following virus adsorption, the monolayers were overlaid with 1% methylcellulose in minimum essential medium Eagle (MEM). Infected cell foci were detected 42-46 hrs after infection. Following fixation with 2% paraformaldehyde for 1 hr at room temperate, plates were incubated with 500 ng/ml of flavivirus cross-reactive mouse MAb E60 (194) for 2 hr at room temperature or overnight at 4ºC. After incubation at room temperate for 2 hr with a 1:5,000 dilution of

horseradish peroxidase (HRP)-conjugated goat anti-mouse IgG (Sigma), foci were detected by addition of TrueBlue substrate (KPL). Foci were quantified with a CTL Immunospot analyzer.

ZIKV infectious clone mutagenesis. We used previously described infectious clones of ZIKV stains H/PF/2013 or PRVABC59, generated using a quadripartite infectious clone system (164)(52). Due to the high sequence identity between H/PF/2013 and PRVABC59, the same naturally occurring class IIG nonpalindromic restriction endonuclease sites within the full-length genome were used for both infectious clones, allowing us to swap fragments between the two strains to generate chimeric viruses. PCR site-directed mutagenesis was used to introduce mutations to H/PF/2013 or PRVABC59 plasmids. The resulting purified plasmids were digested, ligated, *in vitro* transcribed, and electroporated into Vero or C6/36 cells as previously described (195). Supernatants from electroporated Vero or C6/36 cells were harvested after 6 to 7 days and passaged once on Vero cells to generate virus stocks. Virus stocks were titrated by FFA on Vero cells. Restriction enzymes and Phusion High Fidelity PCR kit were obtained from New England BioLabs. SuperScript III First Strand Synthesis kit was obtained from Invitrogen. Oligonucleotide primers and probes for DNA amplification, qRT-PCR, and sequencing primers were obtained from Sigma and IDT. The mMachine T7 Ultra transcription kit was obtained from Ambion. Anti-flavivirus monoclonal antibodies E60 and 4G2 were produced by the UNC Protein Expression and Purification Core Facility (194, 197). Secondary antibodies were obtained from Sigma.

Mouse Experiments. Animal husbandry and experiments were performed under the approval of the University of North Carolina at Chapel Hill Institutional Animal Care and

Use Committee. Five - to six-week old, or 8-week-old, male and female *Ifnar1*$^{-/-}$, *Ifnar1*$^{-/-}$ *Ifngr1*$^{-/-}$ DKO, or *Ifng*$^{-/-}$ mice on a C57BL/6 background were used. Mice were inoculated with 1 x 10^3 or 1 x 10^5 FFU of ZIKV in a volume of 50µl by a subcutaneous route in the footpad. Survival and weight loss were monitored for 14 or 21 days. Animals that lost ≥30% of their starting weight or that exhibited severe disease signs were euthanized.

Measurement of Viral Burden. ZIKV-infected mice were sacrificed at 6 dpi and perfused with 20 ml of PBS. Spleen, kidney, testes, brain, and eyes were harvested and homogenized with zirconia beads (BioSpec) in a MagNA Lyser instrument (Roche Life Science) in 500µl (eyes) or 1ml (all other tissues) of buffer RLT (Qiagen). Blood was collected at 2 and 4 dpi by submandibular bleed with a 5mm Goldenrod lancet and by cardiac puncture at 6 dpi. Blood was collected in serum separator tubes (BD) and serum was separated by centrifugation at 8000rpm for 5 min. Tissues and serum from infected animals were stored at -80^{o}C until virus titration. Tissue samples and serum from ZIKV-infected mice were extracted with the RNeasy Mini Kit (tissues) or Viral RNA Mini Kit (serum) (Qiagen). ZIKV RNA levels were determined by TaqMan one-step qRT-PCR on a CFX96 Touch Real-Time PCR Detection System (BioRad) using standard cycling conditions. Viral burden is expressed as genome copies per ml on a Log_{10} scale after comparison with a standard curve produced using serial 100-fold dilutions of ZIKV A plasmid. A previously published primer set was used to detect ZIKV RNA: forward, CCGCTGCCCAACACAAG; reverse, CCACTAACGTTCTTTTGCAGACAT; probe, /56-FAM/AGCCTACCT/ZEN/TGA CAAGCAATCAGACACTCAA/3IABkFQ/ (Integrated DNA Technologies) (52, 200).

IFN-γ ELISA. Blood was collected from ZIKV-infected mice at 2, 4, 6, or 8 dpi by submandibular bleed with a 5mm Goldenrod lancet. Blood was collected in serum separator tubes (BD) and serum was separated by centrifugation at 8000rpm for 5 min. A mouse IFN-y Uncoated ELISA was performed according to the manufacturers protocol (Invitrogen) as follows. A Corning Costar 96-well plate was coated with 100µl per well of capture Ab in Coating buffer and the plate was incubated overnight at 4^{o}C. The wells were washed three times with PBS and blot dried. Wells were blocked with 200µl per well ELISA/ELISPOT diluent and incubated at room temperature for one hour. Wells were aspirated and washed once with PBS. A standard curve was prepared by performing 2-fold serial dilutions of provided mouse IFN gamma with a starting concentration of 1000 pg/mL. 50µl of serum was added to the appropriate wells and the plate was sealed and incubated overnight at 4^{o}C. Wells were aspirated and washed three times with PBS. Next, 100µl of detection Ab was added to each well and the plate was incubated at room temperature for one hour. Wells were aspirated and washed three times with PBS. Then, 100µl Avidin-HRP was added to each well and the plate was incubated at room temperature for 30 minutes. Wells were aspirated and washed three times with PBS. Then, 100µl of 1X TMB solution was added to each well and incubated at room temperature for 15 minutes. Finally, 50µl Stop Solution was added to each well and the plate was read at 450nm on an Epoch spectrophotometer (BioTeK).

Deep sequencing. Viruses were grown on Vero cells and virions were concentrated over a 20% sucrose cushion by ultracentrifugation and full-length virion RNA was extracted using TRIzol (Ambion) following manufacturer's protocol. PRVABC59 RNA was submitted to the UNC Chapel Hill Vironomics Core for library construction and sequencing

on an Ion S5 (ThermoFisher Scientific). H/PF/2013 cDNA was made using extracted full-length virion RNA using Random Primer 9 (NEB) and SuperScript II and the second strand of the cDNA was synthesized using NEBNext Ultra II Non-Directional RNA Second Strand Synthesis Module (NEB) following the manufacturer's suggested protocol. Libraries were constructed from this double stranded cDNA using Nextera XT DNA Library Prep kit following manufactures suggested protocol, quantified using a 4200 TapeStation System (Agilent Technologies), and quantified using Qubit dsDNA HS Assay Kit (ThermoFisher Scientific). Libraries were sequenced on a MiSeq Desktop Sequencer (Illumina).

Primer ID. Viral RNA was extracted using a QIAamp viral RNA mini kit (Qiagen). Primer ID sequencing libraries were constructed as previously described (224). In brief, we used the SuperScript III kit (ThermoFisher) with cDNA primers containing a block of degenerate nucleotides (the Primer ID) to synthesize cDNA. After bead purification of the cDNA product using RNAClean XP (Beckman), two rounds of PCR were performed to incorporate MiSeq sequencing adaptors. Amplified products were purified, pooled, and sequenced using Illumina MiSeq 300 bp paired-end sequencing. A detailed protocol can be accessed at https://www.protocols.io/view/primer-id-miseq-library-prep-useewbe. We used the Illumina bcl2fastq pipeline for the initial data processing and the TCS pipeline (https://github.com/SwanstromLab/PID) to construct template consensus sequences.

Data Analysis. All data were analyzed with GraphPad Prism software. Kaplan-Meier survival curves were analyzed by the log rank test, and weight losses were compared using two-way ANOVA. For viral burden analysis, the log-transformed titers were

analyzed by the Mann-Whitney test. A p value of < 0.05 indicated statistically significant differences.

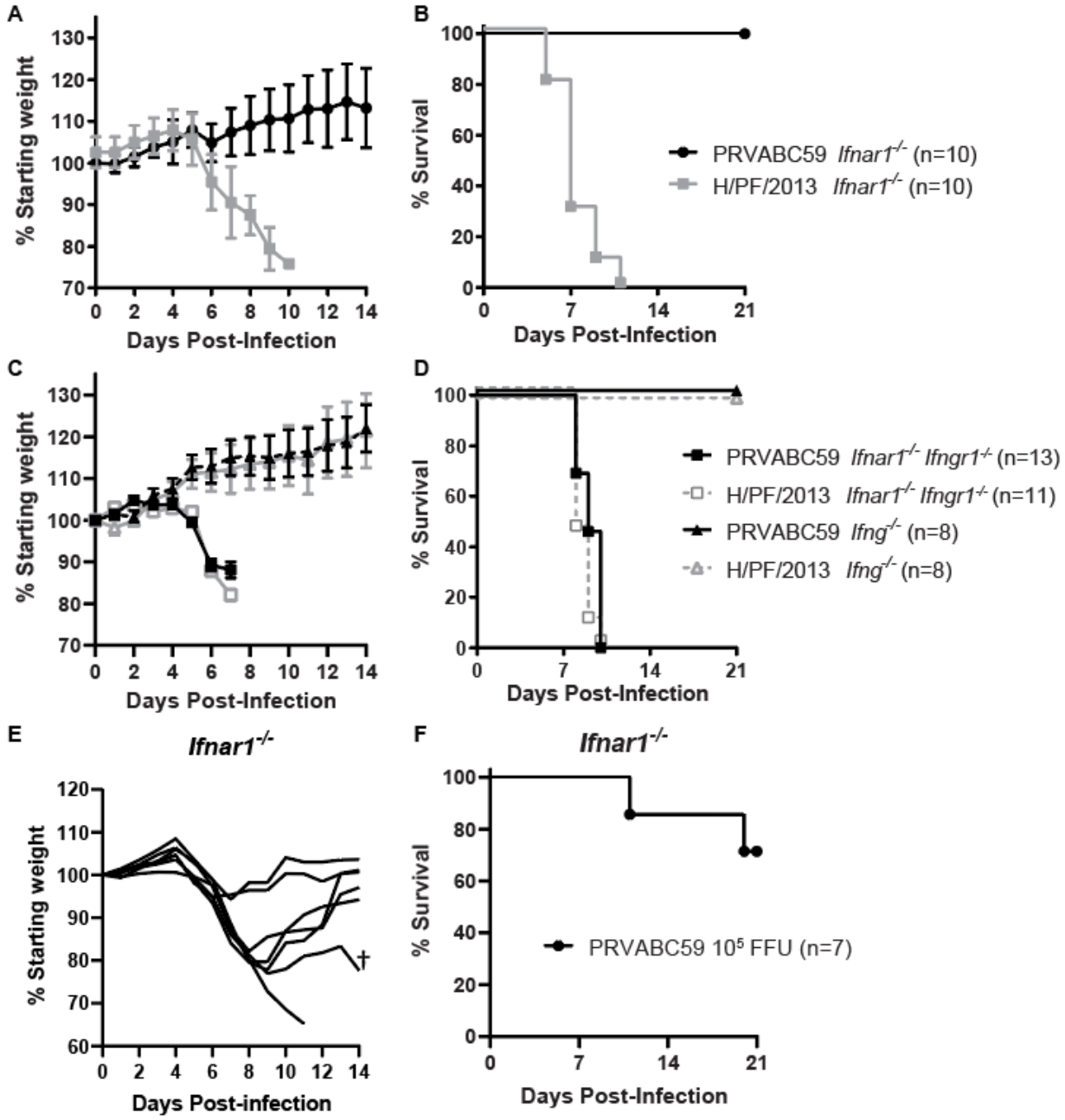

Figure 3.1. **PRVABC59 is attenuated in *Ifnar1*$^{-/-}$ mice.** Five- to six-week-old *Ifnar1*$^{-/-}$, *Ifnar1*$^{-/-}$ *Ifngr*$^{-/-}$, or *Ifng*$^{-/-}$ mice were inoculated with 1 x 10^3 (A to D) or 1 x 10^5 (E and F) FFU of ZIKV strain PRVABC59 or H/PF/2013 isolate viruses by a subcutaneous route. (A, C, and E) Mice were weighed daily for 14 days, and weights are expressed as percentages of body weight prior to infection. Results shown are the mean values ± SEM of the indicated number of mice from one (E and F) or two independent experiments (A-D). Lethality was monitored for 21 days. † = mouse died 20 dpi.

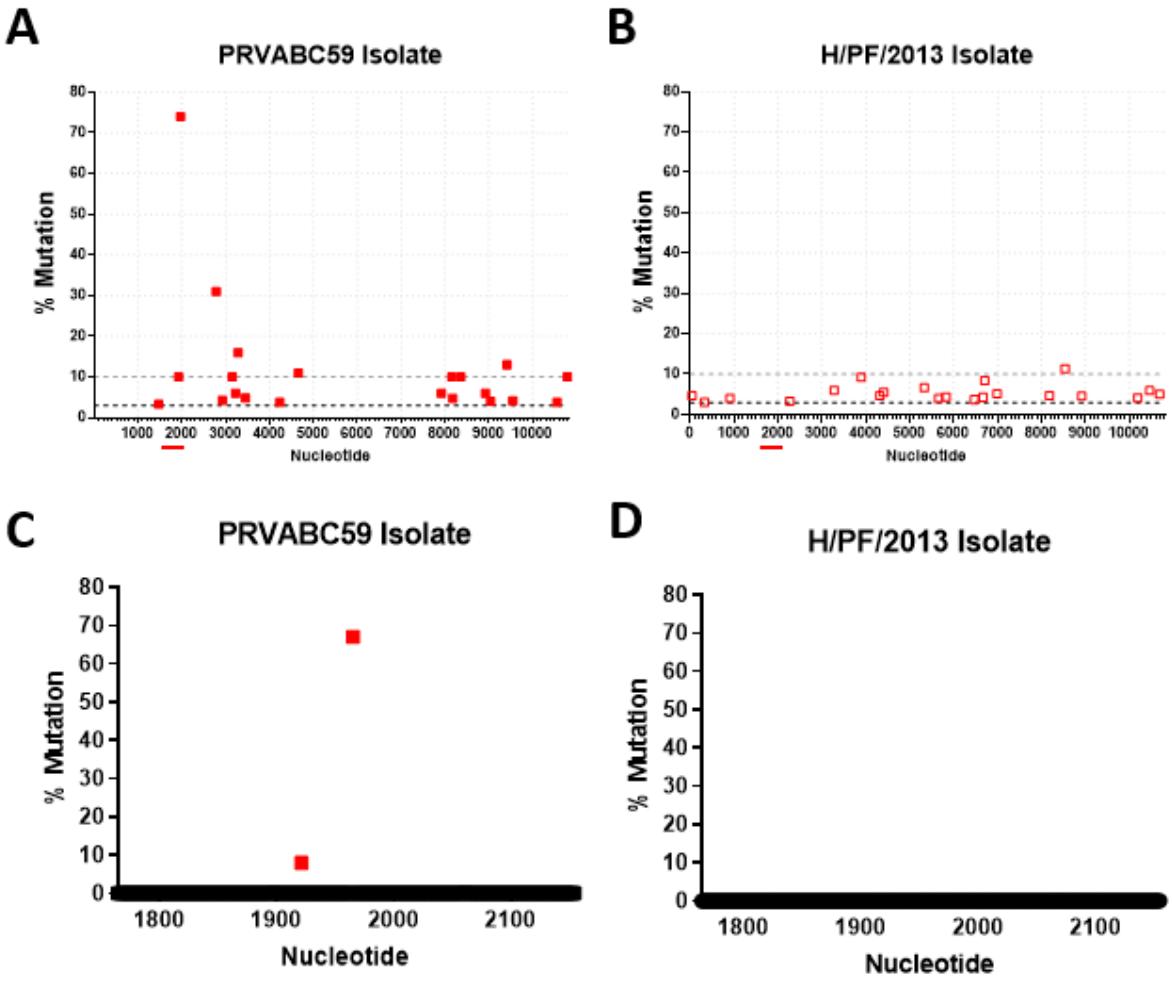

Figure 3.2. PRVABC59 isolate contains high frequency variants. A and B: Deep sequencing was performed on ZIKV strain PRVABC59 and H/PF/2013. The cut-off for single nucleotide polymorphisms was set at a depth ≥ 10 reads and a mutation rate ≥ 3% (black dashed line). The gray dashed line indicates 10% mutation rate. C and D: Primer ID was performed on ZIKV strains PRVABC59 and H/PF/2013 for the indicated 483 nucleotide region (red line under full genome sequencing) covering AA 231 to 392 of envelope.

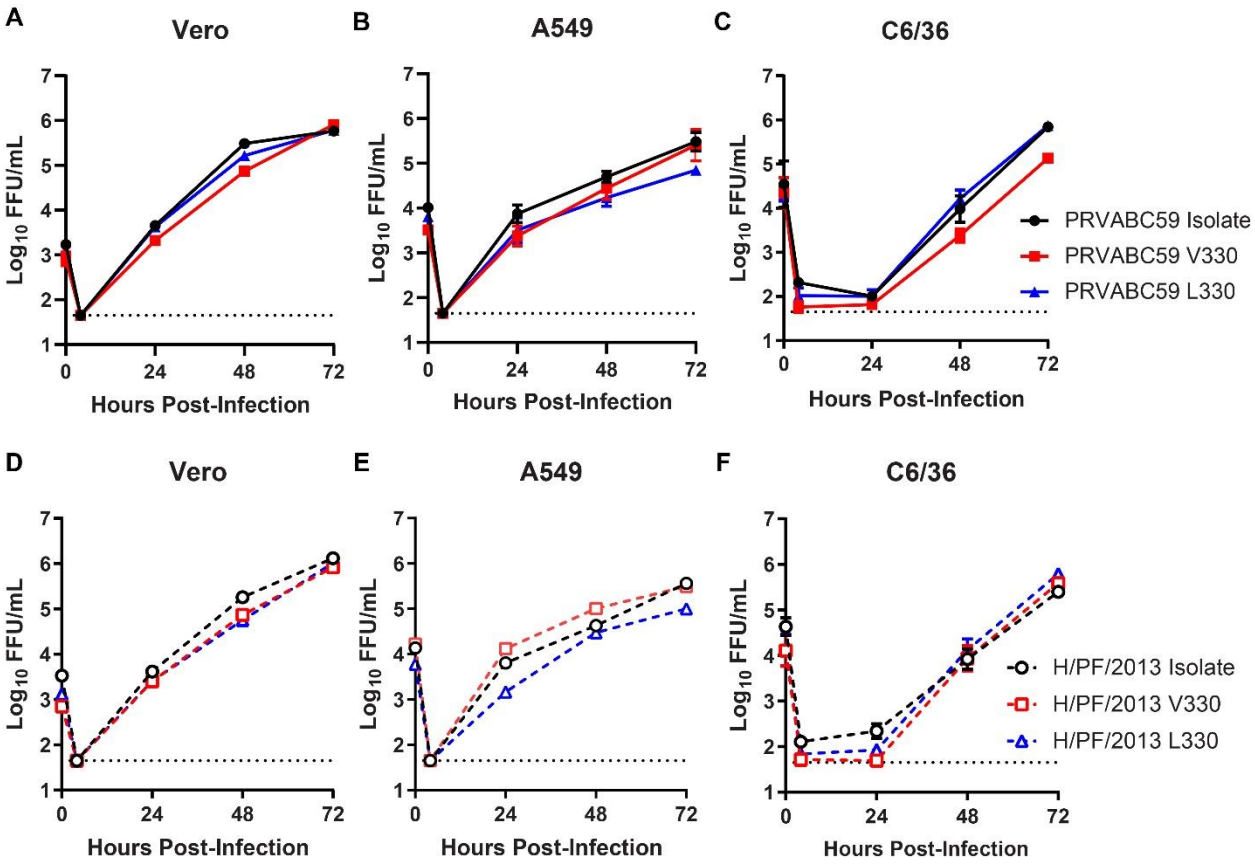

Figure 3.3. V330L substitution does not impact ZIKV replication in cell culture. Vero (A and D), A549 (B and E), or C6/36 (C and F) cells were infected at a MOI of 0.01 with ZIKV PRVABC59 or H/PF/2013 isolate, V330 clone, or L330 clone virus. Viruses in culture supernatants were titrated by focus-forming assay. Data shown are the mean values ± standard errors of the means (SEM) of 9 samples from 3 independent experiments.

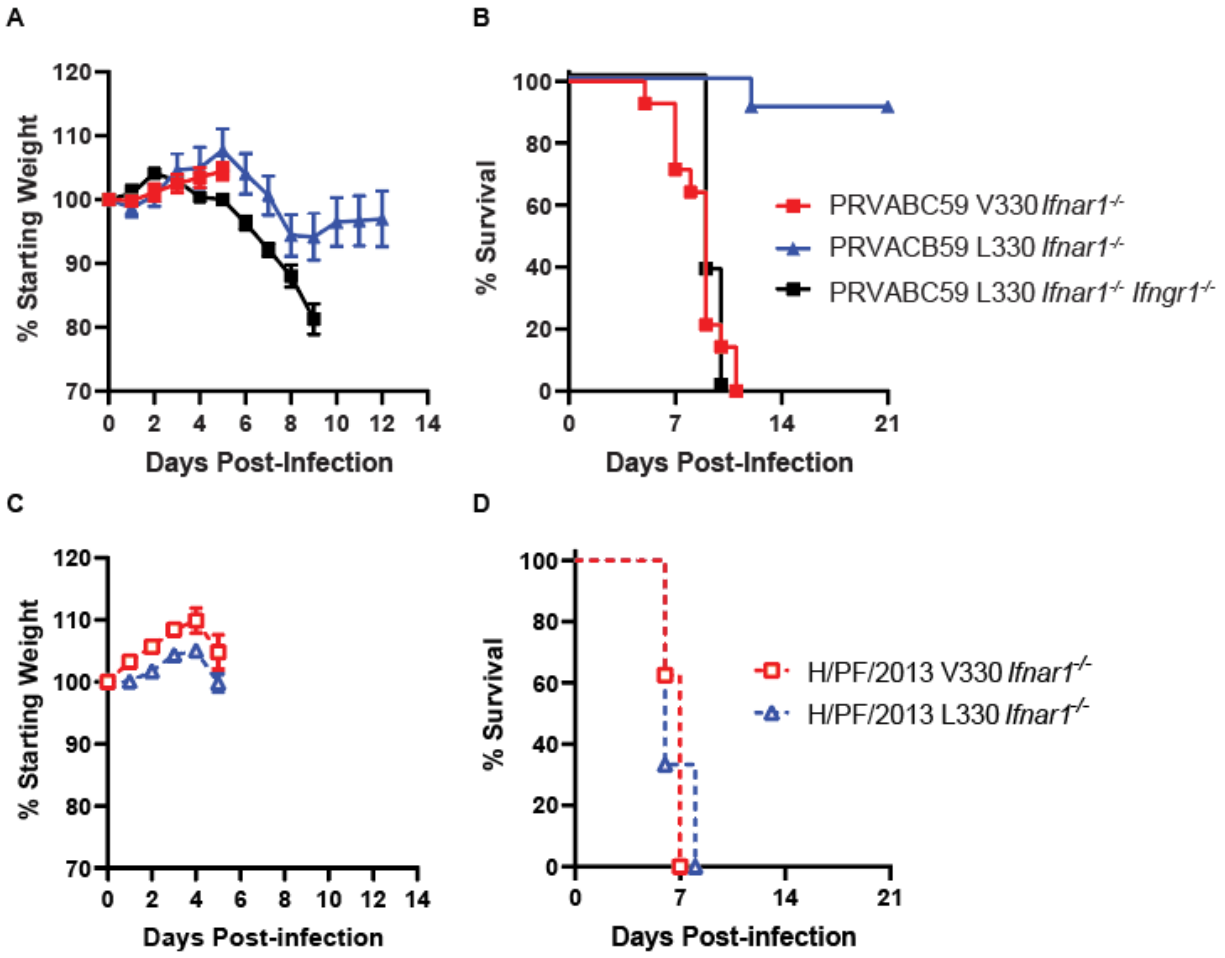

Figure 3.4. V330L substitution is attenuating on a PRVABC59 but not H/PF/2013 background in *Ifnar1*$^{-/-}$ mice. 5-to-6-week-old *Ifnar1*$^{-/-}$ or 8-week-old *Ifnar1*$^{-/-}$ *Ifngr1*$^{-/-}$ DKO mice were inoculated with 1x10^3 FFU ZIKV strain PRVABC59 or H/PF/2013 V330 or L330 viruses by a subcutaneous route. (A and C) Mice were weighed daily for 14 days. Weights are expressed as percent of body weight prior to infection and censored once one mouse in a group died. (B and D) Lethality was monitored for 21 days. Results shown are the mean ± SEM of 11-14 *Ifnar1*$^{-/-}$ mice (PRVABC59 V330 and L330), 9 *Ifnar1*$^{-/-}$ mice (H/PF/2013 V330 and L330), or 8 *Ifnar1*$^{-/-}$ *Ifngr1*$^{-/-}$ DKO mice from one or two independent experiments.

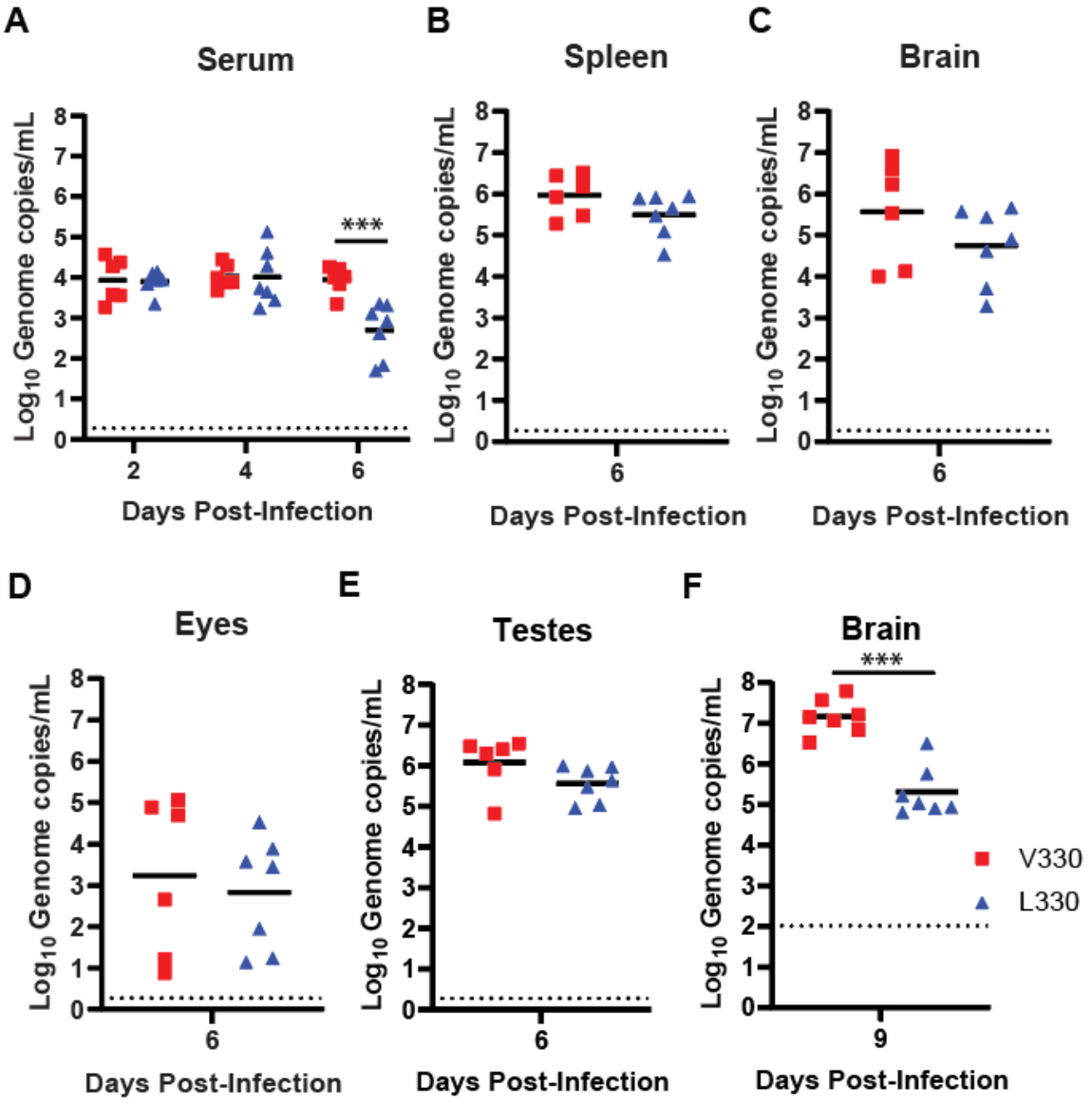

Figure 3.5. PRVABC59 330 variants produce similar viral loads. Five- to six-week-old *Ifnar1*$^{-/-}$ mice were inoculated with 1 x 10^3 FFU of ZIKV strain PRVABC59 V330 or L330 virus by a subcutaneous route in the footpad. (A) Blood was collected at 2, 4, and 6 days after infection, and ZIKV RNA in serum was measured by qRT-PCR. (B to F) Mice were euthanized 6 or 9 days after infection, perfused, and tissues were harvested. ZIKV RNA in tissue was measured by qRT-PCR. ***, P< 0.001 (unpaired 2-tailed t test). Results shown represent 2 independent experiments.

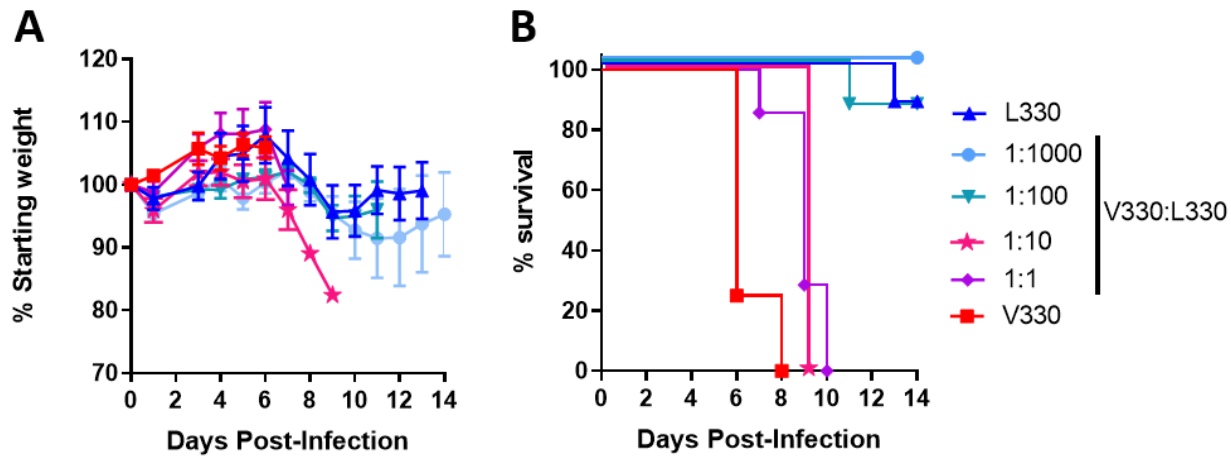

Figure 3.6. A 1:100 ratio of V330 to L330 attenuates V330 lethality. Five- to six-week-old *Ifnar1*$^{-/-}$ mice were inoculated with 1 x 10^3 FFU of ZIKV strain PRVABC59 V330, L330, or the indicated ratio of V330:L330 virus by a subcutaneous route. A. Mice were weighed daily, and weights are expressed as percentages of body weight prior to infection. B. Lethality was monitored for 14 days. Results shown are the mean values ± SEM of 4-8 *Ifnar1*$^{-/-}$ mice per virus from two or three independent experiments. Lethality was monitored for 21 days.

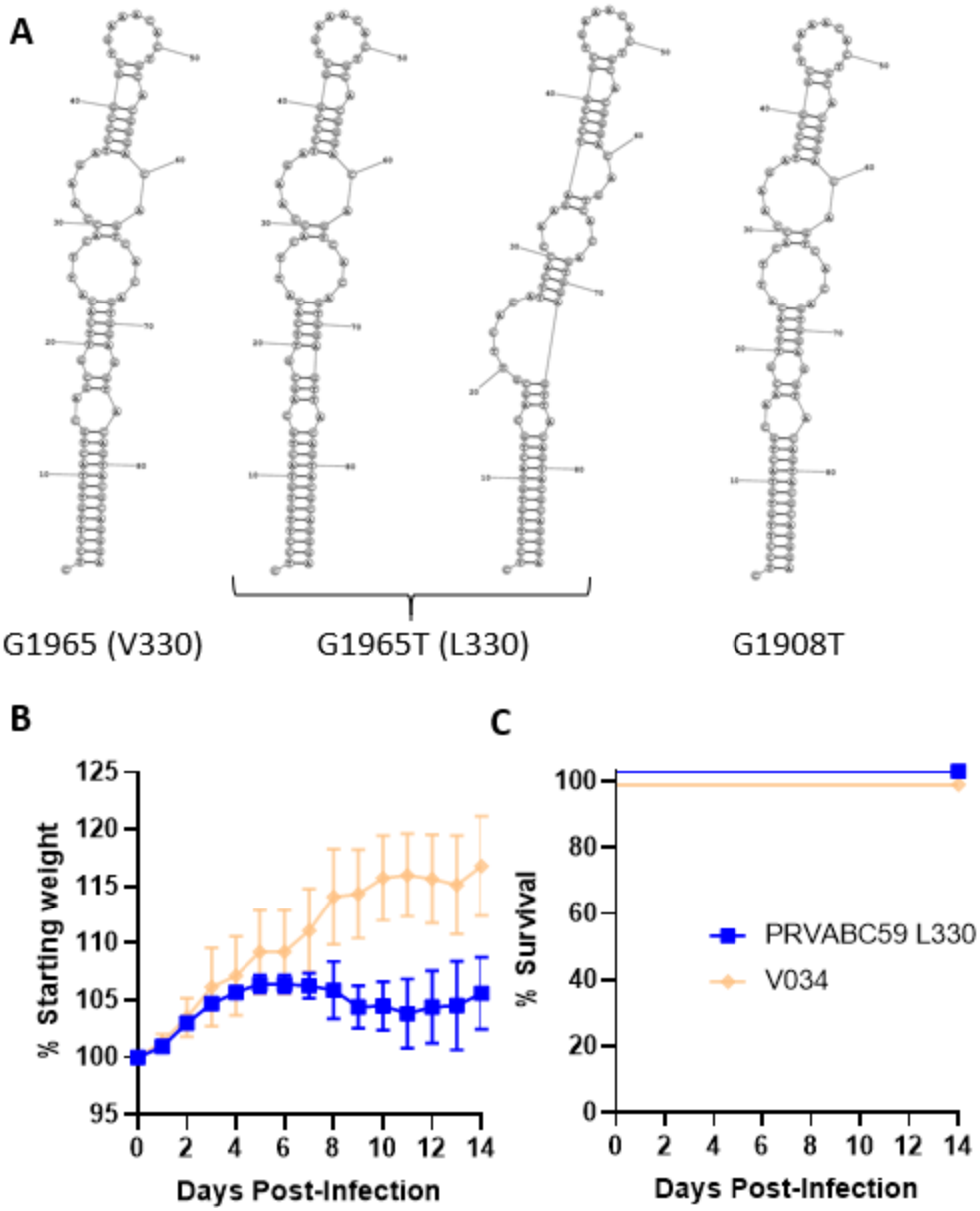

Figure 3.7. RNA secondary structure does not confer differential lethality between PRVABC59 G1965T. (A) Predicted RNA secondary structure of PRVABC59 V330 (G1965), L330 G1965T, and a compensatory mutation to restore the V330 RNA structure (G10908T) while maintaining T1965. (B and C) Five- to six-week-old *Ifnar1*$^{-/-}$ mice were inoculated with 1 x 10^3 FFU of ZIKV strain PRVABC59 L330, or PRVABC59 G1908T (V034) virus by a subcutaneous route. Mice were weighed daily, and weights are expressed as percentages of body weight prior to infection. Lethality was monitored for 14 days. Results shown are the mean values ± SEM of 4 *Ifnar1*$^{-/-}$ mice per virus in

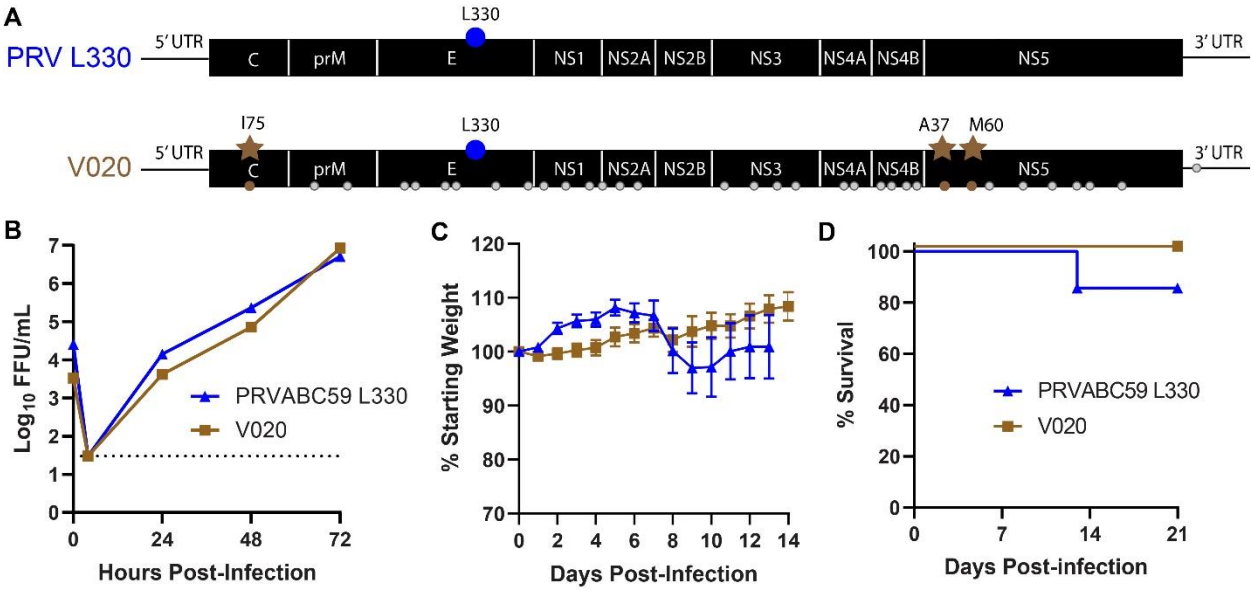

Figure 3.8. **Three amino acids that differ between H/PF/2013 and PRVABC59 do not confer lethality.** (A) Schematic of PRVABC59 L330 and V020 genomes depicts the introduction of 3 H/PF/2013 amino acids (stars); small circles indicate nucleotide differences between PRVABC59 and H/PF/2013. (B) Vero cells were infected at an MOI of 0.01 with ZIKV PRVABC59 L330 or V020. Viruses in culture supernatants were titrated by focus-forming assay. Data shown are the mean ± SEM of 9 samples from 3 independent experiments. (C and D) Five-to six-week-old *Ifnar1*$^{-/-}$ mice were inoculated with 1 x 10^3 FFU ZIKV strain PRVABC59 L330 or V020 virus by a subcutaneous route. Mice were weighed daily for 14 days, and weights are expressed as percentages of body weight prior to infection and censored once one mouse in a group died. Results shown are the mean values ± SEM of 7 mice for PRVABC59 L330 and 11 mice for V020 from four independent experiments. Lethality was monitored for 21 days.

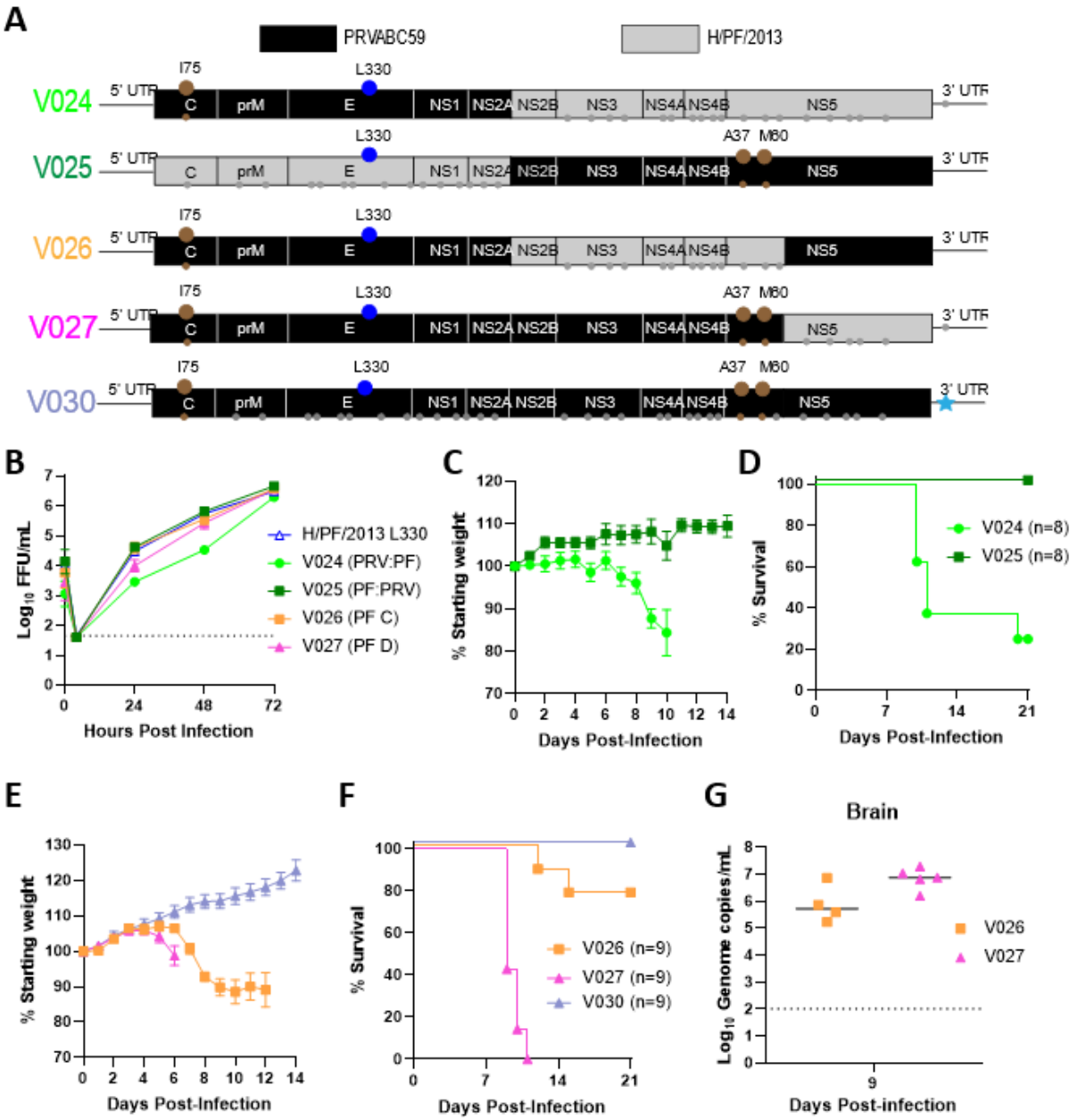

Figure 3.9. H/PF/2013 3' end confers lethality in mice. (A) Schematic of PRVABC59 and H/PF/2013 chimeric viruses (V024-V027) and a single 3' UTR nucleotide change (V031). (B) Vero cells were infected at an MOI of 0.01 with ZIKV H/PF/2013 L330, V024, V025, V026, V027, or V030. Viruses in culture supernatants were titrated by focus-forming assay. Data shown are the mean ± SEM of 9 samples from 3 independent experiments. Five-to six-week-old *Ifnar1*$^{-/-}$ mice were inoculated with 1x10^3 FFU ZIKV V024 or V025 (C and D) and V026, V027, or V030 (E and F) by a subcutaneous route. (C-F) Mice were weighed daily for 21 days and weights are expressed as percentages of body weight prior to infection. Results shown are the mean values ± SEM of the indicated number of *Ifnar1*$^{-/-}$ mice for each virus from three independent experiments. Lethality was monitored for 21 days. (G) Five-to six-week-old *Ifnar1*$^{-/-}$ mice were inoculated with 1x10^3 FFU ZIKV V026 or V027 by subcutaneous route. Mice were euthanized 9 days after infection, perfused, and tissues were harvested. ZIKV RNA in brains was measured by qRT-PCR.

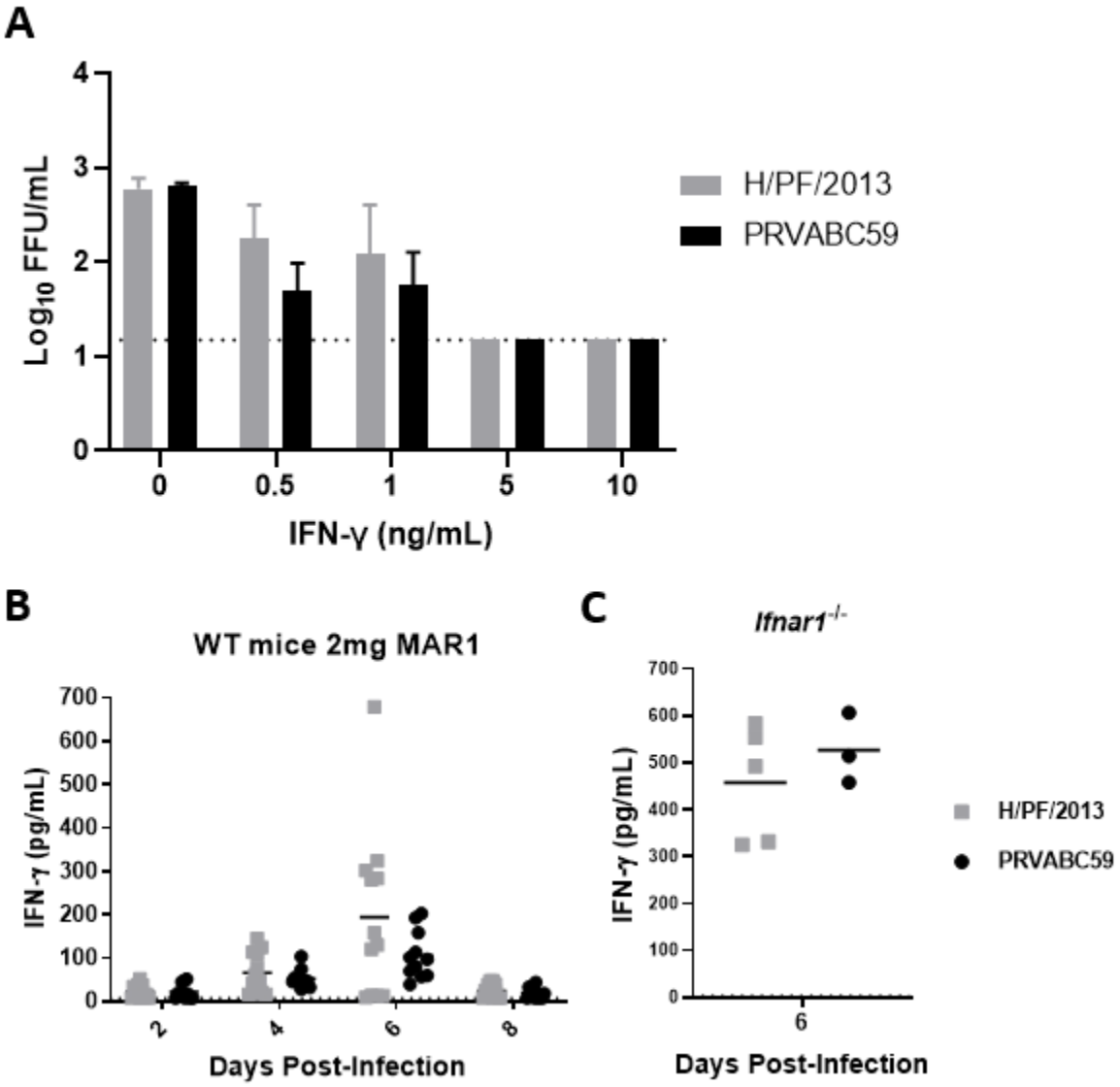

Figure 3.10. **No difference between H/PF/2013 and PRVABC59 inhibition by IFN-γ in tissue culture or in IFN-γ levels in sera of infected mice**. (A) *Ifnar1*$^{-/-}$ mouse embryonic fibroblasts were pre-treated with 0, 0.5, 1, 5, or 10ng of mouse IFN-γ for 24hrs, washed with PBS, and infected with ZIKV strain H/PF/2013 or PRVABC59 at a MOI of 0.1. Viruses in culture supernatants were titrated 24 hours-post infection by focus-forming assay. (B and C) Five- to six-week-old WT mice pretreated with 2mg IFNAR1-blocking MAb MAR1 (B) or *Ifnar1*$^{-/-}$ mice (C) were inoculated with 1 x 10^3 FFU of ZIKV strain H/PF/2013 or PRVABC59 and serum was collected at the indicated days post-infection. Serum IFN-γ levels were measured by ELISA. Data shown are the mean values ± standard errors of the means (SEM) of 4 samples from 2 independent experiments for (A), three independent experiments for (B), and one experiment for (C). Dotted lines indicate limit of detection.

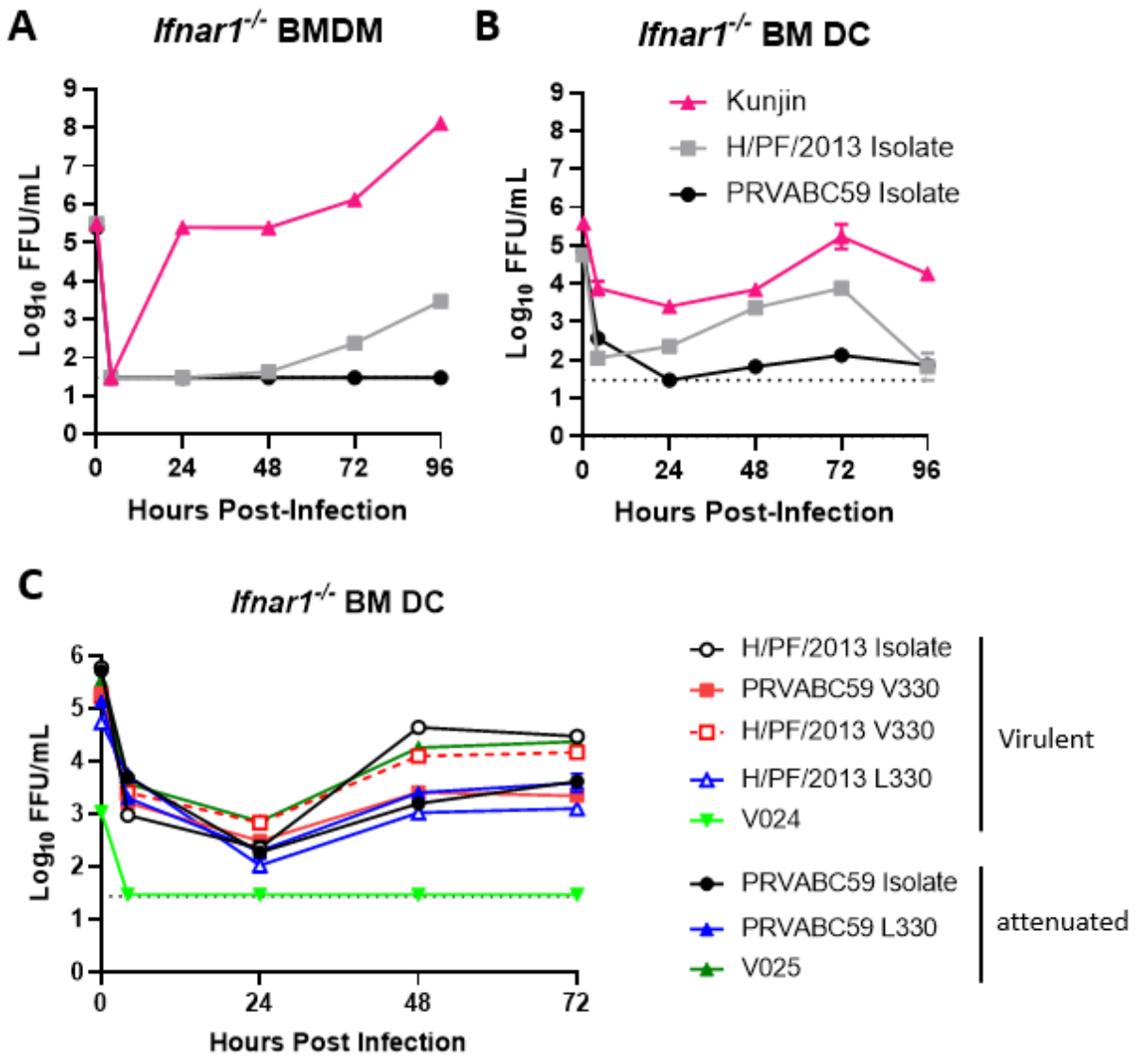

Figure 3.11. **PRVABC59 isolate is attenuated in mouse immune cells**. (A and B) *Ifnar1*$^{-/-}$ bone marrow derived macrophages (BMDM) or bone marrow derived dendritic cells (BMDC) were infected at an MOI of 0.01 with ZIKV H/PF/2013 isolate, PRVABC59 isolate, or WNV Kunjin. (C) *Ifnar1*$^{-/-}$ BMDC were infected at an MOI of 0.01 with H/PF/2013 isolate, PRAVABC59 isolate, H/PF/2013 V330 or L330, PRVABC59 V330 or L330, V024 or V025. Virulent or attenuated viruses in *Ifnar1*$^{-/-}$ mice are indicated. Viruses in culture supernatants were titrated by focus-forming assay. Data shown are the mean ± SEM of 3 samples from 1 independent experiments.

Table 3.1. **Variation at position 1965 of the genome is unique to ZIKV PRVABC59**. Viruses grown in Vero or C6/36 cells were deep sequenced by Primer ID and percent nucleotide variation is shown. The Leu codon for ZIKV is TTA and SPOV codon is CTG.

Virus	Accession #	Cell	% T (Leu)	% G (Val)
H/PF/2013	KJ776791	Vero	-	100
		C6/36	-	100
PRVABC59	KU501215	Vero	69	31
		C6/36	72	28
Paraiba	KX280026	Vero	-	100
		C6/36	-	100
FSS13025	KU955593	Vero	-	100
		C6/36	-	100
Mex-2-81	KX446950	Vero	-	100
		C6/36	-	100
Dakar 41662	KU955592.1	Vero	-	100
		C6/36	-	100
Dakar 41671	KU955595.1	Vero	-	100
		C6/36	-	100
DENV4	KC963424.1	Vero	-	100
		C6/36	-	100
SPOV	KX227370.1	Vero	100 (CTG)	-
		C6/36	100 (CTG)	-

Table 3.2. **ZIKV infectious clones and mutants**. ZIKV clones, mutants, and chimeras were generated from PRVABC59 (PRV) or H/PF/2013 (PF) strains using a quadripartite infectious clone system. The ZIKV strain origin of each backbone fragment (A-D) and any nucleotide changes and the resulting amino acid substitution are indicated. Amino acid numbering is for individual proteins (C, E, or NS5), nucleotide numbering for the complete genome. I75T is in C, V330L is in E, and V2611A and V2634M are in NS5.

Virus	Backbone Fragment				AA change[1] [NT change][2]	Mean time to death
	A	B	C	D		
H/PF/2013 V330	PF	PF	PF	PF	Consensus	6.63
H/PF/2013 L330	PF	PF	PF	PF	V330L [G1965T]	6.67
PRVABC59 V330	PRV	PRV	PRV	PRV	Consensus	8.57
PRVABC59 L330	PRV	PRV	PRV	PRV	V330L [G1965T]	*Ifnar1*$^{-/-}$ = 15 DKO = 9.38
V020	PRV	PRV	PRV	PRV	I75T [C346T], V330L [G1965T], V37A [T7939C], V60M [G8007A]	N/A
V024	PRV	PRV	PF	PF	I75T [C346T], V330L [G1965T]	12.4
V025	PF	PF	PRV	PRV	V330L [G1965T], V37A [T7939C], V60M [G8007A]	N/A
V026	PRV	PRV	PF	PRV	I75T [C346T], V330L [G1965T]	13.5
V027	PRV	PRV	PRV	PF	I75T [C346T], V330L [G1965T], V2611A [T7939C], V2634M [G8007A]	9.44

[1]Amino acid numbering for individual proteins (C, E, or NS5)

[2]Nucleotide numbering for complete genome

CHAPTER 4 – ZIKV XRRNA FACILITATE REPLICATION

4.1 Summary

Flaviviruses produce a 300–500–base long non-coding RNA, termed subgenomic flavivirus RNA (sfRNA), via structures in the 3’ untranslated region (UTR) that stall the cellular 5’-3’ exonuclease Xrn1. The generation of sfRNA by these Xrn1 resistant RNAs (xrRNA), facilitates flavivirus replication and pathogenesis by multiple mechanisms. Characterization of Zika virus (ZIKV) xrRNA by nuclear magnetic resonance (NMR) spectroscopy revealed a distinct thermodynamic fingerprint for indexing Xrn1 resistance. In this study we tested whether mutations that are predicted to destabilize the xrRNA inhibit ZIKV replication. Overall, our data suggest xrRNA activity is essential for ZIKV replication but xrRNA1 and xrRNA2 are largely redundant.

4.2 Importance

The molecular mechanisms that facilitate flavivirus transmission by mosquitoes remain unclear. Here, we demonstrate that highly structured regions in the 3’ UTR that cause the host 5’-3’ exonuclease Xrn1 to stall are essential for ZIKV replication.

4.3 Introduction

Mosquito-borne flaviviruses, such as Zika virus (ZIKV), dengue virus (DENV), West Nile virus (WNV), Japanese encephalitis virus (JEV), and yellow fever virus (YFV), as well as tick-borne flaviviruses, such as tick-borne encephalitis virus (TBEV) are important endemic and emerging human pathogens that can cause hemorrhagic fever,

encephalitis, and birth defects (1, 2, 225, 226). The geographic areas where flaviviruses are transmitted is growing, as climate change and global commerce expands the range of vector mosquitoes and ticks. The ability of flaviviruses to be transmitted by mosquitoes and ticks is crucial to their emergence and spread, but the cellular mechanisms that dictate flavivirus host range are not fully understood. Flaviviruses have a positive-sense single stranded RNA genome that encodes a single open reading frame flanked by 5’ and 3’ untranslated regions (UTR). Located at the 5’ end of the 3’ UTR are two highly structured RNA motifs called Xrn1 resistant RNAs (xrRNA1 and xrRNA2). These xrRNAs cause the host 5’-3’ exonuclease Xrn1 to stall, resulting in stable RNA degradation products known as subgenomic flavivirus RNAs (sfRNAs). These stable sfRNA have been implicated in the induction of pathogenicity in mice and cytopathicity in cell culture, evasion of the type I/II IFN response, decreased mRNA turnover, enhanced virus replication in mammalian cells, and the infection and subsequent transmission by mosquito vectors (145–152). High-resolution X-ray structures of mosquito-borne flavivirus xrRNAs have identified a core conformation that encapsulates the 5’-end of xrRNAs, yet also display variable long-range interactions for pseudoknot formation (227, 228). Our collaborators in the UNC Department of Biochemistry and Biophysics, Rhese Thompson and Dr. Qi Zhang, used nuclear magnetic resonance (NMR) spectroscopy and hydrogen-deuterium-exchange to characterize structural dynamics of ZIKV xrRNA. These thermodynamic fingerprints show that ZIKV xrRNA is orders of magnitude more stable than other RNA structures previously reported, with stability controlled by long-range pseudoknot interactions. The unprecedented stability of ZIKV xrRNA was only revealed by NMR and would not be

evident by other biochemical or biophysical approaches. NMR characterization of ZIKV xrRNA reveals a distinct thermodynamic fingerprint for indexing Xrn1 resistance. Although these methods identified xrRNA1 and xrRNA2 as highly stable RNA structures, they could not ascertain whether these structures were important for viral replication, or whether the two structures served independent functions. These xrRNAs may be redundant, meaning that xrRNA2 serves as a backup if xrRNA1 is degraded. On the other hand, they may both be important and serve distinct roles in flavivirus replication.

In this study, we evaluated the effects of xrRNA stability on ZIKV replication in tissue culture. We used site-directed mutagenesis to introduce mutations that are predicted to destabilize xrRNA1 or xrRNA2 in a previously described infectious clone of the Asian-lineage ZIKV strain H/PF/2013 (164). We show that ZIKV xrRNA mutants replicate equivalently in two mosquito cell lines, C6/36 and U4.4, but are slightly attenuated in mammalian Vero cells. Accordingly, the xrRNA mutants produced a significantly smaller infectious foci by focus-forming assay (FFA), suggesting a small difference in replication and/or impaired cell-to-cell spread. Interestingly, we were unable to recover infectious clones with mutations in both xrRNA1 and xrRNA2. Competition assays showed mutants with destabilized xrRNA1 replicate equivalently to WT virus through 72 hours post-infection (hpi). However, a destabilized xrRNA1 mutant out-competed an xrRNA2 mutant. Overall, our data suggest xrRNA activity is essential for ZIKV replication but xrRNA1 and xrRNA2 are largely redundant.

4.4 Results

Destabilized xrRNA mutants replicate equivalently to WT

To test whether mutations that destabilize xrRNA1 or xrRNA2 affect replication, we used PCR site-directed mutagenesis to introduce mutations predicted to destabilize xrRNA1 or xrRNA2 in a previously described infectious clone of the Asian-lineage ZIKV strain H/PF/2013 (164). We generated two xrRNA1 mutants: a CCCC>AAAA (V028) or a CCCC>CTCT (V029) (Fig 4.1B and C). Both mutations are predicted to disrupt the pseudoknot interaction stabilizing the xrRNA structure, with V028 being less stable than V029. To generate the xrRNA2 mutant we introduced a single base change (C>G) at position 10,946 of the genome, which is predicted to destabilize xrRNA2 (V031) (Fig 4.1D). We also attempted to generate double mutants, combining the xrRNA2 mutation of V031 with either of the two xrRNA1 mutations (from V028 or V029), but were unable to recover these viruses after 6 electroporations into Vero or C6/36 cells. Our ability to rescue xrRNA1 and xrRNA2 mutants individually but not in combination suggests a redundant essential function for these two xrRNA structures in replication of ZIKV. We compared replication of WT, V028, V029, and V031 mutants in Vero cells and mosquito cells (Fig 4.2). C6/36 and U4.4 cells both are derived from *Aedes albopictus*, but C6/36 cells have a mutation in Dicer2 that ablates the RNAi-mediated antiviral response and renders these cells highly permissive to viral infection (229). Since a known function of flavivirus sfRNA is antagonizing Dicer2 and the RNAi response in mosquitoes, we expected xrRNA mutants to be attenuated in U4.4 cells, which retain a functional RNAi response, but not compromised in C6/36 or Vero cells. However, V028, V029, and V031 mutants replicated equivalently to WT virus in C6/36 and U4.4 cells in multi-step growth

curves. Interestingly, in Vero cells, V028 and V031 replicated to statistically significant lower viral titers at 48 and 72 hpi compared to WT virus. V029 replicated to lower levels than WT, but the difference was not statistically significant.

xrRNA mutants produce smaller infectious foci in Vero cells

In accordance with our Vero cell growth curve data, all xrRNA mutants produced significantly smaller foci by focus-forming assay (FFA) on Vero cells (Fig 4.3A). The wild-type virus produced foci ~3.2 x 10^4 μm^2, whereas V028, V029, and V031 produced foci ~9 x 10^3 μm^2 (Fig 4.3B). These data suggest that even though a similar amount of virus is being released into the supernatants (Fig 4.2), the xrRNA mutants may have a modest replication defect not evident in the supernatant titers measured on a $\log_{10}$ scale. We also measured whether there was a difference in genome to FFU ratio between the xrRNA mutants and wild-type virus. WT virus had a ratio of 805, V028 a ratio of 1527, V029 a ratio of 1665, and V031 a ratio of 7638 (Fig 3C). These data suggest the WT virus is more efficiently packaged, followed by V028, V029, and then V031.We next considered whether a competition experiment might reveal a replication impairment not evident in the growth curves. We tested whether wild-type virus would out-compete xrRNA1 mutants (V028 and V029) and whether there is a fitness difference between destabilized xrRNA1 (V028) and destabilized xrRNA2 (V031) (Fig 4.4). We infected U4.4 cells at a total MOI of 0.1 with a 1:1 ratio of WT:V028, WT:V029, or V028:V031 (Fig 4.4A) and assessed the relative proportions of each virus by inspecting chromatograms from Sanger sequencing of the inoculum and of culture supernatants at 72hpi. The proportions of WT:V028 and WT:V029 remained similar at 72 hpi, compared to the inoculum, suggesting that the destabilization of xrRNA1 did not

reduce viral fitness. We found similar results upon testing an inoculum with a 10:1 ratio of V028:WT or V029:WT (Fig 4.4B). In contrast, a destabilized xrRNA1 mutant (V028) out-competed an xrRNA2 mutant (V031), as the V028 genotype dominated at 72 hpi, whether at a starting ratio of 1:1 or 10:1 V031:V028.

4.5 Discussion

The molecular determinants of arbovirus transmission by mosquitoes are not fully understood, and few interactions between arboviruses and their vectors have been described in molecular detail. Flaviviruses produce a 300–500–base long stable RNA degradation product (sfRNA) that results from the stalling of the host 5'-3' exonuclease Xrn1 on RNA structures (xrRNAs) in the 3'UTR. sfRNAs facilitate flavivirus replication and pathogenesis by multiple mechanisms (144, 230). Here, we investigated the effect of mutations predicted to destabilize two structures in the ZIKV 3'UTR, xrRNA1 and xrRNA2. We found that destabilizing either xrRNA1 or xrRNA2 did not significantly affect ZIKV replication as measured in a multi-step growth curve in C6/36 and U4.4 cells, but may cause a modest replication defect in Vero cells as seen by a significantly smaller foci by FFA. The inability to recover double mutant viruses with mutations in both xrRNA1 and xrRNA2 suggests that xrRNA activity is essential for ZIKV replication and that these two structures serve largely redundant functions. In a multi-step growth curve, all three xrRNA mutants replicated equivalently. However, a competition assay revealed that a mutant with a severely destabilized xrRNA1 (V028) was more fit than a mutant destabilizing xrRNA2 (V031), suggesting that the functions of xrRNA1 and xrRNA2 are not identical and that xrRNA2 activity may be more important than xrRNA1 activity for ZIKV replication. Future studies will assess additional xrRNA1 and xrRNA2

mutants with variable stability (as determined by NMR thermodynamic fingerprint analysis), to titrate the relative activity of xrRNA1 and xrRNA2 and thereby better determine their distinct contributions to flavivirus replication. Future studies also will measure sfRNA levels during infection to confirm that xrRNA destabilizing mutations have the expected effect on sfRNA production. While some 3' UTR RNA structures are conserved, there is variation among flaviviruses in the set of xrRNAs present in the 3'UTR and their thermodynamic fingerprints. Furthermore, tick-borne flaviviruses are predicted to have distinct xrRNA structures, though there are no experimentally validated xrRNA structures for tick-borne flaviviruses. Altogether, the combination of new methods for determining thermodynamic fingerprints that predict xrRNA stability along with molecular virology approaches to assess xrRNA function creates an opportunity for new discoveries in the molecular mechanisms that mediate flavivirus replication, transmission, and pathogenesis.

4.6 Materials and methods

Cells and viruses. Vero, C6/36, and U4.4 cells were maintained in Dulbecco's modified Eagle medium (DMEM) containing 5% heat-inactivated fetal bovine serum (FBS) and L-glutamine at 37^{o}C with 5% CO_2 for Vero cells or 28^{o}C without CO_2 for C6/36 and U4.4 cells. Virus stocks were grown in Vero (African green monkey kidney epithelial) cells. Virus stocks were titered on Vero cells by focus-forming assay (FFA) (193). For multi-step growth analysis, cells were infected at a MOI of 0.1 and incubated at 37^{o}C with 5% CO_2 (Vero cells) or 28^{o}C without CO_2 (C6/36 and U4.4 cells). Samples of infected cell culture supernatant were collected at 4, 24, 48 and 72 hpi and stored at -80^{o}C for virus titration. Virus quantification was performed by FFA on Vero cells.

Duplicates of serial 10-fold dilutions of virus in viral growth medium (DMEM containing 2% FBS and 20 mM HEPES) were applied to Vero cells in 96-well plates and incubated at 37^{o}C with 5% CO_2 for 1 hr. Cells were then overlaid with 1% methylcellulose in minimum essential medium Eagle (MEM). Infected cell foci were detected 42-46 hpi. Following fixation with 2% paraformaldehyde for 1 hr at room temperature, plates were incubated with 500 ng/ml of flavivirus cross-reactive mouse MAb E60 (194) for 2 hr at room temperature or overnight at 4^{o}C. After incubation at room temperate for 2 hr with a 1:5,000 dilution of horseradish peroxidase (HRP)-conjugated goat anti-mouse IgG (Sigma), foci were detected by addition of TrueBlue substrate (KPL). Foci were quantified with a CTL Immunospot instrument.

ZIKV infectious clone design and mutagenesis. We generated xrRNA mutants in a previously described infectious clone of ZIKV strain H/PF/2013 (164). Site-directed mutagenesis was used to introduce the mutations CCCC>AAAA at position 10450-10453 of the genome (V028), CCCC>CTCT at position 10451 and 10453 of the genome (V029), and C10496G (V031) in the 3' UTR to destabilize xrRNA secondary structures. Supernatants from electroporated C6/36 cells were harvested after 6 to 7 days and passaged once on Vero cells to generate virus stocks. Virus stocks were titered by FFA on Vero cells. Restriction enzymes and Phusion High Fidelity PCR kit were obtained from New England BioLabs. SuperScript III First Strand Synthesis kit was obtained from Invitrogen. Oligonucleotide primers and probes for DNA amplification, qRT-PCR, and sequencing were obtained from Sigma and IDT. The mMachine T7 Ultra transcription kit was obtained from Ambion.

Competition assay. U4.4 cells were plated at 1 x 10^6 cells/well in 6-well plates. Cells were inoculated with a 1:1 or 10:1 mixture of viruses at a total MOI of 0.1 in triplicate wells. Viral supernatants were harvested at 72 hours post-infection. Viral RNA was extracted from all samples using Viral RNA mini kit (Qiagen), followed by cDNA synthesis with SuperScript III First Strand Synthesis kit (Invitrogen), then PCR to amplify the 3' UTR. PCR products were run on a 1% agarose gel and DNA bands were extracted using a DNA gel extraction kit (Zymo). Amplicons were sequenced by Sanger sequencing through Genewiz. Chromatograms were viewed in SnapGene.

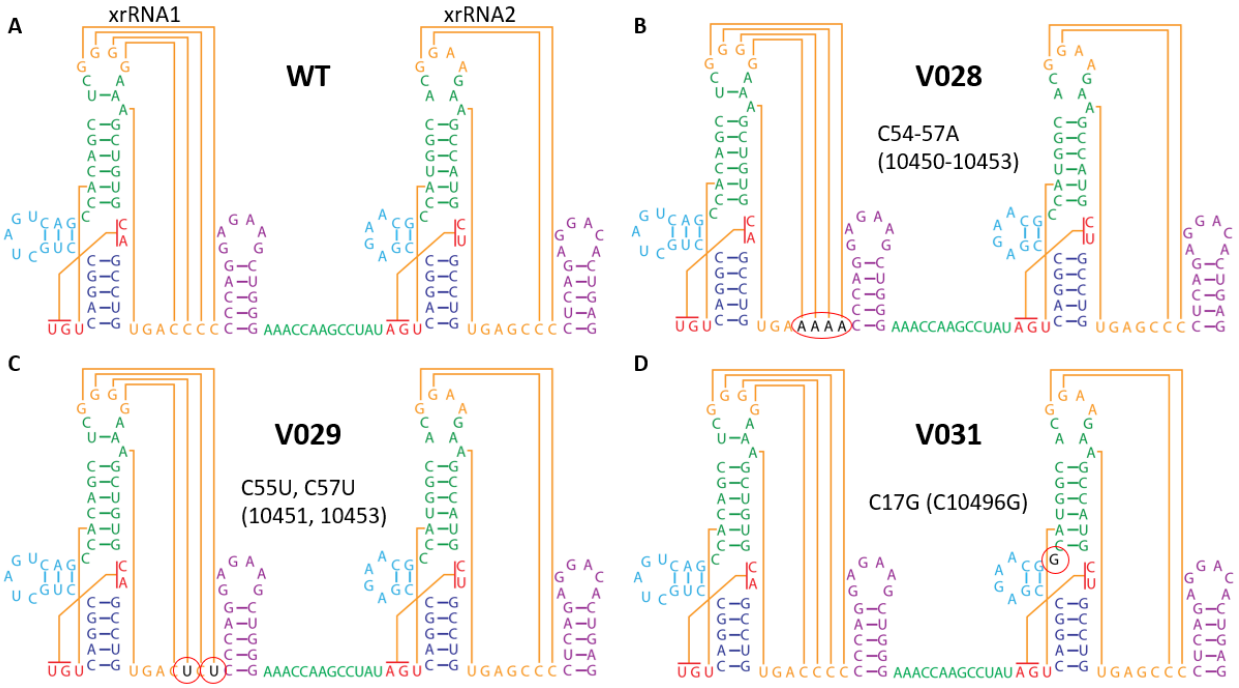

Figure 4.1. ZIKV xrRNA1 and xrRNA2 and destabilizing mutations. (A) WT xrRNA1 and xrRNA2 structures (B) Mutations (CCCC>AAAA) made to generate V028, which severely destabilizes the xrRNA1 pseudoknot (C) mutations (CCCC>CTCT) made to generate V029, which modestly destabilizes the xrRNA1 pseudoknot and (D) mutation (C10496G) made to generate V031, which destabilizes xrRNA2. Mutations are highlighted with red circles.

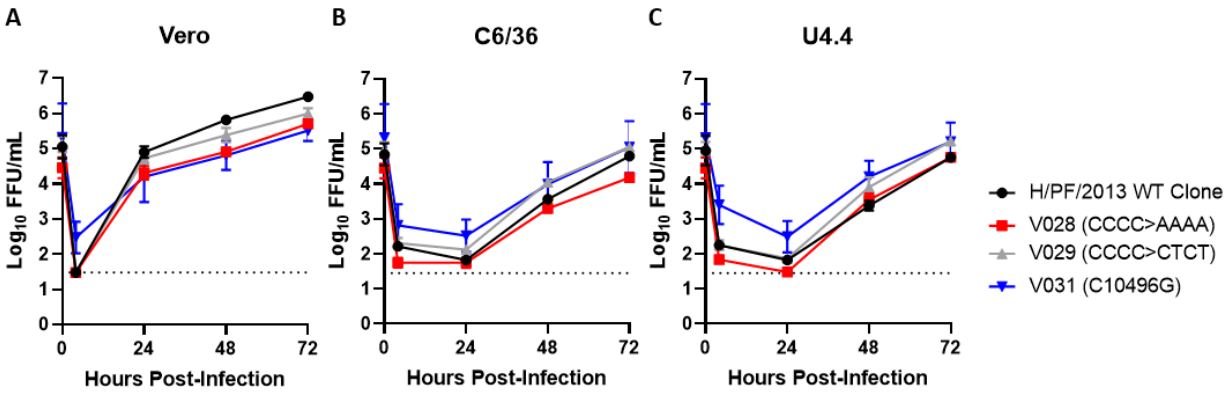

Figure 4.2. xrRNA mutants replicate similarly to WT virus in multi-step growth curves. Vero (A), C6/36 (B), or U4.4 (C) cells were infected at a MOI of 0.1 with ZIKV H/PF/2013 WT clone, V028, V029, or V031. Viruses in culture supernatants were titered by focus-forming assay. Data shown are the mean values ± standard errors of the means (SEM) of 12 samples from 4 independent experiments for WT, V028, and V029 and 6 samples from two independent experiments for V031.

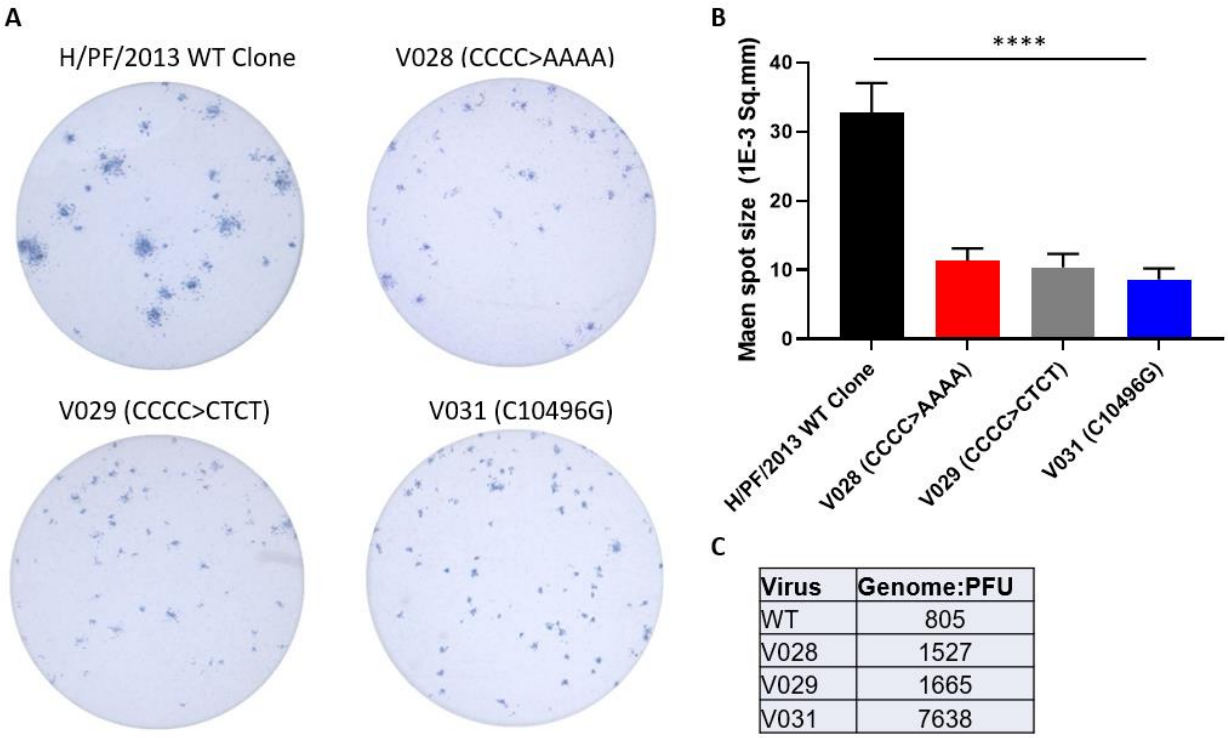

C

Virus	Genome:PFU
WT	805
V028	1527
V029	1665
V031	7638

Figure 4.3. xrRNA mutants produce smaller infectious foci. (A) Vero cells infected with the indicated viruses were fixed 44hpi and infected cell foci visualized by antibody staining. (B) Area of WT, V028, V029, or V031 infectious foci. (C) Genome:PFU ratio for each virus. Data shown are the mean values ± standard errors of the means (SEM) of 9 wells from one FFA.

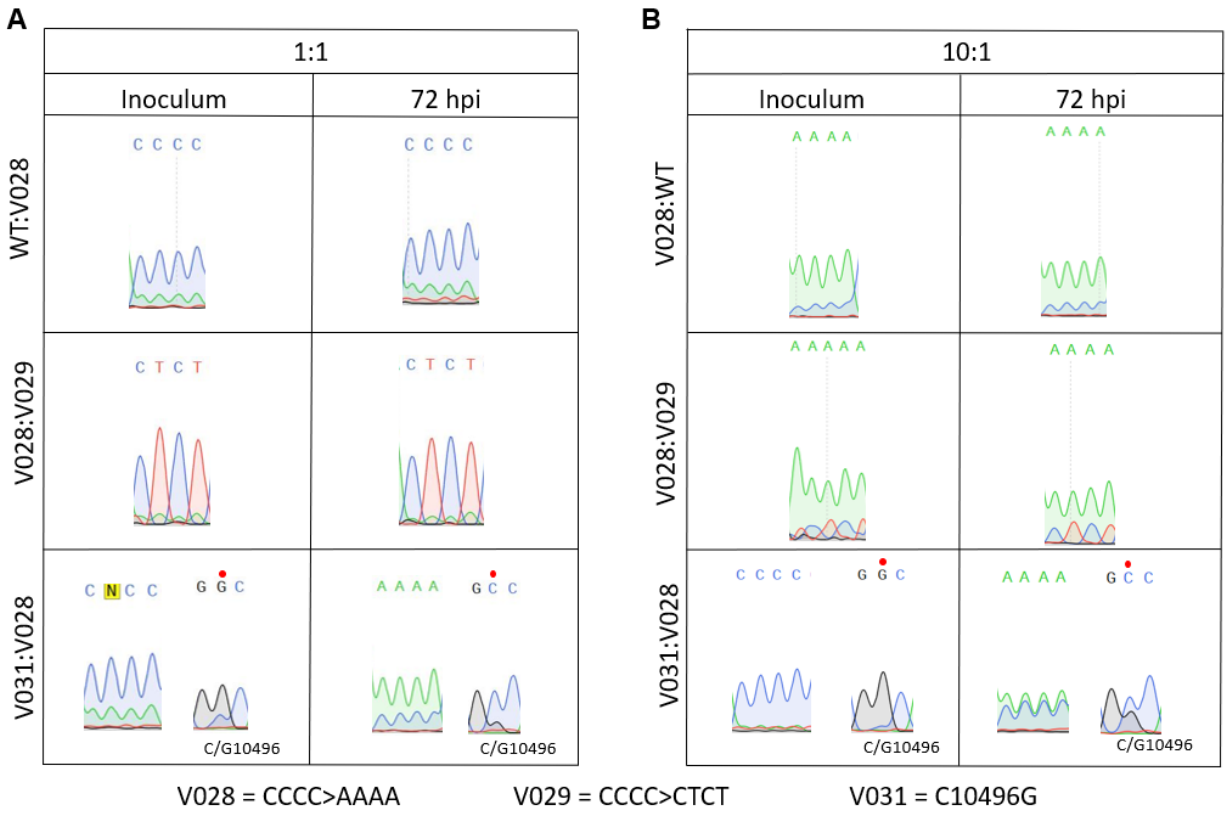

Figure 4.4. xrRNA mutants retain fitness in competition assays. U4.4 cells were infected with the indicated pair of viruses at a 1:1 (A) or 10:1 (B) ratio at a total MOI of 0.1. Input virus and 72hpi supernatant virus were analyzed by Sanger sequencing, with chromatograms indicating the mixture of sequences present. The experiments were performed in triplicate, and one representative chromatogram is shown. Red dots indicate C/G10496 peak.

CHAPTER 5 – DISCUSSION

5.1 Overview of reported ZIKV genetic determinants of pathogenesis

How ZIKV changed from a seemingly mild virus to a human pathogen capable of causing severe clinical manifestations remains unclear. Since the emergence of ZIKV into the Western Hemisphere there has been a surge in ZIKV related research to elucidate the cause of the unexpected clinical manifestations, including Guillain-Barré syndrome and congenital Zika syndrome (2, 34, 39, 40). The 2015-2016 ZIKV outbreak in Brazil was orders of magnitude larger than prior outbreaks, and large outbreaks allow us to observe rare outcomes. It is likely that at least some of the new disease phenotypes are due to the size of the outbreak and extensive surveillance, however it may not explain everything. Phylogenetic analyses of ZIKV isolates from past and recent outbreaks have revealed amino acid differences between historic African-lineage strains and the contemporary Asian-lineage strains that are currently circulating in the Western Hemisphere (41, 155, 179). Several of these amino acid differences have been implicated in transmission, immune suppression, and enhanced disease.

A single amino acid substitution in prM (S139N) has been shown to increase ZIKV replication in human neural progenitor cells (NPCs) and may contribute to a more severe microcephalic phenotype in mice (159). This residue is exposed on the surface of the immature virion and homology modelling from the crystal structure of the DENV

pr peptide showed that the 139 residue is located within a loop region that connects two β-strands (127). In neonatal mouse models, the contemporary Asian strains, with N139, were substantially more virulent than the 2010 Cambodian FSS13035 strain, which has S139 (159). Direct injection of the viruses into the lateral ventricle of embryonic mouse brains led to microcephaly for both the Asian and the contemporary American strains; however, the contemporary strains caused a more severe microcephalic phenotype than the Cambodian strain. In a reverse genetics experiments, the single amino acid substitution of S139N was also shown to increase the neurovirulence of the Cambodian strain, whereas the N139S reciprocal mutant on the contemporary GZ01 strain, isolated in 2016 from a patient in Venezuela (231), had decreased neurovirulence in neonatal mice compared with the parental strain (159). Consistent with these findings, the S139N mutant virus also showed increased replication in embryonic mouse brains and enhanced tropism for mouse and human NPCs (159). This report suggested that the S139N substitution does not function as the sole contributor to microcephaly, but it may increase ZIKV capability to cause a severe microcephalic phenotype. However, others found that this mutation is not essential for fetal pathology in a mouse transplacental transmission model (180). Thus, we should be critical of such pronouncements that a single mutation is the sole cause for the microcephalic phenotype, as it can cause harm to public health. For example, health authorities in India advised their community not to worry about a 2016-2017 ZIKV outbreak after sequencing revealed the ZIKV strain circulating did not have the S139N substitution (154).

A second genetic change implicated in ZIKV pathogenesis is an A188V amino acid substitution located at the dimer interface of the NS1 protein (127, 157). The

secretion of the NS1 protein into the host circulatory system has been shown to be required for the efficient infection of mosquitoes when they feed on the infected host (232). Compared with the parental Cambodian FSS13025 strain, the A188V mutant led to the secretion of more NS1 and increased virus transmission from mice to mosquitoes in both a mouse–mosquito acquisition model and a mosquito– mouse–mosquito transmission model (157). The mechanism by which the A188V mutation increases NS1 secretion remains unclear. However, the presence of A188V in NS1 led to reduced phosphorylation of TBK1 and the subsequent inhibition of the production of interferon-β (IFN-β) (158), which may facilitate viral replication.

Genetic changes could also have downstream effects on post-translational modifications, such as protein glycosylation. Contemporary Asian-lineage strains possess an intact E glycosylation motif at amino acid N154. In contrast, many historic African-lineage ZIKV strains lack this motif (29, 174), though limited sampling of African ZIKV strains precludes robust conclusions about how common non-glycosylated viruses are in nature. E glycosylation plays a role in attachment and infectivity for DENV (83), WNV (67, 81, 96), and JEV (84) and has been associated with enhanced mosquito transmission and/or increased virulence and neuroinvasion in vertebrates for other flaviviruses (82, 95, 105, 107, 114, 116–118, 161, 162). ZIKV strain MR766 lacking E glycosylation due to a 4 amino acid deletion or a N154A substitution produced lower viral loads in serum and brains of A129 mice compared to glycosylated virus (98). Similarly, a Cambodian ZIKV strain lacking E glycosylation due to a N154Q substitution also resulted in decreased viral loads in serum of A129 mice compared to the WT glycosylated virus (99).

In addition to genetic changes between historic and contemporary ZIKV strains, there are reported virulence differences between closely related contemporary strains, as well as effects of variants within a single stain on virulence in mice. Many different ZIKV strains have been isolated during the recent outbreaks and distributed to research labs around the world (e.g. ~12 contemporary strains available from BEI resources). All contemporary ZIKV strains share high nucleotide identity and minimal amino acid differences throughout their genomes and thus have been used largely interchangeably to draw conclusions about the pathogenesis of contemporary ZIKV strains. However, not all contemporary ZIKV strains share the same pathogenic outcome in mice. A ZIKV strain isolated in 2013 from French Polynesia (H/PF/2013) and a strain isolated in 2015 from Brazil (Paraiba_01/2015) both have been shown to cause 100% lethality in *Ifnar1*$^{-/-}$ mice (134, 135). In contrast, a ZIKV strain isolated in 2010 from Cambodia (FSS13025) was only 20-30% lethal in *Stat2*$^{-/-}$ or *Ifnar1*$^{-/-}$ mice, and a strain isolated in 2015 from Puerto Rico (PRVABC59) was not lethal in either mouse model (136). However, the H/PF/2013, Paraiba_01/2015, FSS13025, and PRVABC59 strains were uniformly lethal in *Ifnar1*$^{-/-}$ *Ifngr1*$^{-/-}$ DKO mice (137–140). These data indicate ZIKV strain-specific contributions to virulence in mice, and highlight that differences in pathogenesis may not be evident in highly susceptible models, such as *Ifnar1*$^{-/-}$ *Ifngr1*$^{-/-}$ DKO mice. Strain characteristics such as virus source (human versus mosquito), disease outcome, geographic origin, or year of isolation, do not obviously correlate with pathogenic phenotype in mice, though such relationships might be revealed by comparing a larger number of strains under identical experimental conditions (136, 166, 216).

Two variants, V330L in the E protein and W98G in the NS1 protein, were identified in ZIKV PRVABC59 strain that affected virulence in mice. The V330L substitution attenuated the virus in *Ifnar1*$^{-/-}$ *Ifngr1*$^{-/-}$ DKO mice, increasing the mean time to death, and the addition of the NS1 W98G substitution further attenuated the virus, highlighting the ability of this variant to act epistatically to modulate virulence.

Another variant in a different protein of another ZIKV strain has been reported to confer differential lethality in mice (233). Paraiba_01/2015, isolated from a patient serum sample in 2015, and a ZIKV strain isolated from a fetal brain in Rio Grande do Norte Natal (RGN) in 2015, showed differential lethality in *Ifnar1*$^{-/-}$ mice. Deep sequencing revealed a variant (A177V) in the NS2A protein of Paraiba_01/2015 that conferred lethality in *Ifnar1*$^{-/-}$ mice. They further showed that the A177V substitution reduced host innate immune responses and viral-induced apoptosis *in vitro*.

These reports highlight the ability of small genetic changes between different viruses, as well as variants within a single virus strain, to have significant phenotypic effects on viral replication and pathogenesis.

5.2 My contributions to investigating the role of E glycosylation in ZIKV pathogenesis

To further understand the role of ZIKV E protein glycosylation in tissue tropism and pathogenesis, I measured viral replication *in vitro* and *in vivo*, as well as studied viral attachment and infectivity, using glycosylated and non-glycosylated ZIKV from both African and Asian lineage strains. I used a reverse genetics platform to generate novel ZIKV mutants to better understand how E protein glycosylation facilitates infectivity and pathogenesis. My results indicated that both Asian and African lineage ZIKV strains

lacking E glycosylation sustained lower serum and tissue viral loads compared to WT virus. These results are consistent with other reports of a role for E glycosylation in mediating ZIKV virulence (98, 99). Notably, even though I found that ZIKV lacking E glycosylation resulted in lower viral loads in the serum, eyes, and brains compared to glycosylated virus, I observed similar viral loads in the spleen and testes, consistent with a previous report that glycosylated and non-glycosylated ZIKV strain MR766 sustained similar viral loads in the spleen and liver (98), suggesting these tissues harbor cell types that can be targeted by the virus regardless of E glycosylation status. Furthermore, my observation that the ZIKV H/PF/2013 N154Q mutation was maintained upon intracranial inoculation, but selected against after subcutaneous inoculation, suggests that glycosylation provides a selective advantage to ZIKV in peripheral tissues but not within the brain.

E glycosylation likely facilitates attachment to and infection of lectin-expressing cells, including CD14+ monocytes that are targets of ZIKV in humans (182–185). DC-SIGN and DC-SIGNR are among several attachment factors described for flaviviruses such as DENV (83, 177, 186), JEV (82, 84), and WNV (67, 81, 96) as well as for ZIKV (85, 187, 188), though it is less clear which lectins or other attachment factors actually mediate ZIKV infection in mice or humans (189–191). Though mice do not have clear DC-SIGN or DC-SIGNR orthologs, they have eight DC-SIGN homologs clustered within the same genomic region (182). I found that E glycosylation facilitates infectivity of lectin expressing cells. However, unexpectedly, I found DC-SIGNR was able to augment infection by the N154Q mutant even in the absence of E glycosylation, whereas the T156I mutant showed little to no infectivity in DC-SIGNR-expressing cells.

The different infection efficiencies of the two non-glycosylated mutants on Raji DC-SIGNR cells could result from less efficient maturation of N154Q virions compared to T156I virions; in this case, glycosylated prM on immature N154Q virions may partially complement the loss of E glycosylation (188). Alternatively, the difference in infection efficiencies in DC-SIGNR cells could indicate a specific role for Gln 154 or Thr 156 independent of glycosylation, perhaps through modulation of the glycan loop and resulting effects on attachment and fusion (188, 191). Different amino acid substitutions at E154/156 of WNV conferred distinct avian host and vector competence phenotypes independent of E-protein glycosylation status (101).

I also showed that the location of the glycosylation on ZIKV E is important for viral replication in cell culture and in mice. A single N67 (D67N/N154Q) or double N67/N154 (D67N) glycosylated ZIKV were attenuated in Vero and A549 cells. ZIKV D67N also was attenuated in C6/36 cells, however the D67N/N154Q virus replicated equivalently to WT in C6/36 cells. In mice, both the D67N/N154Q and D67N viruses were attenuated, replicating to lower levels than the N154Q, non-glycosylated virus. These data may suggest that the location per se of the glycosylation on E is important, or distinct glycans may be added at the different positions, which in turn could influence attachment and infectivity. The distinct glycosylation patterns also may impact the antibody repertoire produced in response to infection.

Overall, my findings have contributed to our understanding of the role of E glycosylation in ZIKV pathogenesis. My work demonstrates a role for E glycosylation in ZIKV pathogenesis, possibly by facilitating attachment and infection of lectin-expressing leukocytes, and shows that the location of ZIKV E glycosylation, specifically at position

N154, is important for replication in certain cell types in tissue culture and for replication in mice.

5.3 My contributions to elucidating ZIKV strain genetic determinants of virulence in mice

To investigate differences in ZIKV viral strain virulence, I used a reverse genetics platform to systematically generate novel ZIKV mutants and chimeric viruses of two closely related ZIKV strains (H/PF/2013 and PRVABC59). I identified and described two distinct genetic determinants of ZIKV strain-specific virulence; notably, both phenotypes were evident in *Ifnar1*$^{-/-}$ mice but masked in *Ifnar1*$^{-/-}$ *Ifngr1*$^{-/-}$ DKO mice.

ZIKV replicates poorly in mice with intact IFN-αβ signaling, due to an inability to antagonize murine STAT2 and STING (131, 132, 217, 218). Thus, mouse pathogenesis studies typically use mice deficient in IFN-αβ signaling and both *Ifnar1*$^{-/-}$ and *Ifnar1*$^{-/-}$ *Ifngr1*$^{-/-}$ DKO mice are widely used in the field (137, 139, 166, 219–221). However, *Ifnar1*$^{-/-}$ *Ifngr1*$^{-/-}$ DKO mice develop more severe disease and succumb more rapidly to ZIKV infection, independent of the inoculation route, compared to *Ifnar1*$^{-/-}$ mice (139, 222).

I identified a variant (V330L) in the PRVABC59 virus stock that was not present in any of the other ZIKV strains we had in lab (Table 3.1). I found that the Val to Leu substitution in E was sufficient to attenuate on the PRVABC59 genetic backbone (10% lethality with PRVABC59 L330, compared to 100% lethality with PRVABC59 V330 in *Ifnar1*$^{-/-}$ mice), but this same substitution had no effect on the H/PF/2013 backbone (the L330 virus remained 100% lethal). The mechanism by which a Val to Leu substitution in domain III of the envelope protein would attenuate virulence, and why this would be specific to the PRVABC59 strain remains unclear. Apart from V330L variation, the

PRVABC59 and H/PF/2013 strains have identical E protein amino acid sequences, so the L330 substitution would be expected to have a similar effect on both strains. An alternative explanation is that the distinct virulence phenotypes are determined not by the V330L change in the E protein, but by the effect of the G1965T nucleotide change on RNA structure or other RNA functions. Unfortunately, the codons in this position preclude generating mutants that would distinguish the effects of nucleotide and amino acid changes at this site. Though I was able to generate a compensatory mutant that was predicted to restore the RNA structure of the attenuated L330 virus to that of the virulent V330 virus, while maintaining the Leu at position 330, this compensatory mutation did not restore virulence. However, these results do not exclude a role for RNA structure in the differential lethality of the V330 and L330 viruses, as the RNA structure prediction software may not be accurate, and/or we cannot exclude that the Ala to Pro change independently attenuates the compensatory mutant.

Since the L330 substitution was not attenuating on the H/PF/2013 background, and the other three amino acids that differ between the two strains did not have an effect on virulence, I sought to identify which of the other 31 nucleotide differences between the two strains were responsible for the differential lethality. Using chimeric viruses, I was able to narrow down the virulence determinant to 6 nucleotide differences in the 3' region of the H/PF/2013 genome (including NS5 and the 3'UTR), though the mechanism by which these nucleotide changes modulate virulence remains unclear. Possible mechanisms could include effects on RNA structure and/or post-transcriptional modifications, though these changes did not obviously disrupt predicted RNA structures or predicted m6A modification sites. And though the one nucleotide difference that falls 6

nucleotides upstream of the first stem loop structure in the 3' UTR was not solely able to confer lethality, it is plausible that one or more of the other nucleotide changes between PRVABC59 and H/PF/2013 could impact the production, stability, or function of subgenomic flavivirus RNA (sfRNA). sfRNA is a stable RNA degradation product resulting from stalling of the cellular 5'–3'-exoribonuclease Xrn1 on RNA structures in the flavivirus 3' UTR, which has been shown to modulate replication and virulence of ZIKV and other flaviviruses (227, 230, 234–236).

Altogether, my work identifies a large and previously unreported difference in virulence between two commonly used ZIKV strains, in two widely used mouse models of ZIKV pathogenesis (*Ifnar1*$^{-/-}$ and *Ifnar1*$^{-/-}$ *Ifngr1*$^{-/-}$ DKO mice). My data further describe the effect of a previously reported variant in the PRVABC59 strain that appears to be attenuating only on the PRVABC59 genetic background. I also identified a novel role for non-coding changes as ZIKV virulence determinants, suggesting possible effects on RNA structure or post-transcriptional modifications. My results highlight that even very closely related virus strains can produce significantly different pathogenic phenotypes in common laboratory models.

5.4 My contributions to evaluating the effect of xrRNA stability on ZIKV replication

To test whether mutations that destabilize xrRNA1 or xrRNA2 affect replication, I used PCR site-directed mutagenesis to introduce mutations predicted to destabilize xrRNA1 or xrRNA2 in a previously described infectious clone of the Asian-lineage ZIKV strain H/PF/2013 (164). I found that mutations in xrRNA1 or xrRNA2 do not significantly affect the production of infectious virus particles into the supernatants, but may cause a slight replication defect as seen by a significantly smaller foci by FFA. However,

competition assays revealed no detectible replication advantage of WT virus over xrRNA1 or xrRNA2 mutants, though a destabilized xrRNA1 mutant replicated better than an xrRNA2 mutant. The inability to recover double mutant virus with mutations in both xrRNA1 and xrRNA2 suggests these structures are essential for ZIKV replication. Overall, my data suggests xrRNA activity is essential for ZIKV replication but xrRNA1 and xrRNA2 are largely redundant.

5.5 Future directions for the flavivirus field

Results presented in this dissertation have contributed to expanding our knowledge of genetic determinants of ZIKV pathogenesis. Along with concurrent work defining other genetic determinants of ZIKV infection, replication, and pathogenesis in related strains, as well as other flaviviruses, we are continually learning more about flavivirus biology and the molecular determinants that impact pathogenesis.

Despite all the progress we have made towards unraveling which aspects of the viral genome are important, and how genetic changes may lead to more pathogenic viruses, we still have much to learn. Understanding how ZIKV is able to spread through sexual transmission, cause neurological disease and congenital Zika syndrome are not fully understood. Elucidating further how the location of E glycosylation can impact what kind of glycan is added, from different cell types, and how that glycan impacts the next round of replication will further our understanding of ZIKV biology. Also understanding how distinct glycans on E can impact the antibody repertoire elicited in response to infection, especially in DENV endemic regions where most individuals have existing antibodies to DENV that may cross react with ZIKV, is of great importance. Unraveling which viral genetic changes may have epistatic effects or impact long range RNA- RNA

interactions that affect viral replication and pathogenies requires more research. Further studies to understand the extent to which ZIKV sfRNA interact with host and vector proteins to modulate infection and replications are required. Continuous fundamental research of both the viruses and the hosts will elucidate these complex relationships between flaviviruses and the hosts they infect. Uncovering the answers to these questions will further fill in our existing knowledge gaps in ZIKV biology and pathogenesis.

REFERENCES

1. Gould EA, Solomon T. 2008. Pathogenic flaviviruses. Lancet 371:500–09.

2. Pierson TC, Diamond MS. 2018. The emergence of Zika virus and its new clinical syndromes. Nature 560:573–581.

3. George TL, Harrigan RJ, Lamanna JA, Desante DF, Saracco JF, Smith TB. 2015. Persistent impacts of West Nile virus on North American bird populations. Proc Natl Acad Sci U S A 112:14290–14294.

4. Angenvoort J, Brault AC, Bowen RA, Groschup MH. 2013. West Nile viral infection of equids. Vet Microbiol 167:168–180.

5. Marm Kilpatrick A, Wheeler SS. 2019. Impact of West Nile Virus on Bird Populations: Limited Lasting Effects, Evidence for Recovery, and Gaps in Our Understanding of Impacts on Ecosystems. J Med Entomol 56:1491–1497.

6. Benzarti E, Linden A, Desmecht D, Garigliany M. 2019. Mosquito-borne epornitic flaviviruses: An update and review. J Gen Virol 100:119–132.

7. Ng WC, Soto-Acosta R, Bradrick SS, Garcia-Blanco MA, Ooi EE. 2017. The 5' and 3' untranslated regions of the flaviviral genome. Viruses 9:1–14.

8. Chambers, T.J.; Hahn, C.S.; Galler, R.; Rice C. 1990. Flavivirus genome organization, expression, and replication. Annu Rev Microbiol 44:649–688.

9. Roby JA, Setoh YX, Hall RA, Khromykh AA. 2015. Post-translational regulation and modifications of flavivirus structural proteins. J Gen Virol 96:1551–1569.

10. Slon Campos JL, Mongkolsapaya J, Screaton GR. 2018. The immune response against flaviviruses. Nat Immunol 19:1189–1198.

11. Konishi E, Mason PW. 1993. Proper maturation of the Japanese encephalitis

virus envelope glycoprotein requires cosynthesis with the premembrane protein. J Virol 67:1672–1675.

12. Kuhn RJ, Zhang W, Rossmann MG, Pletnev S V, Corver J, Lenches E, Jones CT, Mukhopadhyay S, Chipman PR, Strauss EG, Baker TS, Strauss JH. 2002. Structure of dengue virus: Implications for flavivirus organization, maturation, and fusion. Cell 108:717–725.

13. Zhang Y, Zhang W, Ogata S, Clements D, Strauss JH, Timothy S, Kuhn RJ, Rossmann MG. 2014. Conformational changes of flavivirus E protein. Structure 12:1607–1618.

14. Kostyuchenko VA, Lim EXY, Zhang S, Fibriansah G, Ng TS, Ooi JSG, Shi J, Lok SM. 2016. Structure of the thermally stable Zika virus. Nature 533:425–428.

15. Felix A. Rey *, Franz X. Heinz t, Christian Mandlt CK t BSCH. 1995. The envelope glycoprotein from tick-borne encephalitis virus at 2 A resolution. Nature 375:291–298.

16. Heinz FX, Allison SL. 2001. The machinery for flavivirus fusion with host cell membranes. Curr Opin Microbiol 4:450–455.

17. Weissenhorn W, Dessen A, Calder LJ, Harrison SC, Skehel JJ, Wiley DC. 1999. Structural basis for membrane fusion by enveloped viruses. Mol Membr Biol 16:3–9.

18. Yorgo Modis, Steven Ogata, David Clements and SCH. 2003. A ligand-binding pocket in the dengue virus envelope glycoprotein. PNAS 100:6989–6991.

19. Pöhlmann, Simmons G. 2013. Viral Entry into Host Cells, p. 83–94. *In* .

20. Pierson TC, Diamond MS. 2012. Degrees of maturity: The complex structure and biology of flaviviruses. Curr Opin Virol 2:168–175.

21. Long Li, Shee-Mei Lok, I-Mei Yu, Ying Zhang, Richard J. Kuhn, Jue Chen MGR.

2008. The Flavivirus Precursor Membrane-Envelope Protein Complex: Structure and Maturation. Science 319:1830–1835.

22. Stadler K, Allison SL, Schalich J, Heinz FX. 1997. Proteolytic activation of tick-borne encephalitis virus by furin. J Virol 71:8475–81.

23. Hayes EB. 2009. Zika virus outside Africa. Emerg Infect Dis 15:1347–1350.

24. Dick GWA. 1952. Zika Virus I. Trans R Soc Trop Med Hyg 34:282.

25. Fagbami AH. 1979. Zika virus infections in Nigeria: Virological and seroepidemiological investigations in Oyo State. J Hyg (Lond) 83:213–219.

26. McCrae AWR, Kirya BG. 1982. Yellow fever and Zika virus epizootics and enzootics in Uganda. Trans R Soc Trop Med Hyg 76:552–562.

27. Darwish MA, Hoogstraal H, Roberts TJ, Ahmed IP, Omar F. 1983. A sero-epidemiological survey for certain arboviruses (Togaviridae) in Pakistan. Trans R Soc Trop Med Hyg 77:442–445.

28. Olson JG, Ksiazek TG, Suhandiman G, Triwibowo V. 1981. Zika virus, a cause of fever in central java, indonesia. Trans R Soc Trop Med Hyg 75:389–393.

29. Faye O, Freire CCM, Iamarino A, Faye O, de Oliveira JVC, Diallo M, Zanotto PMA, Sall AA. 2014. Molecular Evolution of Zika Virus during Its Emergence in the 20th Century. PLoS Negl Trop Dis 8:36.

30. Duffy M. Chen T.Hancock T. Powers A. Kool J. Lanciotti R. Pretrick M. 2009. Zika Virus Outbreak on Yap Island, Federated States of Micronesia. N Engl J Med 360:2536–2543.

31. Heang V, Yasuda CY, Sovann L, Haddow AD, da Rosa APT, Tesh RB, Kasper MR. 2012. Zika virus infection, Cambodia, 2010. Emerg Infect Dis 18:349–351.

32. Cao-Lormeau V-M, Roche C, Teissier A, Robin E, Mallet HP, Sall AA, Musso D. 2014. Zika Vírus, French Polynesia, South Pacific. Emerg Infect Dis 20:1572–4.

33. Campos GS, Bandeira AC, Sardi SI. 2015. Zika virus outbreak, Bahia, Brazil. Emerg Infect Dis 21:1885–1886.

34. Oehler E, Watrin L, Larre P, Leparc-go I, Lastère S, Valour F, Baudouin L, Mallet HP, Musso D. 2014. Zika virus infection complicated by Guillain-Barré syndrome – case report , French Polynesia , December 2013. Euro Surveill 19:20720.

35. Munoz LS, Parra B, Pardo CA. 2017. Neurological Implications of Zika Virus Infection in Adults. J Infect Dis 216:897–905.

36. Zanluca C, De Melo VCA, Mosimann ALP, Dos Santos GIV, dos Santos CND, Luz K. 2015. First report of autochthonous transmission of Zika virus in Brazil. Mem Inst Oswaldo Cruz 110:569–572.

37. Metsky HC, Matranga CB, Wohl S, Schaffner SF, Freije CA, Winnicki SM, West K, Qu J, Baniecki ML, Gladden-young A, Lin AE, Tomkins-tinch CH, Ye SH, Park DJ, Luo CY, Barnes KG, Shah RR, Chak B, Barbosa-lima G, Delatorre E, Vieira YR, Paul LM, Tan AL, Barcellona CM, Porcelli MC, Vasquez C, Cannons AC, Cone MR, Hogan KN, Brown CM, Hennigan S, Sabina B, Scotland S, Montoya MCM, Diana P. 2017. Zika virus evolution and spread in the Americas. Nat Publ Gr 546:411–415.

38. Huo Y, Aboud K, Kang H, Cutting LE, Bennett A. 2017. Establishment and cryptic transmission of Zika virus in Brazil and the Americas. Nature 546:1–13.

39. Coyne CB, Lazear HM. 2016. Zika virus-reigniting the TORCH. Nat Rev Microbiol 14:707–715.

40. Brady OJ, Osgood-Zimmerman A, Kassebaum NJ, Ray SE, de Araújo VEM, da Nóbrega AA, Frutuoso LC V., Lecca RCR, Stevens A, Zoca de Oliveira B, de Lima JM, Bogoch II, Mayaud P, Jaenisch T, Mokdad AH, Murray CJL, Hay SI, Reiner RC, Marinho F. 2019. The association between Zika virus infection and microcephaly in Brazil 2015–2017: An observational analysis of over 4 million births. PLOS Med 16:e1002755.

41. Pettersson JHO, Eldholm V, Seligman SJ, Lundkvist ??ke, Falconar AK, Gaunt MW, Musso D, Nougair??de A, Charrel R, Gould EA, De Lamballerie X. 2016. How did zika virus emerge in the Pacific Islands and Latin America? MBio 7:e01239-16.

42. Aebi M. 2013. N-linked protein glycosylation in the ER. Biochim Biophys Acta - Mol Cell Res 1833:2430–2437.

43. Mukhopadhyay S, Kuhn RJ, Rossmann MG. 2005. A STRUCTURAL PERSPECTIVE OF THE FLAVIVIRUSLIFE CYCLE. Nat Rev Microbiol 3:13–22.

44. Mandl CW, Guirakhoo F, Holzmann H, Heinz FX, Kunz C. 1989. Antigenic structure of the flavivirus envelope protein E at the molecular level, using tick-borne encephalitis virus as a model. J Virol 63:564–571.

45. Winkler G, Heinz FX, Kunz C. 1987. Studies on the glycosylation of flavivirus E proteins and the role of carbohydrate in antigenic structure. Virology 159:237–243.

46. Post PR, Santos CND, Carvalho R, Cruz ACR, Ricet CM, Galler R. 1992. Heterogeneity in envelope protein sequence and N-Linked glycosylation among yellow fever virus vaccine strains. Virology 188:160–167.

47. Johnson AJ, Guirakhoo F, Roehhrig JT. 1994. The Envelope Glycoproteins of Dengue 1 and Dengue 2 Viruses Grown in Mosquito Cells Differ in Their Utilization of Potential Glycosylation Sites. Virology 203:241–249.

48. Alsaleh K, Khou C, Frenkiel MP, Lecollinet S, Vàzquez A, de Arellano ER, Després P, Pardigon N. 2016. The E glycoprotein plays an essential role in the high pathogenicity of European-Mediterranean IS98 strain of West Nile virus. Virology 492:53–65.

49. Berthet N, Nakouné E, Kamgang B, Selekon B, Descorps-Declère S, Gessain A, Manuguerra JC, Kazanji M. 2014. Molecular characterization of three zika flaviviruses obtained from sylvatic mosquitoes in the Central African Republic. Vector-Borne Zoonotic Dis 14:862–865.

50. Yun S, Song B, Frank JC, Julander JG, Polejaeva IA, Davies CJ, White KL, Lee Y. 2016. Complete Genome Sequences of Three Historically Important , Spatiotemporally Distinct , and Genetically Divergent Strains of Zika Virus. Genome Announc 4:1–4.

51. Ladner JT, Wiley MR, Prieto K, Yasuda CY, Nagle E, Kasper MR, Reyes D, Vasilakis N, Heang V, Weaver SC, Haddow A, Tesh RB, Sovann L, Palacios G. 2016. Complete Genome Sequences of Five Zika Virus Isolates. Genome Announc 4:6–7.

52. Carbaugh DL, Baric RS, Lazear HM. 2019. Envelope protein glycosylation mediates Zika virus pathogenesis. J Virol 93:1–16.

53. Lee E, Leang SK, Davidson A, Lobigs M. 2010. Both E Protein Glycans Adversely Affect Dengue Virus Infectivity but Are Beneficial for Virion Release. J Virol 84:5171–5180.

54. Rush JS. 2004. Transmembrane movement of a water-soluble analogue of mannosylphosphoryldolichol is mediated by an endoplasmic reticulum protein. J Cell Biol 130:529–536.

55. Rush JS, Waechter CJ, Wolucka B, Ouerfelli O, van Leyen K. 2002. Transbilayer movement of Glc-P-dolichol and its function as a glucosyl donor: protein-mediated transport of a water-soluble analog into sealed ER vesicles from pig brain. Glycobiology 8:1195–1205.

56. Chen W, Zhong Y, Su R, Qi H, Deng W, Sun Y, Ma T, Wang X, Yu H, Wang X, Li Z. 2017. N-glycan profiles in H9N2 avian influenza viruses from chicken eggs and human embryonic lung fibroblast cells. J Virol Methods 249:10–20.

57. An Y, Parsons LM, Jankowska E, Melnyk D, Joshi M, Cipollo F. 2019. crossm N - Glycosylation of Seasonal Influenza Vaccine Hemagglutinins : J Virol 93:1–22.

58. Rendic D, Wilson IBH, Paschinger K. 2008. The Glycosylation Capacity of Insect Cells. ChemInform 39:7–21.

59. Shi X, Jarvis D. 2007. Protein N-Glycosylation in the Baculovirus-Insect Cell System. Curr Drug Targets 8:1116–1125.

60. Hsieh P, Robbins PW. 1984. Regulation of Asparagine-linked Oligosaccharide Processing 259:2375–2382.

61. Hsieh P, Rosner MR, Robbins PW. 1983. Host-dependent variation of asparagine-linked oligosaccharides at individual glycosylation sites of sindbis virus glycoproteins. J Biol Chem 258:2548–2554.

62. Butters TD, Hughes RC, Vischer P. 1981. Steps in the biosynthesis of mosquito cell membrane glycoproteins and the effects of tunicamycin. BBA - Biomembr 640:672–686.

63. Yap SSL, Nguyen-Khuong T, Rudd PM, Alonso S. 2017. Dengue virus glycosylation: What do we know? Front Microbiol 8:1–16.

64. Khoo US, Chan KYK, Chan VSF, Lin CLS. 2008. DC-SIGN and L-SIGN: The SIGNs for infection. J Mol Med 86:861–874.

65. Geijtenbeek TBH, Kwon DS, Torensma R, Van Vliet SJ, Van Duijnhoven GCF, Middel J, Cornelissen ILMHA, Nottet HSLM, KewalRamani VN, Littman DR, Figdor CG, Van Kooyk Y. 2000. DC-SIGN, a dendritic cell-specific HIV-1-binding protein that enhances trans-infection of T cells. Cell 100:587–597.

66. Curtis BM, Scharnowske S, Watson AJ. 1992. Sequence and expression of a membrane-associated C-type lectin that exhibits CD4-independent binding of human immunodeficiency virus envelope glycoprotein gp120. Proc Natl Acad Sci U S A 89:8356–8360.

67. Martina BEE, Koraka P, van den Doel P, Rimmelzwaan GF, Haagmans BL, Osterhaus ADME. 2008. DC-SIGN enhances infection of cells with glycosylated West Nile virus in vitro and virus replication in human dendritic cells induces production of IFN-α and TNF-α. Virus Res 135:64–71.

68. Lozach PY, Lortat-Jacob H, De Lacroix de Lavalette A, Staropoli I, Foung S,

Amara A, Houlès C, Fieschi F, Schwartz O, Virelizier JL, Arenzana-Seisdedos F, Altmeyer R. 2003. DC-SIGN and L-SIGN are high affinity binding receptors for hepatitis C virus glycoprotein E2. J Biol Chem 278:20358–20366.

69. Alvarez CP, Lasala F, Carrillo J, Muñiz O, Corbí AL, Delgado R. 2002. C-Type Lectins DC-SIGN and L-SIGN Mediate Cellular Entry by Ebola Virus in cis and in trans. J Virol 76:6841–6844.

70. Gardner JP, Durso RJ, Arrigale RR, Donovan GP, Maddon PJ, Dragic T, Olson WC. 2003. L-SIGN (CD 209L) is a liver-specific capture receptor for hepatitis C virus. Proc Natl Acad Sci U S A 100:4498–4503.

71. Halary F, Amara A, Lortat-Jacob H, Messerle M, Delaunay T, Houlès C, Fieschi F, Arenzana-Seisdedos F, Moreau JF, Déchanet-Merville J. 2002. Human Cytomegalovirus binding to DC-SIGN is required for dendritic cell infection and target cell trans-infection. Immunity 17:653–664.

72. Klimstra WB, Nangle EM, Smith MS, Yurochko AD, Ryman KD. 2004. DC-SIGN and L-SIGN Can Act as Attachment Receptors for Alphaviruses and Distinguish between Mosquito Cell- and Mammalian Cell-Derived Viruses. J Virol 78:7862–7862.

73. Birx DL, Trumpfheller C, Finke J, Schlesinger S, Granelli-Piperno A, Eller MA, Burgess TH, Sun W, Sarasombath S, Pattanapanyasat K, Steinman RM, Marovich MA, Tassaneetrithep B. 2003. DC-SIGN (CD209) Mediates Dengue Virus Infection of Human Dendritic Cells. J Exp Med 197:823–829.

74. Navarro-Sanchez E, Altmeyer R, Amara A, Schwartz O, Fieschi F, Virelizier JL, Arenzana-Seisdedos F, Desprès P. 2003. Dendritic-cell-specific ICAM3-grabbing non-integrin is essential for the productive infection of human dendritic cells by mosquito-cell-derived dengue viruses. EMBO Rep 4:723–728.

75. Marzi A, Gramberg T, Simmons G, Möller P, Rennekamp AJ, Krumbiegel M, Geier M, Eisemann J, Turza N, Saunier B, Steinkasserer A, Becker S, Bates P, Hofmann H, Pöhlmann S. 2004. DC-SIGN and DC-SIGNR Interact with the Glycoprotein of Marburg Virus and the S Protein of Severe Acute Respiratory Syndrome Coronavirus. J Virol 78:12090–12095.

76. Goo L, Demaso CR, Pelc RS, Kuhn RJ, Pierson TC, Ledgerwood JE, Graham BS. 2018. The Zika virus envelope protein glycan loop regulates virion antigenicity. Virology 515:191–202.

77. Pokidysheva E, Hendrickson WA, Battisti AJ, Bator-Kelly CM, Zhang Y, Rossmann MG, Gregorio GG, Chipman PR, Kuhn RJ, Xiao C. 2006. Cryo-EM Reconstruction of Dengue Virus in Complex with the Carbohydrate Recognition Domain of DC-SIGN. Cell 124:485–493.

78. Balzarini J, Neyts J, Schols D, Alen MMF, Dallmeier K. 2012. Crucial role of the N-glycans on the viral E-envelope glycoprotein in DC-SIGN-mediated dengue virus infection. Antiviral Res 96:280–287.

79. Davis CW, Mattei LM, Nguyen HY, Ansarah-Sobrinho C, Doms RW, Pierson TC. 2006. The location of asparagine-linked glycans on west nile virions controls their interactions with CD209 (dendritic cell-specific ICAM-3 grabbing nonintegrin). J Biol Chem 281:37183–37194.

80. Hacker K, White L, Silva AM De. 2009. N -Linked glycans on dengue viruses grown in mammalian and insect cells. J Gen Virol 90:2097–2106.

81. Davis CW, Nguyen H-Y, Hanna SL, Sánchez MD, Doms RW, Pierson TC. 2006. West Nile virus discriminates between DC-SIGN and DC-SIGNR for cellular attachment and infection. J Virol 80:1290–301.

82. Liang J-J, Chou M-W, Lin Y-L. 2018. DC-SIGN Binding Contributed by an Extra N-Linked Glycosylation on Japanese Encephalitis Virus Envelope Protein Reduces the Ability of Viral Brain Invasion. Front Cell Infect Microbiol 8:239.

83. Mondotte JA, Lozach P-Y, Amara A, Gamarnik A V. 2007. Essential Role of Dengue Virus Envelope Protein N Glycosylation at Asparagine-67 during Viral Propagation. J Virol 81:7136–7148.

84. Wang P, Hu K, Luo S, Zhang M, Deng X, Li C, Jin W, Hu B, He S, Li M, Du T, Xiao G, Zhang B, Liu Y, Hu Q. 2016. DC-SIGN as an attachment factor mediates Japanese encephalitis virus infection of human dendritic cells via interaction with a single high-mannose residue of viral E glycoprotein. Virology 488:108–119.

85. Gong D, Zhang T-H, Zhao D, Du Y, Chapa TJ, Shi Y, Wang L, Contreras D, Zeng G, Shi P-Y, Wu T-T, Arumugaswami V, Sun R. 2018. High-Throughput Fitness Profiling of Zika Virus E Protein Reveals Different Roles for Glycosylation during Infection of Mammalian and Mosquito Cells. iScience 1:97–111.

86. Hamel R, Dejarnac O, Wichit S, Ekchariyawat P, Neyret A, Luplertlop N, Perera-Lecoin M, Surasombatpattana P, Talignani L, Thomas F, Cao-Lormeau V-M, Choumet V, Briant L, Desprès P, Amara A, Yssel H, Missé D. 2015. Biology of Zika Virus Infection in Human Skin Cells. J Virol 89:8880–8896.

87. Dejnirattisai W, Wongwiwat W, Supasa S, Zhang X, Dai X, Rouvinsky A, Jumnainsong A, Edwards C, Quyen NTH, Duangchinda T, Grimes JM, Tsai WY, Lai CY, Wang WK, Malasit P, Farrar J, Simmons CP, Zhou ZH, Rey FA, Mongkolsapaya J, Screaton GR. 2015. A new class of highly potent, broadly neutralizing antibodies isolated from viremic patients infected with dengue virus. Nat Immunol 16:170–177.

88. Sommerstein R, Flatz L, Remy MM, Malinge P, Magistrelli G, Fischer N, Sahin M, Bergthaler A, Igonet S, ter Meulen J, Rigo D, Meda P, Rabah N, Coutard B, Bowden TA, Lambert PH, Siegrist CA, Pinschewer DD. 2015. Arenavirus Glycan Shield Promotes Neutralizing Antibody Evasion and Protracted Infection. PLoS Pathog 11:1–25.

89. Korber B, Gaschen B, Yusim K, Thakallapally R, Kesmir C, Detours V. 2001. Evolutionary and immunological implications of contemporary HIV-1 variation. Br Med Bull 58:19–42.

90. Ma X, Lu M, Gorman J, Terry DS, Hong X, Zhou Z, Zhao H, Altman RB, Arthos J, Blanchard SC, Kwong PD, Munro JB, Mothes W. 2018. HIV-1 env trimer opens through an asymmetric intermediate in which individual protomers adopt distinct conformations. Elife 7:1–18.

91. Ward AB, Wilson IA. 2017. The HIV-1 envelope glycoprotein structure: nailing down a moving target. Immunol Rev 275:21–32.

92. Wyatt R, Kwong PD, Desjardins E, Sweet RW, Robinson J, Hendrickson W a, Sodroski JG. 1998. The antigenic structure of the HIV gp120 envelope glycoprotein 393:705–711.

93. Watanabe Y, Bowden TA, Wilson IA, Crispin M. 2019. Exploitation of glycosylation in enveloped virus pathobiology. Biochim Biophys Acta - Gen Subj 1863:1480–1497.

94. Goto A, Yoshii K, Obara M, Ueki T, Mizutani T, Kariwa H, Takashima I. 2005. Role of the N-linked glycans of the prM and E envelope proteins in tick-borne encephalitis virus particle secretion. Vaccine 23:3043–3052.

95. Yoshii K, Yanagihara N, Ishizuka M, Sakai M, Kariwa H. 2013. N-linked glycan in tick-borne encephalitis virus envelope protein affects viral secretion in mammalian cells, but not in tick cells. J Gen Virol 94:2249–2258.

96. Hanna SL, Pierson TC, Sanchez MD, Ahmed AA, Murtadha MM, Doms RW. 2005. N-linked glycosylation of west nile virus envelope proteins influences particle assembly and infectivity. J Virol 79:13262–74.

97. Mossenta M, Marchese S, Poggianella M, Slon Campos JL, Burrone OR. 2017. Role of N-glycosylation on Zika virus E protein secretion, viral assembly and infectivity. Biochem Biophys Res Commun 492:579–586.

98. Annamalai AS, Pattnaik A, Sahoo BR. 2017. Zika Virus Encoding Nonglycosylated Envelope Protein Is Attenuated and Defective in Neuroinvasion. J Virol 91:1–16.

99. Fontes-garfias CR, Shan C, Luo H, Wang T, Scott C. 2017. Functional Analysis of Glycosylation of Zika Virus Article Functional Analysis of Glycosylation of Zika Virus Envelope Protein. CellReports 21:1180–1190.

100. Bryant JE, Calvert AE, Mesesan K, Crabtree MB, Volpe KE, Silengo S, Kinney RM, Huang CYH, Miller BR, Roehrig JT. 2007. Glycosylation of the dengue 2 virus E protein at N67 is critical for virus growth in vitro but not for growth in intrathoracically inoculated Aedes aegypti mosquitoes. Virology 366:415–423.

101. Maharaj PD, Langevin SA, Bolling BG, Andrade CC, Engle XA, Ramey WN, Bosco-Lauth A, Bowen RA, Sanders TA, Huang CY-H, Reisen WK, Brault AC. 2019. N-linked glycosylation of the West Nile virus envelope protein is not a

requisite for avian virulence or vector competence. PLoS Negl Trop Dis 13:e0007473.

102. Braack L, Gouveia De Almeida AP, Cornel AJ, Swanepoel R, De Jager C. 2018. Mosquito-borne arboviruses of African origin: Review of key viruses and vectors. Parasites and Vectors 11:29.

103. de la Fuente J, Antunes S, Bonnet S, Cabezas-Cruz A, Domingos AG, Estrada-Peña A, Johnson N, Kocan KM, Mansfield KL, Nijhof AM, Papa A, Rudenko N, Villar M, Alberdi P, Torina A, Ayllón N, Vancova M, Golovchenko M, Grubhoffer L, Caracappa S, Fooks AR, Gortazar C, Rego ROM. 2017. Tick-Pathogen Interactions and Vector Competence: Identification of Molecular Drivers for Tick-Borne Diseases. Front Cell Infect Microbiol 7:1–13.

104. Franz AWE, Kantor AM, Passarelli AL, Clem RJ. 2015. Tissue barriers to arbovirus infection in mosquitoes. Viruses 7:3741–3767.

105. Moudy RM, Zhang B, Shi PY, Kramer LD. 2009. West Nile virus envelope protein glycosylation is required for efficient viral transmission by Culex vectors. Virology 387:222–228.

106. Dinglasan RR, Jacobs-Lorena M. 2005. Insight into a conserved lifestyle: Protein-carbohydrate adhesion strategies of vector-borne pathogens. Infect Immun 73:7797–7807.

107. Wen D, Li S, Dong F, Zhang Y, Lin Y, Wang J, Zou Z, Zheng A. 2018. N-glycosylation of viral e protein is the determinant for vector midgut invasion by flaviviruses. MBio 9:1–14.

108. Banet-Noach C, Simanov L, Malkinson M. 2003. Direct (non-vector) transmission of West Nile virus in geese. Avian Pathol 32:489–494.

109. Ricklin ME, García-Nicolás O, Brechbühl D, Python S, Zumkehr B, Nougairede A, Charrel RN, Posthaus H, Oevermann A, Summerfield A. 2016. Vector-free transmission and persistence of Japanese encephalitis virus in pigs. Nat Commun 7:1–9.

110. Llorente F, Pérez-Ramírez E, Fernández-Pinero J, Elizalde M, Figuerola J, Soriguer RC, Jiménez-Clavero MÁ. 2015. Bagaza virus is pathogenic and transmitted by direct contact in experimentally infected partridges, but is not infectious in house sparrows and adult mice. Vet Res 46:93.

111. Brockmann SO, Oehme R, Buckenmaier T, Beer M, Jeffery-Smith A, Spannenkrebs M, Haag-Milz S, Wagner-Wiening C, Schlegel C, Fritz J, Zange S, Bestehorn M, Lindau A, Hoffmann D, Tiberi S, Mackenstedt U, Dobler G. 2018. A cluster of two human cases of tick-borne encephalitis (TBE) transmitted by unpasteurised goat milk and cheese in Germany, May 2016. Eurosurveillance 23:(15).

112. Hudopisk N, Korva M, Janet E, Simetinger M, Grgič-Vitek M, Gubenšek J, Natek V, Kraigher A, Strle F, Avšič-Županc T. 2013. Tick-borne encephalitis associated with consumption of raw goat milk, Slovenia, 2012. Emerg Infect Dis 19:806–808.

113. Li X, Shi Y, Liu Q, Wang Y, Li G, Teng Q, Zhang Y, Liu S, Li Z. 2015. Airborne transmission of a novel Tembusu virus in ducks. J Clin Microbiol 53:2734–2736.

114. Yan D, Shi Y, Wang H, Li G, Li X, Wang B, Su X, Wang J, Teng Q, Yang J, Chen H, Liu Q, Ma W, Li Z. 2018. A Single Mutation at Position 156 in the Envelope Protein of Tembusu Virus Is Responsible for Virus Tissue Tropism and Transmissibility in Ducks. J Virol 92:1–16.

115. Garmendia AE, Van Kruiningen HJ, French RA. 2001. The West Nile virus: Its recent emergence in North America. Microbes Infect 3:223–229.

116. Shirato K, Miyoshi H, Goto A, Ako Y, Ueki T, Kariwa H, Takashima I. 2004. Viral envelope protein glycosylation is a molecular determinant of the neuroinvasiveness of the New York strain of West Nile virus. J Gen Virol 85:3637–3645.

117. Beasley DWC, Whiteman MC, Zhang S, Huang CY-H, Schneider BS, Smith DR, Gromowski GD, Higgs S, Kinney RM, Barrett ADT. 2005. Envelope Protein Glycosylation Status Influences Mouse Neuroinvasion Phenotype of Genetic Lineage 1 West Nile Virus Strains. J Virol 79:8339–8347.

118. Prow NA, May FJ, Westlake DJ, Hurrelbrink RJ, Biron RM, Leung JY, McMinn PC, Clark DC, Mackenzie JS, Lobigs M, Khromykh AA, Hall RA. 2011. Determinants of attenuation in the envelope protein of the flavivirus Alfuy. J Gen Virol 92:2286–2296.

119. MACKENZIE JS, BROOM AK, LINDSAY MDA, WRIGHT AE, SMITH DW. 2018. Epizootic Activity of Murray Valley Encephalitis and Kunjin Viruses in an Aboriginal Community in the Southeast Kimberley Region of Western Australia: Results of Mosquito Fauna and Virus Isolation Studies. Am J Trop Med Hyg 69:277–283.

120. Lobigs M, Marshall ID, Weir RC, Dalgarno L. 1988. Murray Valley encephalitis virus field strains from Australia and Papua New Guinea: Studies on the sequence of the major envelope protein gene and virulence for mice. Virology 165:245–255.

121. MacKenzie JS, Williams DT. 2009. The zoonotic flaviviruses of southern, south-eastern and eastern Asia, and australasia: The potential for emergent viruses. Zoonoses Public Health 56:338–356.

122. May FJ, Lobigs M, Lee E, Gendle DJ, Mackenzie JS, Broom AK, Conlan J V., Hall RA. 2006. Biological, antigenic and phylogenetic characterization of the flavivirus Alfuy. J Gen Virol 87:329–337.

123. AG P, M B, CJ L, Pletnev AG, Bray M, Lai CJ. 1993. Chimeric tick-borne encephalitis and dengue type 4 viruses: effects of mutations on neurovirulence in mice. J Virol 67:4956–63.

124. Pletnev AG, Karganova GG, Dzhivanyan TI, Lashkevich VA, Bray M. 2000. Chimeric Langat/dengue viruses protect mice from heterologous challenge with the highly virulent strains of tick-borne encephalitis virus. Virology 274:26–31.

125. Pletnev AG, Putnak R, Speicher J, Wagar EJ, Vaughn DW. 2002. West Nile virus/dengue type 4 virus chimeras that are reduced in neurovirulence and peripheral virulence without loss of immunogenicity or protective efficacy. Proc Natl Acad Sci 99:3036–3041.

126. Chambers TJ, Nestorowicz A, Mason PW, Rice CM. 1999. Yellow fever/Japanese encephalitis chimeric viruses: construction and biological properties. J Virol 73:3095–101.

127. Liu ZY, Shi WF, Qin CF. 2019. The evolution of Zika virus from Asia to the Americas. Nat Rev Microbiol. Springer US 131-139.

128. Haddow AD, Schuh AJ, Yasuda CY, Kasper MR, Heang V, Huy R, Guzman H, Tesh RB, Weaver SC. 2012. Genetic characterization of zika virus strains: Geographic expansion of the asian lineage. PLoS Negl Trop Dis 6.

129. Frost MJ, Zhang J, Edmonds JH, Prow NA, Gu X, Davis R, Hornitzky C, Arzey KE, Finlaison D, Hick P, Read A, Hobson-Peters J, May FJ, Doggett SL, Haniotis J, Russell RC, Hall RA, Khromykh AA, Kirkland PD. 2012. Characterization of virulent West Nile virus Kunjin strain, Australia, 2011. Emerg Infect Dis 18:792–800.

130. Vrmt B, Ja B, Sv B, Virologie S, Gr E, Heinen F. 2017. A novel Zika virus mouse model reveals strain specific differences in virus pathogenesis and host inflammatory immune responses Inhalt • TheorePscher Hintergrund Zielsetzung des Papers Ergebnisse. PLoS Pathog 13:1–19.

131. Kumar A, Hou S, Airo AM, Limonta D, Mancinelli V, Branton W, Power C, Hobman TC. 2016. Zika virus inhibits type-I interferon production and downstream signaling. EMBO Rep 17:1766–1775.

132. Grant A, Ponia SS, Tripathi S, Balasubramaniam V, Miorin L, Sourisseau M, Schwarz MC, Sánchez-Seco MP, Evans MJ, Best SM, García-Sastre A. 2016. Zika Virus Targets Human STAT2 to Inhibit Type i Interferon Signaling. Cell Host Microbe 19:882–890.

133. Lee AJ, Ashkar AA. 2018. The dual nature of type I and type II interferons. Front Immunol 9:1–10.

134. Lazear HM, Govero J, Smith AM, Platt DJ, Miner JJ, Diamond MS. 2016. A Mouse Model of Zika Virus Pathogenesis. Cell Host Microbe 19:1–11.

135. Marzi A, Emanuel J, Callison J, McNally KL, Arndt N, Chadinha S, Martellaro C, Rosenke R, Scott DP, Safronetz D, Whitehead SS, Best SM, Feldmann H. 2018. Lethal Zika virus disease models in young and older interferon α/β receptor knock out mice. Front Cell Infect Microbiol 8:1–10.

136. Tripathi S, Balasubramaniam VRMT, Brown JA, Mena I, Grant A, Bardina S V., Maringer K, Schwarz MC, Maestre AM, Sourisseau M, Albrecht RA, Krammer F, Evans MJ, Fernandez-Sesma A, Lim JK, García-Sastre A. 2017. A novel Zika virus mouse model reveals strain specific differences in virus pathogenesis and host inflammatory immune responses. PLoS Pathog 13:1–19.

137. Weger-lucarelli J, Duggal NK, Bullard-feibelman K, Ebel GD. 2017. Development and Characterization of Recombinant Virus Generated from a New World Zika Virus Infectious Clone. Science 91:1–10.

138. Duggal NK, McDonald EM, Weger-Lucarelli J, Hawks SA, Ritter JM, Romo H, Ebel GD, Brault AC. 2019. Mutations present in a low-passage Zika virus isolate result in attenuated pathogenesis in mice. Virology 530:19–26.

139. Rossi SL, Tesh RB, Azar SR, Muruato AE, Hanley KA, Auguste AJ, Langsjoen RM, Paessler S, Vasilakis N, Weaver SC. 2016. Characterization of a novel murine model to study zika virus. Am J Trop Med Hyg 94:1362–1369.

140. Aliota MT, Caine EA, Walker EC, Larkin KE, Camacho E, Osorio JE. 2016. Characterization of Lethal Zika Virus Infection in AG129 Mice. PLoS Negl Trop Dis 10:1–2.

141. Brinton MA, Basu M. 2015. Functions of the 3’ and 5’ genome RNA regions of members of the genus Flavivirus. Virus Res 206:108–119.

142. Khromykh AA, Meka H, Guyatt KJ, Westaway EG. 2001. Essential Role of Cyclization Sequences in Flavivirus RNA Replication. J Virol 75:6719–6728.

143. Basu M, Brinton MA. 2011. West Nile virus (WNV) genome RNAs with up to three adjacent mutations that disrupt long distance 5′-3′ cyclization sequence basepairs are viable. Virology 412:220–232.

144. Slonchak A, Khromykh AA. 2018. Subgenomic flaviviral RNAs: What do we know after the first decade of research. Antiviral Res 159:13–25.

145. Yeh SC, Pompon J. 2018. Flaviviruses produce a subgenomic flaviviral RNA that enhances mosquito transmission. DNA Cell Biol 37:154–159.

146. Pompon J, Manuel M, Ng GK, Wong B, Shan C, Manokaran G, Soto-Acosta R, Bradrick SS, Ooi EE, Missé D, Shi PY, Garcia-Blanco MA. 2017. Dengue subgenomic flaviviral RNA disrupts immunity in mosquito salivary glands to increase virus transmission. PLoS Pathog 13:1–27.

147. Göertz GP, Fros JJ, Miesen P, Vogels CBF, van der Bent ML, Geertsema C, Koenraadt CJM, van Rij RP, van Oers MM, Pijlman GP. 2016. Noncoding Subgenomic Flavivirus RNA Is Processed by the Mosquito RNA Interference Machinery and Determines West Nile Virus Transmission by Culex pipiens Mosquitoes. J Virol 90:10145–10159.

148. Manokaran G, Finol E, Wang C, Gunaratne J, Bahl J, Ong EZ, Tan HC, Sessions OM, Ward AM, Gubler DJ, Harris E, Garcia-Blanco MA, Ooi EE. 2015. Dengue subgenomic RNA binds TRIM25 to inhibit interferon expression for epidemiological fitness. Science 350:217–221.

149. Bidet K, Garcia-Blanco MA. 2014. Flaviviral RNAs: Weapons and targets in the war between virus and host. Biochem J 462:215–230.

150. Schnettler E, Sterken MG, Leung JY, Metz SW, Geertsema C, Goldbach RW, Vlak JM, Kohl A, Khromykh AA, Pijlman GP. 2012. Noncoding Flavivirus RNA Displays RNA Interference Suppressor Activity in Insect and Mammalian Cells. J Virol 86:13486–13500.

151. Schuessler A, Funk A, Lazear HM, Cooper DA, Torres S, Daffis S, Jha BK, Kumagai Y, Takeuchi O, Hertzog P, Silverman R, Akira S, Barton DJ, Diamond MS, Khromykh AA. 2012. West Nile Virus Noncoding Subgenomic RNA Contributes to Viral Evasion of the Type I Interferon-Mediated Antiviral Response. J Virol 86:5708–5718.

152. Moon SL, Dodd BJT, Brackney DE, Wilusz CJ, Ebel GD, Wilusz J. 2015.

Flavivirus sfRNA suppresses antiviral RNA interference in cultured cells and mosquitoes and directly interacts with the RNAi machinery. Virology 485:322–329.

153. Petersen LR, Jamieson DJ, Powers AM, Honein MA. 2016. Zika Virus. N Engl J Med 374:1552–1563.

154. Grubaugh ND, Ishtiaq F, Setoh YX, Ko AI. 2019. Misperceived Risks of Zika-related Microcephaly in India. Trends Microbiol xx:1–3.

155. Zhu Z, Chan JFW, Tee KM, Choi GKY, Lau SKP, Woo PCY, Tse H, Yuen KY. 2016. Comparative genomic analysis of pre-epidemic and epidemic Zika virus strains for virological factors potentially associated with the rapidly expanding epidemic. Emerg Microbes Infect 5:e22-11.

156. Wang L, Valderramos SG, Wu A, Ouyang S, Li C, Brasil P, Bonaldo M, Coates T, Nielsen-Saines K, Jiang T, Aliyari R, Cheng G. 2016. From Mosquitos to Humans: Genetic Evolution of Zika Virus. Cell Host Microbe 19:561–565.

157. Liu Y, Liu J, Du S, Shan C, Nie K, Zhang R, Li X, Zhang R. 2017. Evolutionary enhancement of Zika virus infectivity in Aedes aegypti mosquitoes. Nat Publ Gr 545:482–486.

158. Xia H, Luo H, Shan C, Muruato AE, Nunes BTD, Medeiros DBA, Zou J, Xie X, Giraldo MI, Vasconcelos PFC, Weaver SC, Wang T, Rajsbaum R, Shi PY. 2018. An evolutionary NS1 mutation enhances Zika virus evasion of host interferon induction. Nat Commun.

159. Ling Yuan, Xing-Yao Huang, Zhong-Yu Liu, Feng Zhang, Xing-Liang Zhu, Jiu-Yang Yu3, Xue Ji, Yan-Peng Xu, Guanghui Li, Cui Li, Hong-Jiang Wang, Yong-Qiang Deng, Menghua Wu, Meng-Li Cheng, Qing Ye, Dong-Yang Xie Xiao-Feng Li, Xiangxi Wang, Weifeng Shi, Baoya C-FQ, Yuan L, Huang XY, Liu ZY, Zhang F, Zhu XL, Yu JY, Ji X, Xu YP, Li G, Li C, Wang HJ, Deng YQ, Wu M, Cheng ML, Ye Q, Xie DY, Li XF, Wang X, Shi W, Hu B, Shi PY, Xu Z, Qin CF. 2017. A single mutation in the prM protein of Zika virus contributes to fetal microcephaly. Science 7120:933–936.

160. Carbaugh DL, Lazear HM. 2020. Flavivirus Envelope Protein Glycosylation: Impacts on Viral Infection and Pathogenesis. J Virol 94:1–10.

161. Jiang WR, Lowe A, Higgs S, Reid H, Gould EA. 1993. Single amino acid codon changes detected in louping ill virus antibody-resistant mutants with reduced neurovirulence. J Gen Virol 74:931–935.

162. Murata R, Eshita Y, Maeda A, Maeda J, Akita S, Tanaka T, Yoshii K, Kariwa H, Umemura T, Takashima I. 2010. Glycosylation of the West Nile virus envelope protein increases in vivo and in vitro viral multiplication in birds. Am J Trop Med Hyg 82:696–704.

163. Wen D, Li S, Dong F, Zhang Y, Lin Y, Wang J, Zou Z, Zheng A. 2018. N-glycosylation of viral e protein is the determinant for vector midgut invasion by flaviviruses. MBio 9:1–14.

164. Widman DG, Young E, Yount BL, Plante KS, Gallichotte EN, Carbaugh DL, Peck KM, Plante J, Swanstrom J, Heise MT, Lazear HM, Baric RS. 2017. A reverse genetics platform that spans the Zika virus family tree. MBio 8:e02014-16.

165. Sheehan KCF, Lai KS, Dunn GP, Bruce AT, Diamond MS, Heutel JD, Dungo-Arthur C, Carrero J a., White JM, Hertzog PJ, Schreiber RD. 2006. Blocking Monoclonal Antibodies Specific for Mouse IFN-ab Receptor Subunit 1 (IFNAR-1) from Mice Immunized by In Vivo Hydrodynamic Transfection. J Interf Cytokine Res 26:804–819.

166. Lazear HM, Govero J, Smith AM, Platt DJ, Fernandez E, Miner JJ, Diamond MS. 2016. A Mouse Model of Zika Virus Pathogenesis. Cell Host Microbe 19:720–730.

167. Rossi SL, Tesh RB, Azar SR, Muruato AE, Hanley KA, Auguste AJ, Langsjoen RM, Paessler S, Vasilakis N, Weaver SC. 2016. Characterization of a novel murine model to study zika virus. Am J Trop Med Hyg 94:1362–1369.

168. Yockey LJ, Varela L, Rakib T, Khoury-Hanold W, Fink SL, Stutz B, Szigeti-Buck K, Van den Pol A, Lindenbach BD, Horvath TL, Iwasaki A. 2016. Vaginal Exposure to Zika Virus during Pregnancy Leads to Fetal Brain Infection. Cell 166:1247-1256.e4.

169. Miner JJ, Cao B, Govero J, Smith AM, Fernandez E, Cabrera OH, Garber C, Noll M, Klein RS, Noguchi KK, Mysorekar IU, Diamond MS. 2016. Zika Virus Infection during Pregnancy in Mice Causes Placental Damage and Fetal Demise. Cell 165:1081–1091.

170. Musso D, Bossin H, Mallet HP, Besnard M, Broult J, Baudouin L, Levi JE, Sabino EC, Ghawche F, Lanteri MC, Baud D. 2018. Zika virus in French Polynesia 2013–14: anatomy of a completed outbreak. Lancet Infect Dis 18:e172–e182.

171. Cauchemez S, Besnard M, Bompard P, Dub T, Guillemette-Artur P, Eyrolle-Guignot D, Salje H, Van Kerkhove MD, Abadie V, Garel C, Fontanet A, Mallet HP. 2016. Association between Zika virus and microcephaly in French Polynesia, 2013-15: A retrospective study. Lancet 387:2125–2132.

172. Baronti C, Piorkowski G, Charrel RN, Boubis L, Leparc-Goffart I, de Lamballerie X. 2014. Complete Coding Sequence of Zika Virus from a French Polynesia Outbreak in 2013. Genome Announc 2:2013–2014.

173. Lanciotti RS, Lambert AJ, Holodniy M, Saavedra S, del Carmen Castillo Signor L. 2016. Phylogeny of zika virus in western Hemisphere, 2015. Emerg Infect Dis 22 933-935.

174. Berthet N, Nakouné E, Kamgang B, Selekon B, Descorps-Declère S, Gessain A, Manuguerra J-C, Kazanji M. 2014. Molecular Characterization of Three Zika Flaviviruses Obtained from Sylvatic Mosquitoes in the Central African Republic. Vector-Borne Zoonotic Dis 14:862–865.

175. Faria NR, Azevedo R d. S d. S, Kraemer MUG, Souza R, Cunha MS, Hill SC, Theze J, Bonsall MB, Bowden TA, Rissanen I, Rocco IM, Nogueira JS, Maeda AY, Vasami FG d. S, Macedo FL d. L, Suzuki A, Rodrigues SG, Cruz ACR, Nunes BT, Medeiros DB d. A, Rodrigues DSG, Nunes Queiroz AL, Silva EVP d., Henriques DF, Travassos da Rosa ES, de Oliveira CS, Martins LC, Vasconcelos HB, Casseb LMN, Simith D d. B, Messina JP, Abade L, Lourenco J, Alcantara LCJ, Lima MM De, Giovanetti M, Hay SI, de Oliveira RS, Lemos P d. S, Oliveira LF De, de Lima CPS, da Silva SP, Vasconcelos JM d., Franco L, Cardoso JF, Vianez-Junior JL d. SG, Mir D, Bello G, Delatorre E, Khan K, Creatore M, Coelho GE, de Oliveira WK, Tesh R, Pybus OG, Nunes MRT, Vasconcelos PFC. 2016. Zika virus in the Americas: Early epidemiological and genetic findings. Science 5036:1–9.

176. Ladner JT, Wiley MR, Prieto K, Yasuda CY, Nagle E, Kasper MR, Reyes D, Vasilakis N, Heang V, Weaver SC, Haddow A, Tesh RB, Sovann L, Palacios G. 2016. Complete Genome Sequences of Five Zika Virus Isolates. Genome Announc 4:e00377-16.

177. Tassaneetrithep B, Burgess TH, Granelli-Piperno A, Trumpfheller C, Finke J, Sun W, Eller MA, Pattanapanyasat K, Sarasombath S, Birx DL, Steinman RM, Schlesinger S, Marovich MA. 2003. DC-SIGN (CD209) mediates dengue virus infection of human dendritic cells. J Exp Med 197:823–829.

178. Rouvinski A, Guardado-Calvo P, Barba-Spaeth G, Duquerroy S, Vaney MC, Kikuti CM, Navarro Sanchez ME, Dejnirattisai W, Wongwiwat W, Haouz A, Girard-Blanc C, Petres S, Shepard WE, Desprès P, Arenzana-Seisdedos F, Dussart P, Mongkolsapaya J, Screaton GR, Rey FA. 2015. Recognition determinants of broadly neutralizing human antibodies against dengue viruses. Nature 520:109–113.

179. Wang L, Valderramos SG, Wu A, Ouyang S, Li C, Brasil P, Bonaldo M, Coates T, Nielsen-Saines K, Jiang T, Aliyari R, Cheng G. 2016. From Mosquitos to Humans: Genetic Evolution of Zika Virus. Cell Host Microbe 5: 561-565.

180. Jaeger AS, Murrieta RA, Goren LR, Crooks CM, Moriarty R V, Weiler AM, Rybarczyk S, Semler MR, Huffman C, Mejia A, Simmons HA, Fritsch M, Osorio JE, Eickhoff JC, O'Connor SL, Ebel GD, Friedrich TC, Aliota MT. 2019. Zika viruses of African and Asian lineages cause fetal harm in a mouse model of vertical transmission. PLoS Negl Trop Dis 13.

181. Gu SH, Song DH, Lee D, Jang J, Kim MY, Jung J, Woo KI, Kim M, Seog W, Oh HS, Choi BS, Ahn JS, Park Q, Jeong ST. 2017. Whole-genome sequence analysis of Zika virus, amplified from urine of traveler from the Philippines. Virus Genes 53:918–921.

182. Garcia-vallejo JJ, Kooyk Y Van. 2013. The physiological role of DC-SIGN : A tale of mice and men. Trends Immunol 34:482–486.

183. Michlmayr D, Andrade P, Gonzalez K, Balmaseda A, Harris E. 2017. CD14 + CD16 + monocytes are the main target of Zika virus infection in peripheral blood mononuclear cells in a paediatric study in Nicaragua. Nat Microbiol 2.

184. Foo SS, Chen W, Chan Y, Bowman JW, Chang LC, Choi Y, Yoo JS, Ge J, Cheng G, Bonnin A, Nielsen-Saines K, Brasil P, Jung JU. 2017. Asian Zika virus strains target CD14+ blood monocytes and induce M2-skewed immunosuppression during pregnancy. Nat Microbiol 2:1558–1570.

185. Domínguez-Soto A, Sierra-Filardi E, Puig-Kröger A, Pérez-Maceda B, Gómez-Aguado F, Corcuera MT, Sánchez-Mateos P, Corbí AL. 2011. Dendritic Cell-Specific ICAM-3–Grabbing Nonintegrin Expression on M2-Polarized and Tumor-Associated Macrophages Is Macrophage-CSF Dependent and Enhanced by Tumor-Derived IL-6 and IL-10. J Immunol 186:2192–2200.

186. Navarro-Sanchez E, Altmeyer R, Amara A, Schwartz O, Fieschi F, Virelizier JL, Arenzana-Seisdedos F, Desprès P. 2003. Dendritic-cell-specific ICAM3-grabbing non-integrin is essential for the productive infection of human dendritic cells by mosquito-cell-derived dengue viruses. EMBO Rep 4:723–728.

187. Hamel R, Dejarnac O, Wichit S, Ekchariyawat P, Neyret A, Luplertlop N, Perera-Lecoin M, Surasombatpattana P, Talignani L, Thomas F, Cao-Lormeau V-M, Choumet V, Briant L, Desprès P, Amara A, Yssel H, Missé D. 2015. Biology of Zika Virus Infection in Human Skin Cells. J Virol 89:8880–8896.

188. Goo L, Demaso CR, Pelc RS, Kuhn RJ, Pierson TC, Ledgerwood JE, Graham BS. 2018. The Zika virus envelope protein glycan loop regulates virion antigenicity. Virology 515:191–202.

189. Perera-Lecoin M, Meertens L, Carnec X, Amara A. 2013. Flavivirus entry receptors: An update. Viruses 6:69–88.

190. Agrelli A, de Moura RR, Crovella S, Brandão LAC. 2019. ZIKA virus entry mechanisms in human cells. Infect Genet Evol 69:22–29.

191. Sirohi D, Kuhn RJ. 2017. Zika Virus Structure, Maturation, and Receptors. J Infect Dis.

192. De Alwis R, Williams KL, Schmid MA, Lai CY, Patel B, Smith SA, Crowe JE, Wang WK, Harris E, De Silva AM. 2014. Dengue Viruses Are Enhanced by Distinct Populations of Serotype Cross-Reactive Antibodies in Human Immune

Sera. PLoS Pathog 10:e1004386.

193. Brien JD, Lazear HM, Diamond MS. 2013. Propagation, quantification, detection, and storage of west nile virus. Curr Protoc Microbiol 1–18.

194. Oliphant T, Nybakken GE, Engle M, Xu Q, Nelson CA, Sukupolvi-Petty S, Marri A, Lachmi B-E, Olshevsky U, Fremont DH, Pierson TC, Diamond MS. 2006. Antibody Recognition and Neutralization Determinants on Domains I and II of West Nile Virus Envelope Protein. J Virol 80:12149–12159.

195. Messer WB, Yount B, Hacker KE, Donaldson EF, Huynh JP, De AM, Baric RS. 2012. Development and Characterization of a Reverse Genetic System for Studying Dengue Virus Serotype 3 Strain Variation and Neutralization. PLoS Negl Trop Dis 6:e1486.

196. Smith SA, de Alwis AR, Kose N, Harris E, Ibarra KD, Kahle KM, Pfaf JM, Xiang X, Doranz BJ, de Silva AM, Austin SK, Sukupolvi-Petty S, Diamond MS, Crowe JE. 2013. The potent and broadly neutralizing human dengue virus-specific monoclonal antibody 1C19 reveals a unique cross-reactive epitope on the bc loop of domain II of the envelope protein. MBio 4:1–12.

197. Henchal EA, Gentry MK, McCown JM, Brandt WE. 1982. Dengue virus-specific and flavivirus group determinants identified with monoclonal antibodies by indirect immunofluorescence. Am J Trop Med Hyg 31:830–836.

198. Lai C-Y, Tsai W-Y, Lin S-R, Kao C-L, Hu H-P, King C-C, Wu H-C, Chang G-J, Wang W-K. 2008. Antibodies to Envelope Glycoprotein of Dengue Virus during the Natural Course of Infection Are Predominantly Cross-Reactive and Recognize Epitopes Containing Highly Conserved Residues at the Fusion Loop of Domain II. J Virol 82:6631–6643.

199. Sheehan KCF, Lai KS, Dunn GP, Bruce AT, Diamond MS, Heutel JD, Dungo-Arthur C, Carrero J a., White JM, Hertzog PJ, Schreiber RD. 2006. Blocking Monoclonal Antibodies Specific for Mouse IFN-αβ Receptor Subunit 1 (IFNAR-1) from Mice Immunized by In Vivo Hydrodynamic Transfection. J Interf Cytokine Res 26:804–819.

200. Lanciotti RS, Kosoy OL, Laven JJ, Velez JO, Lambert AJ, Johnson AJ, Stanfield SM, Duffy MR. 2008. Genetic and serologic properties of Zika virus associated with an epidemic, Yap State, Micronesia, 2007. Emerg Infect Dis 14:1232–1239.

201. Lyle R. Petersen MDMPH, Denise J. Jamieson, M.D. MPH, Ann M. Powers PD, Margaret A. Honein, Ph.D. MP. 2016. Zika Virus. N Engl J Med 374:1552–63.

202. Tsetsarkin KA, Kenney H, Chen R, Liu G, Manukyan H, Whitehead SS. 2016. A Full-Length Infectious cDNA Clone of Zika Virus from the 2015 Epidemic in Brazil as a Genetic Platform for Studies of Virus-Host 7:1–8.

203. Lazear HM, Schoggins JW, Diamond MS. 2019. Shared and Distinct Functions of Type I and Type III Interferons. Immunity 50:907–923.

204. Manangeeswaran M, Ireland DDC, Verthelyi D. 2016. Zika (PRVABC59) Infection Is Associated with T cell Infiltration and Neurodegeneration in CNS of Immunocompetent Neonatal C57Bl/6 Mice. PLoS Pathog 12:1–20.

205. McDonald EM, Duggal NK, Delorey MJ, Oksanish J, Ritter JM, Brault AC. 2019. Duration of seminal Zika viral RNA shedding in immunocompetent mice inoculated with Asian and African genotype viruses. Virology 535:1–10.

206. Weger-lucarelli J, Garcia SM, Rückert C, Byas A, Connor SLO, Aliota MT, Friedrich TC, Connor DHO, Ebel GD. 2018. Using barcoded Zika virus to assess virus population structure in vitro and in Aedes aegypti mosquitoes. Virology 521:138–148.

207. Pardy RD, Valbon SF, Richer MJ. 2019. Running interference: Interplay between Zika virus and the host interferon response. Cytokine 119:7–15.

208. Singh PK, Guest J, Kanwar M, Boss J, Gao N, Juzych MS, Abrams GW, Yu F, Kumar A. 2017. Zika virus infects cells lining the blood-retinal barrier and causes chorioretinal atrophy in mouse eyes. JCI Insight 2:1–14.

209. Shrivastava S, Puri V, Dilley KA, Ngouajio E, Shifflett J, Oldfield LM, Fedorova NB, Hu L, Williams T, Durbin A, Amedeo P, Rashid S, Shabman RS, Pickett BE.

2018. Whole genome sequencing, variant analysis, phylogenetics, and deep sequencing of Zika virus strains. Sci Rep 8:1–11.

210. Jabara CB, Jones CD, Roach J, Anderson JA, Swanstrom R. 2011. Accurate sampling and deep sequencing of the HIV-1 protease gene using a Primer ID. Proc Natl Acad Sci 108:20166–20171.

211. Rayamajhi M, Humann J, Penheiter K, Andreasen K, Lenz LL. 2010. Induction of IFN-αβ enables Listeria monocytogenes to suppress macrophage activation by IFN-γ. J Exp Med 207:327–337.

212. Österlund P, Jiang M, Westenius V, Kuivanen S, Järvi R, Kakkola L, Lundberg R, Melén K, Korva M, Avšič – Županc T, Vapalahti O, Julkunen I. 2019. Asian and African lineage Zika viruses show differential replication and innate immune responses in human dendritic cells and macrophages. Sci Rep 9:1–15.

213. Shen J, Devery JM, King NJC. 1995. Adherence status regulates the primary cellular activation responses to the flavivirus West Nile. Immunology 84:254–264.

214. García-Nicolás O, Lewandowska M, Ricklin ME, Summerfield A. 2019. Monocyte-derived dendritic cells as model to evaluate species tropism of mosquito-borne flaviviruses. Front Cell Infect Microbiol 9:1–13.

215. Daffis S, Lazear HM, Liu WJ, Audsley M, Engle M, Khromykh AA, Diamond MS. 2011. The Naturally Attenuated Kunjin Strain of West Nile Virus Shows Enhanced Sensitivity to the Host Type I Interferon Response. J Virol 85:5664–5668.

216. Smith DR, Sprague TR, Hollidge BS, Valdez SM, Padilla SL, Bellanca SA, Golden JW, Coyne SR, Kulesh DA, Miller LJ, Haddow AD, Koehler JW, Gromowski GD, Jarman RG, Alera MTP, Yoon IK, Buathong R, Lowen RG, Kane CD, Minogue TD, Bavari S, Tesh RB, Weaver SC, Linthicum KJ, Pitt ML, Nasar F. 2018. African and asian zika virus isolates display phenotypic differences both in vitro and in vivo. Am J Trop Med Hyg 98:432–444.

217. Ding Q, Gaska JM, Douam F, Wei L, Kim D, Balev M, Heller B, Ploss A. 2018. Species-specific disruption of STING-dependent antiviral cellular defenses by the Zika virus NS2B3 protease. Proc Natl Acad Sci U S A 115:E6310–E6318.

218. Gorman MJ, Caine EA, Zaitsev K, Begley MC, Weger-Lucarelli J, Uccellini MB, Tripathi S, Morrison J, Yount BL, Dinnon KH, Rückert C, Young MC, Zhu Z, Robertson SJ, McNally KL, Ye J, Cao B, Mysorekar IU, Ebel GD, Baric RS, Best SM, Artyomov MN, Garcia-Sastre A, Diamond MS. 2018. An Immunocompetent Mouse Model of Zika Virus Infection. Cell Host Microbe 23:672-685.e6.

219. Dowall SD, Graham VA, Rayner E, Atkinson B, Hall G, Watson RJ, Bosworth A, Bonney LC, Kitchen S, Hewson R. 2016. A Susceptible Mouse Model for Zika Virus Infection. PLoS Negl Trop Dis 10:1–13.

220. Li H, Saucedo-Cuevas L, Regla-Nava JA, Chai G, Sheets N, Tang W, Terskikh A V., Shresta S, Gleeson JG. 2016. Zika Virus Infects Neural Progenitors in the Adult Mouse Brain and Alters Proliferation. Cell Stem Cell 19:593–598.

221. Aliota MT, Caine EA, Walker EC, Larkin KE, Camacho E, Osorio JE. 2016. Characterization of Lethal Zika Virus Infection in AG129 Mice. PLoS Negl Trop Dis 10:e0004682.

222. Morrison TE, Diamond MS. 2017. Animal Models of Zika Virus Infection, Pathogenesis, and Immunity. J Virol 67:242–252.

223. Sukupolvi-Petty S, Brien JD, Austin SK, Shrestha B, Swayne S, Kahle K, Doranz BJ, Johnson S, Pierson TC, Fremont DH, Diamond MS. 2013. Functional Analysis of Antibodies against Dengue Virus Type 4 Reveals Strain-Dependent Epitope Exposure That Impacts Neutralization and Protection. J Virol 87:8826–8842.

224. Keys JR, Zhou S, Anderson JA, Eron JJ, Rackoff LA, Jabara C, Swanstrom R. 2015. Primer ID informs next-generation sequencing platforms and reveals preexisting drug resistance mutations in the HIV-1 reverse transcriptase coding domain. AIDS Res Hum Retroviruses 31:658–668.

225. Klitting R, Gould EA, Paupy C, de Lamballerie X. 2018. What does the future hold for yellow fever virus? (I). Genes (Basel) 9:12–16.

226. Hermance ME, Thangamani S. 2017. Powassan Virus: An Emerging Arbovirus of Public Health Concern in North America. Vector-Borne Zoonotic Dis 17:453–462.

227. Akiyama BM, Laurence HM, Massey AR, Costantino DA, Xie X, Yang Y, Shi PY, Nix JC, Beckham JD, Kieft JS. 2016. Zika virus produces noncoding RNAs using a multi-pseudoknot structure that confounds a cellular exonuclease. Science 354:1148–1152.

228. Chapman EG, Costantino DA, Rabe JL, Moon SL, Wilusz J, Nix JC, Kieft JS. 2014. The structural basis of pathogenic subgenomic flavivirus RNA (sfRNA) production. Science 344:307–310.

229. Scott JC, Brackney DE, Campbell CL, Bondu-Hawkins V, Hjelle B, Ebel GD, Olson KE, Blair CD. 2010. Comparison of dengue virus type 2-specific small RNAs from RNA interference-competent and - incompetent mosquito cells. PLoS Negl Trop Dis 4.

230. Göertz GP, Abbo SR, Fros JJ, Pijlman GP. 2018. Functional RNA during Zika virus infection. Virus Res 254:41–53.

231. Li XF, Dong HL, Huang XY, Qiu YF, Wang HJ, Deng YQ, Zhang NN, Ye Q, Zhao H, Liu ZY, Fan H, An XP, Sun SH, Gao B, Fa YZ, Tong YG, Zhang FC, Gao GF, Cao WC, Shi PY, Qin CF. 2016. Characterization of a 2016 Clinical Isolate of Zika Virus in Non-human Primates. EBioMedicine 12:170–177.

232. Liu J, Liu Y, Nie K, Du S, Qiu J, Pang X, Wang P, Cheng G. 2016. Flavivirus NS1 protein in infected host sera enhances viral acquisition by mosquitoes. Nat Microbiol 1:1–11.

233. Ávila-Pérez G, Nogales A, Park JG, Márquez-Jurado S, Iborra FJ, Almazan F, Martínez-Sobrido L. 2019. A natural polymorphism in Zika virus NS2A protein responsible of virulence in mice. Sci Rep 9:1–17.

234. Michalski D, Gustavo Ontiveros J, Russo J, Charley PA, Anderson JR, Heck AM, Geiss BJ, Wilusz J. 2019. Zika virus noncoding sfRNAs sequester multiple host-derived RNA-binding proteins and modulate mRNA decay and splicing during infection. J Biol Chem 294:16282–16296.

235. Göertz GP, van Bree JWM, Hiralal A, Fernhout BM, Steffens C, Boeren S, Visser TM, Vogels CBF, Abbo SR, Fros JJ, Koenraadt CJM, van Oers MM, Pijlman GP.

2019. Subgenomic flavivirus RNA binds the mosquito DEAD/H-box helicase ME31B and determines Zika virus transmission by Aedes aegypti. Proc Natl Acad Sci U S A 116:19136–19144.

236. Donald CL, Brennan B, Cumberworth SL, Rezelj V V., Clark JJ, Cordeiro MT, Freitas de Oliveira França R, Pena LJ, Wilkie GS, Da Silva Filipe A, Davis C, Hughes J, Varjak M, Selinger M, Zuvanov L, Owsianka AM, Patel AH, McLauchlan J, Lindenbach BD, Fall G, Sall AA, Biek R, Rehwinkel J, Schnettler E, Kohl A. 2016. Full Genome Sequence and sfRNA Interferon Antagonist Activity of Zika Virus from Recife, Brazil. PLoS Negl Trop Dis 10:1–20.